seit 1558

FRIEDRICH-SCHILLER-UNIVERSITÄT JENA

Physikalisch-Astronomische Fakultät

Characterisation of young nearby stars – The Ursa Major group

Dissertation

zur Erlangung des akademischen Grades

doctor rerum naturalium (Dr. rer. nat.)

vorgelegt dem Rat der Physikalischen-Astronomischen Fakultät
der Friedrich-Schiller-Universität Jena

von Dipl.-Phys. Matthias Ammler

geboren am 10.01.1977 in Neuburg a. d. Donau

Gutachter

1. Prof. Dr. Ralph Neuhäuser
2. Dr. habil. Matthias Hünsch
3. Prof. Dr. Artie P. Hatzes

Tag der letzten Rigorosumsprüfung: 26. Juni 2006

Tag der öffentlichen Verteidigung: 11. Juli 2006

Meinen Eltern

Contents

List of Figures

List of Tables

Abstract

This work presents a homogeneous set of stellar parameters for a larger sample of kinematic Ursa Major (UMa) group members with spectral types late-F to early-K.

The UMa group is comprised of the stars in the UMa cluster in the Big Dipper constellation and of many co-moving stars spread over the whole sky. The definition of kinematic membership criteria has ever been difficult so that spectroscopic criteria should be added. Previous work indicated that the UMa group members are young with an age of roughly 300 Myrs. The youth leaves traces in the stellar spectrum, i.e. the Li I λ6707.8 Å absorption line, and activity features, e.g. partial filling-in of the core of the Hα line due to chromospheric emission. Furthermore rotational line broadening is stronger than that of older stars. Additional to the youth indicators, iron abundance is an appropriate membership criterion in case it is different from that of other groups of stars. Spectroscopic properties of the UMa group already have been specified but resulting membership criteria are rather inconclusive.

For this thesis, a sample of kinematic members was drawn from Montes et al. (2001a) and King et al. (2003) in order to derive the spectroscopic properties of mid- and late-type UMa group members homogeneously. Spectra with high resolving power ($\frac{\lambda}{\Delta\lambda} \approx 60000$) and signal-to-noise ratio ($\gtrsim 200$) were obtained for twenty stars with spectral types late-F to M.

Based on the quantitative spectral analysis of Fuhrmann (2004), the stellar parameters such as effective temperatures, surface gravities, iron and magnesium abundance, and projected rotational velocities of ten kinematic UMa group members with spectral types late-F to early-K are derived. These are combined with results for six further members obtained the same way by Fuhrmann (2004) and König et al. (2006) giving a homogeneous list of stellar parameters for in total sixteen kinematic UMa group members.

The stellar parameters of the young star and possible UMa group member HD 217813 from Fuhrmann (2004) were reproduced in order to ensure the consistent application of Fuhrmann's methods.

Spectroscopic distances are calculated from the derived stellar parameters. They are consistent with *Hipparcos* distances corroborating the derived surface gravities. Hereby the quantitative spectral analysis of UMa group members by Fuhrmann (2004) is extended to distances beyond 25 pc.

The effective temperatures and surface gravities place the UMa group on the main sequence but do not provide any further constraints on the age.

The homogeneously derived iron abundances increase the previously determined UMa group iron abundance slightly to [Fe/H]= -0.03 ± 0.04. They can be distinguished from the Hyades moving group but are similar to the Pleiades. Including the magnesium abundances, the UMa group coincides well with the thin disk population defined by Fuhrmann (2004).

Projected rotational velocities were measured for two further kinematic members by Fuhrmann (2000). Together with the sixteen data points from the present work, from Fuhrmann (2004), and from König et al. (2006), these data points trace well the onset of main sequence magnetic braking of rotation at an effective temperature of ≈6200 K. The current rotation rates are consistent with an age of 250 – 1000 Myrs when applying a so-called Skumanich law.

In the present work, lithium absorption was analysed for all of the twenty observed stars. At effective temperatures cooler than that of the Sun and higher than 5000 K, the lithium absorption can be distinguished well from the open clusters Pleiades, Hyades, and M 35, supporting the age estimates of roughly 300 Myrs. The distribution argues against a large intrinsic age spread in the UMa group though based on few data points only.

A preliminary study of the Hα filling-in was done for 24 stars in the present work including measurements for five stars from Fuhrmann (2004). The core of the Hα line is partially filled-in for most of the stars. However the homogeneous level of filling-in encountered by Fuhrmann (2004) is not confirmed.

A promising prospect is the adaption of some of these properties as membership criteria. The decision on the membership of many unsure UMa group candidates might be simplified substantially when combining lithium absorption and iron abundance with kinematic membership criteria.

Zusammenfassung

In dieser Arbeit werden die stellaren Parameter einer größeren Zahl von kinematischen Mitgliedern später F-Spektraltypen bis früher K-Spektraltypen der Ursa-Major-Gruppe (UMa-Gruppe) homogen abgeleitet.

Die UMa-Gruppe setzt sich aus Sternen des UMa-Haufens im Sternbild des Großen Wagens und vielen weiteren Sternen zusammen, die sich in die gleiche Richtung wie der Haufen bewegen und über den gesamten Himmel verteilt sind. Die Festlegung von Kriterien zur Entscheidung über die Mitgliedschaft von Sternen ist schon immer schwierig gewesen, so dass sich die Hinzunahme von spektroskopischen Kriterien empfiehlt. Bisherige Arbeiten stellen heraus, dass die Mitglieder der UMa-Gruppe mit einem Alter von ungefähr 300 Mio. Jahren noch recht jung sind. Die Jugend hinterlässt Spuren im Spektrum dieser Sterne, z.B. die Absorptionslinie des neutralen Lithiums bei 6707,8 Å, und Anzeichen von Aktivität, z.B. die teilweise Auffüllung der Balmer-α-Linie durch chromosphärische Emission. Weiterhin ist die Rotationsverbreiterung der Spektrallinien größer als bei älteren Sternen. Neben diesen Anzeichen für das junge Alter dieser Sterne kann sich auch die Eisenhäufigkeit als Kriterium der Mitgliedschaft erweisen, sollte sie sich deutlich von derjenigen anderer Sterngruppen unterscheiden. Obwohl die spektroskopischen Eigenschaften der UMa-Gruppe schon untersucht wurden, sind resultierende Kriterien der Mitgliedschaft noch wenig prägnant.

Diese Arbeit wählt sichere kinematische Mitglieder späten Spektraltyps aus den Arbeiten von D. Montes und Mitarbeitern (2001a) und J. King und Mitarbeitern (2003) aus, um ihre spektroskopischen Eigenschaften homogen zu bestimmen. Spektren mit hoher spektraler Auflösung von etwa $\frac{\lambda}{\Delta\lambda} \approx 60.000$ und einem hohen Signal-zu-Rausch-Verhältnis von meist über ≈200 wurden für 20 Sternen mit späterem F-Spektraltyp bis zu M-Spektraltypen aufgenommen.

In dieser Arbeit ergeben sich mittels der quantitativen Spektralanalyse nach K. Fuhrmann (2004) für zehn kinematische Mitgliedern der späten Spektraltypen F bis frühen Spektraltypen K stellare Parameter wie die Effektivtemperatur, die Oberflächenschwerebeschleunigung, die Eisen- und Magnesiumhäufigkeiten und die projizierte Rotationsgeschwindigkeit. In die Interpretation der Daten sind die kürzlich erzielten Ergebnisse von Fuhrmann (2004) und König und Mitarbeitern (2006) einbezogen, die mit derselben Methode bestimmt wurden. Auf diese Weise erwächst eine homogene Liste stellarer Parameter für insgesamt 16 kinematische Mitglieder.

Die Reproduzierbarkeit der Ergebnisse K. Fuhrmanns zeigt sich durch die erneute Beobachtung und Analyse des jungen Sterns und möglichen UMa-Mitglieds HD 217813.

Spektroskopische Entfernungen errechnen sich aus den abgeleiteten Eigenschaften der Sterne. Sie stimmen mit den Entfernungen überein, die mittels der *Hipparcos*-Mission gefunden wurden. Im gleichen Zuge wird die Anwendung der Methode Fuhrmanns auf Sterne der UMa-Gruppe jenseits von 25 pc ausgedehnt.

Die Effektivtemperaturen und Oberflächenschwerebeschleunigungen sind mit den Werten der Hauptreihe vereinbar, erlauben jedoch keine weiteren Rückschlüsse über das Alter.

Die homogen abgeleiteten Eisenhäufigkeiten erhöhen den bisher bestimmten Mittelwert, nämlich von $[\mathrm{Fe/H}] \approx -0{,}08$ auf $[\mathrm{Fe/H}] = -0{,}03$. Dieser ist verschieden von demjenigen der Gruppe der Hyaden, jedoch ähnlich zu demjenigen der Plejaden. Unter Hinzunahme der Magnesiumhäufigkeiten passt die UMa-Gruppe gut zum Häufigkeitsmuster der dünnen galaktischen Scheibe nach Fuhrmann (2004). Fuhrmann (2002) vermaß die projizierten Rotationsgeschwindigkeiten zweier weiterer kinematischer Mitglieder. Zusammen mit den anderen 16 Werten, sowohl aus der vorliegenden Arbeit als auch von Fuhrmann (2004) und König und Mitarbeitern (2006), zeichnen sie deutlich das Einsetzen der magnetischen Abbremsung der Rotation auf der Hauptreihe bei einer Effektivtemperatur von etwa 6200 K nach. Die gegenwärtigen Rotationsgeschwindigkeiten lassen auf ein Alter von 250 Mio. Jahren bis zu einer Milliarde Jahren schließen, sofern man ein sogenanntes Skumanich-Gesetz zu Grunde legt.

Das Ausmaß der Lithiumabsorption wird in der vorliegenden Arbeit für alle der beobachteten 20 Sterne bestimmt. Bei kühleren Effektivtemperaturen als derjeniger der Sonne, aber heißer als 5000 K, ist das Ausmaß der Absorption durch Lithium wohlunterschieden von den offenen Haufen der Plejaden, der Hyaden und M 35. Dies unterstützt die bisherige Altersabschätzung von etwa 300 Mio. Jahren. Die Zahl der zu Grunde liegenden Datenpunkte ist gering. Ihre geringe Streuung spricht jedoch gegen eine größere Streuung im Alter der Sterne der UMa-Gruppe.

Eine vorläufige Studie der Einfüllung der Hα-Linie wurde in der vorliegenden Arbeit für 24 kinematische Mitgliedern vorgenommen, einschließlich von fünf Sternen von Fuhrmann (2004). Der Kern der Hα-Linie der meisten Sterne ist teilweise aufgefüllt. Das gleichmäßige Niveau der Auffüllung, die Fuhrmann (2004) gefunden hatte, kann jedoch nicht bestätigt werden.

Ein vielversprechender Ausblick ist die Annahme einiger der vorgenannten Eigenschaften als Kriterien für die Mitgliedschaft zur UMa-Gruppe. Eine Zusammenführung des Ausmaßes der Lithiumabsorption und der Eisenhäufigkeiten mit kinematischen Kriterien könnte die Einordnung von unsicheren Kandidaten deutlich vereinfachen.

Remarks and Acknowledgements

The term “Ursa Major (UMa) group” is used throughout this work for the structure comprising the UMa cluster and the UMa stream/ UMa moving group.

The designations “Fig.” and “Tab.” refer to figures and tables, respectively, included in the present work while “fig.” and “tab.” refer to figures and tables in other work.

Throughout this work, “Myrs” abbreviates “millions of years” and “Gyrs” is the short form for “billions of years”.

This work is based on observations with the Coudé-Échelle spectrograph of the *Alfred-Jentsch-Teleskop* at the *Thüringer Landessternwarte Tautenburg* and on observations collected at the *Centro Astronómico Hispano Alemán (CAHA)* at Calar Alto, operated jointly by the *Max-Planck-Institut für Astronomie* and the *Instituto de Astrofísica de Andalucía (CSIC)*.

This work was supported by a graduate scholarship of the *Bischöfliche Studienförderung Cusanuswerk*. Travel funds were granted by the *DFG* under the projects *NE 515/16 and 17*.

The services *SIMBAD* and *NASA/ADS* as well as the *VALD* data base (see text for details) were used.

Use was made of the operating system *Linux* and the typesetting software LaTeX, both open source.

1 Introduction

The Ursa Major (UMa) group consists of co-moving stars spread over the whole sky (Sect. 1.1). The proximity of these stars warrants high signal-to-noise ratio for many kinds of studies. A similar age of roughly 300 Myrs makes the UMa group members an ideal sample for evolutional studies (Sect. 1.2). However the age is not well-known and there is disagreement on the member list. The UMa group has undergone several attempts to define its properties and to establish a final list of members (Sect. 1.3) while the existence of moving groups always has been controversial. Realising that this work has not yet come to an end, I decided to choose a sample of kinematic members and to extend the homogeneous quantitative spectroscopic analysis of Fuhrmann (2004) who already analysed UMa group members closer than 25 pc (Sect. 1.4).

1.1 What is the Ursa Major group?

1.1.1 Co-moving stars in the Big Dipper constellation

The *Big Dipper*[1] (see the top panel of Fig. 1.1) has ever been known to mankind – seven bright stars – Dubhe, Merak, Phekda, Megrez, Alioth, Mizar with Alcor, and Benet Nash – solely circling around the polar star in an otherwise apparently empty region of the sky (see Fig. 1.3). Halley (1718) discovered that fixed stars actually move slowly – disordered at a first glance – on the celestial sphere. In the middle of the 19th century, Proctor (1869) and Huggins (1871) found that five of the A stars in the Big Dipper were moving into the same direction (bottom panel of Fig. 1.1). Hertzsprung (1909) found stars far off the Big Dipper also moving into this direction, forming the *Ursa Major (UMa) moving group*[2]. Sirius, the brightest star in the sky, is among these new members. The classification of the whole structure is quite difficult as is illustrated by the following sections. The designation *UMa group* is used throughout this work.

A current census of the group is displayed in Fig. 1.2. The understanding of this figure requires the knowledge of some characteristics of moving groups presented in the next section.

1.1.2 Stellar motion and moving groups

The *proper motion* μ [″/yr] of a star describes its proper angular motion on the celestial sphere after correcting for the *parallactic motion* due to Earth's orbit. It is related to the

[1] also Wagon, Bear, Plow, Coffin, depending on the culture. See Sesti (1991) for a good presentation.
[2] For a more popular presentation of the UMa group, see e.g. Croswell (2005).

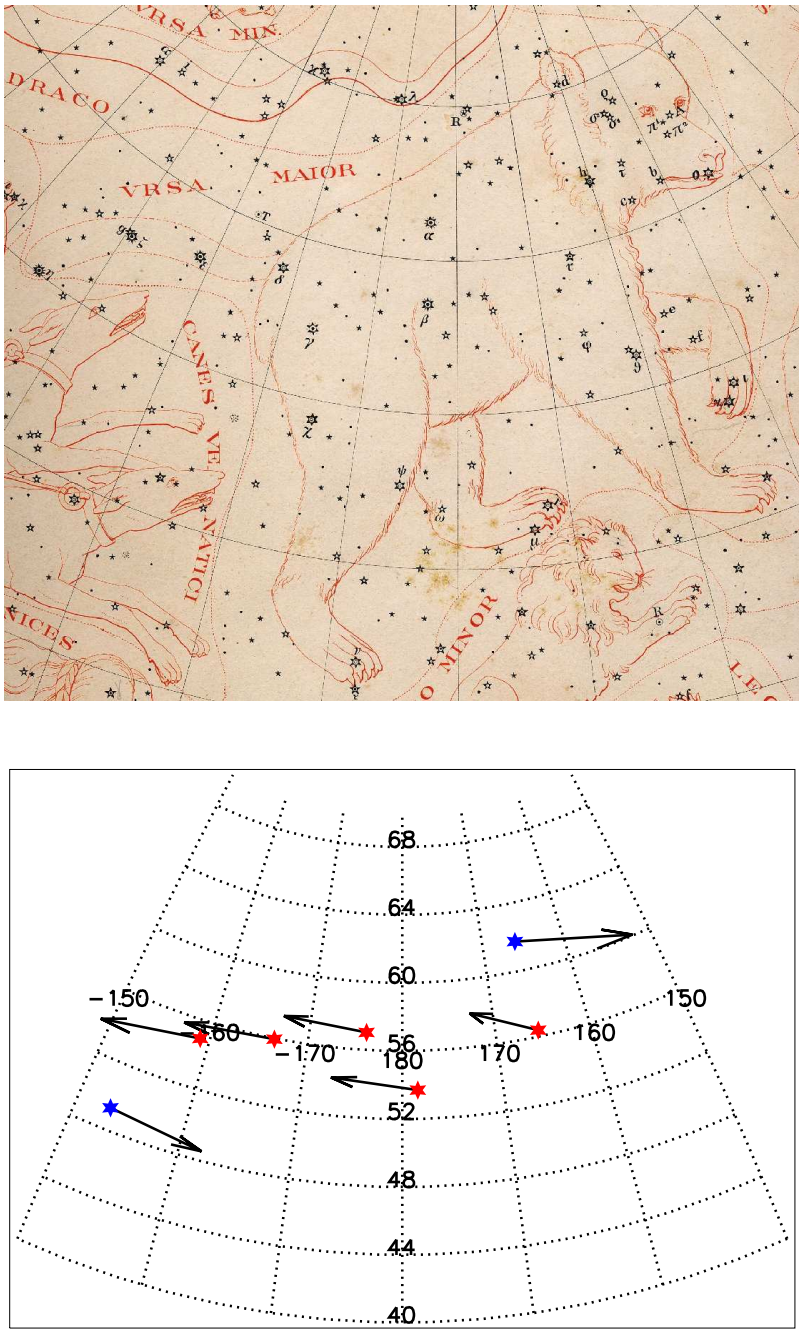

Figure 1.1: The Big Dipper in the constellation Ursa Major – Top: The constellation *Ursa Major* with the *Big Dipper* made up by the stars α (Dubhe), β (Merak), γ (Phekda), δ (Megrez), ϵ (Alioth) ζ (Mizar), and η UMa (Benet Nash). The map is taken from Heis (1872).
Bottom: A Hammer-Aitoff equal area projection of the Big Dipper is shown. Five stars are co-moving while the remaining two stars (α and η UMa) move exactly into the opposite direction.

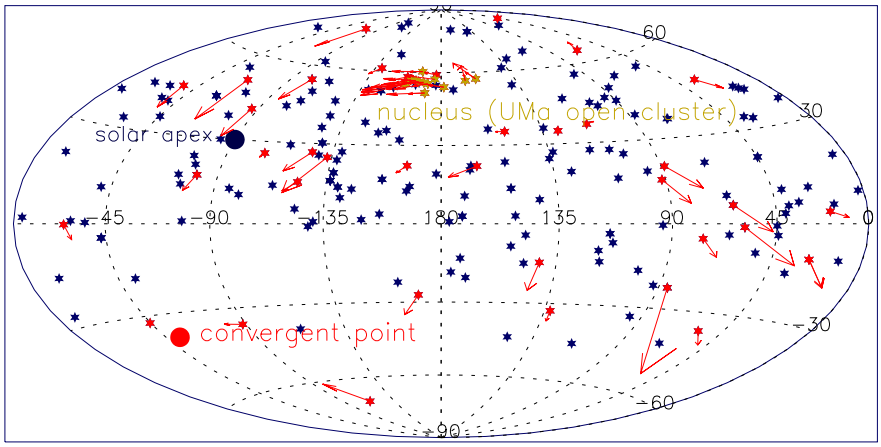

Figure 1.2: The UMa group – The graph shows a Hammer-Aitoff equal area projection of the complete sky. Yellow star symbols mark the core of the UMa group, i.e. the *UMa cluster* in the Big Dipper constellation. These and further co-moving members (red) are attached with arrows indicating the direction and magnitude of proper motion. The remaining stars (blue) are further possible members.

Figure 1.3: A photograph of the Big Dipper – A conspicuous amount of evenly bright stars forms the Big Dipper. By courtesy of Noel Carboni. The original photograph was rotated and cut.

three-dimensional *space velocity* taking into account the distance and the *radial velocity*. The latter is the velocity component along the line of sight and can be measured by spectroscopic observations only. The space velocity components U, V, and W are oriented towards the galactic centre, towards the direction of galactic rotation and towards the north galactic pole, respectively.

Moving groups are constituted by stars which are *co-moving*, i.e. have common space motion and move with the same speed into the same direction. In one respect, their study is very special. Large sections of the sky are considered which can no longer be regarded flat. The proper projection of space velocities onto the celestial sphere becomes indispensable and co-moving stars do not necessarily have parallel proper motions. Consider the paths of co-moving stars (Fig. 1.4, top panel). The graph shows two co-moving stars with the same *total space velocity* $V_{\rm tot}$. The *tangential velocity* $V_{\rm tan}$ of these stars is aligned along great circles as seen from the observer situated in the centre of the figure. The observer further measures the *radial velocity* ρ. Apparently, the stars diverge from a *radiant* and converge to a *convergent point*. Following Klinkerfues (1873) and Bohlin (1905), the poles of the great semi-circles form a new great circle on the celestial sphere. The poles of this circle are the radiant and the convergent point. In Fig. 1.4 (bottom panel), a very suggestive example is shown – the *Hyades* cluster. The space motion of the Hyades is parallel. Due to the projection onto the celestial sphere, the stars apparently converge to their convergent point situated outside of the field of view in this case.

The tangential velocity $V_{\rm tan}$ is related to the proper motion μ, the stellar distance r and the stellar *parallax* π by:

$$V_{\rm tan}[\mathrm{km/s}] = r\,[\mathrm{km}] \cdot \mu \left[\frac{\mathrm{rad}}{\mathrm{s}}\right] = 4.738\,\frac{\mu[''/yr]}{\pi['']} \tag{1.1}$$

Note that

- the observed proper motions are the smallest for co-moving stars close to the convergent point or the radiant,
- the observed radial velocities are the largest close to the convergent point or the radiant, and
- for co-moving stars in the same region of the sky, the proper motions of the closer stars are larger (solve Eq. 1.1 for proper motion).

The space motions have to be corrected for the motion of the Sun in order to find the space velocities relative to the mean galactic field. Due to this motion, the solar neighbourhood moves towards a convergent point on average, the *solar apex* at a right ascension of $A_\odot = 270°$ and a declination of $D_\odot = +30°$ (Scheffler & Elsässer 1992).

Ludendorff (1910) realised the possibility of *vertex deviation*, i.e. that the group members do not share exactly the same space motion. This is discussed in the following section in terms of formation and evolution.

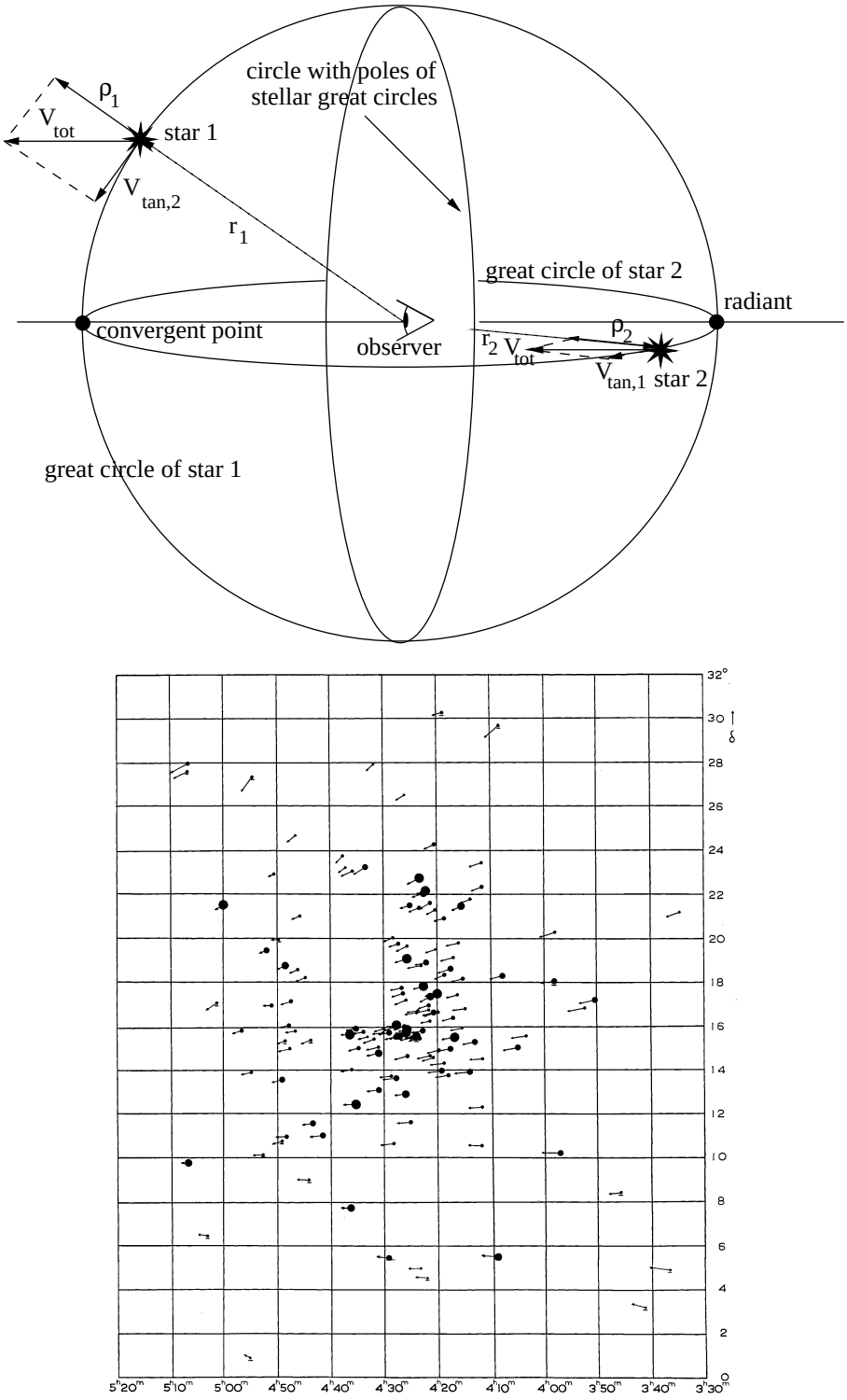

Figure 1.4: Top: Comoving stars on the celestial sphere – See the text for details. **Bottom: Proper motions of Hyades cluster members** – The direction and magnitude of the proper motion is indicated by arrows. The figure is taken from van Bueren (1952).

1.1.3 Formation and evolution of open clusters and associations

Moving groups or stellar kinematic groups might be the link between open clusters or associations on the one side and field stars on the other side. Some words have to be said about the characteristics of these groups of stars in order to address this matter in more detail.

Stars form in groups within dense and cool molecular clouds[3]. The solar neighbourhood is surrounded by several *star forming regions*, e.g. Orion, Taurus, and Scorpius-Centaurus. Orion and Scorpius-Centaurus are constituents of the so-called *Gould Belt* (Gould 1879; Pöppel 1997) which surrounds the Cassiopeia-Taurus star forming region and the solar vicinity. The star forming regions host very young open clusters and associations. The densities and sizes of *open clusters* range widely[4].

Associations are spatial concentrations of stars of a certain type, e.g. stars with spectral types O and B. These *OB associations* (e.g. the Ori OB1 association including the Trapezium) are very young having ages from a few Myrs up to 30 Myrs . The star forming region in Taurus gives an example of a *T association* comprising very young late-type stars, the *T Tauri stars* with the eponymous prototype *T Tauri* (Joy 1945). The Taurus T association has an age of some 10^7 years.

The Pleiades, M 35, and the Hyades are examples for older clusters with ages of 110 Myrs (Terndrup et al. 2000), 175 Myrs (Barrado y Navascués, Deliyannis, & Stauffer 2001), and 625 Myrs (Perryman et al. 1998), respectively.

Cluster members are aligned along well-defined sequences in the *Hertzsprung-Russell diagram* and the *colour-magnitude diagram* (see Fig. 1.5) with mass being the main parameter. This alignment is interpreted in terms of age and evolution. The sequences are *isochrones*, i.e. they connect *co-eval* points having equal age. They are divided into several parts: *pre-main sequence*, *zero-age main sequence*[5] (*ZAMS*), *main sequence* and *post-main sequence*. The evolution of higher-mass stars is faster than the evolution of lower-mass stars so that usually more than one part of the sequence is populated. Higher-mass stars already have entered the post-main sequence phase while the low-mass stars may still be on the pre-main sequence and have not yet started stable hydrogen burning. The cluster sequences are snap-shots in time and thus major keys for the understanding of stellar evolution.

Open clusters older than the Sun are rare. They have lifetimes of typically a few hundred Myrs (Wielen 1971). Cluster evaporation alone cannot explain the short lifetimes. Passing massive objects (e.g. giant molecular clouds) possibly play a role (Wielen 1991). The stars mix with the Galactic field during the process of dissolution and kinematic information on previous cluster membership as well as the stellar birthplace cannot be recovered (Wielen 1977). Eggen (1994) assumed that clusters form a halo of evaporated stars giving rise to the concept of a *supercluster*. The stars retaining similar kinematics after the disruption of the cluster are called a *stellar group*. Then a *moving group* is the appearance of an open cluster or a supercluster extending into the solar neighbourhood.

[3] See Stahler & Palla (2004) for a recent text book on star formation.

[4] The classification of open clusters follows the scheme of Trumpler (see Neckel 1994).

[5] The *ZAMS* is the position of stars which start stable hydrogen burning.

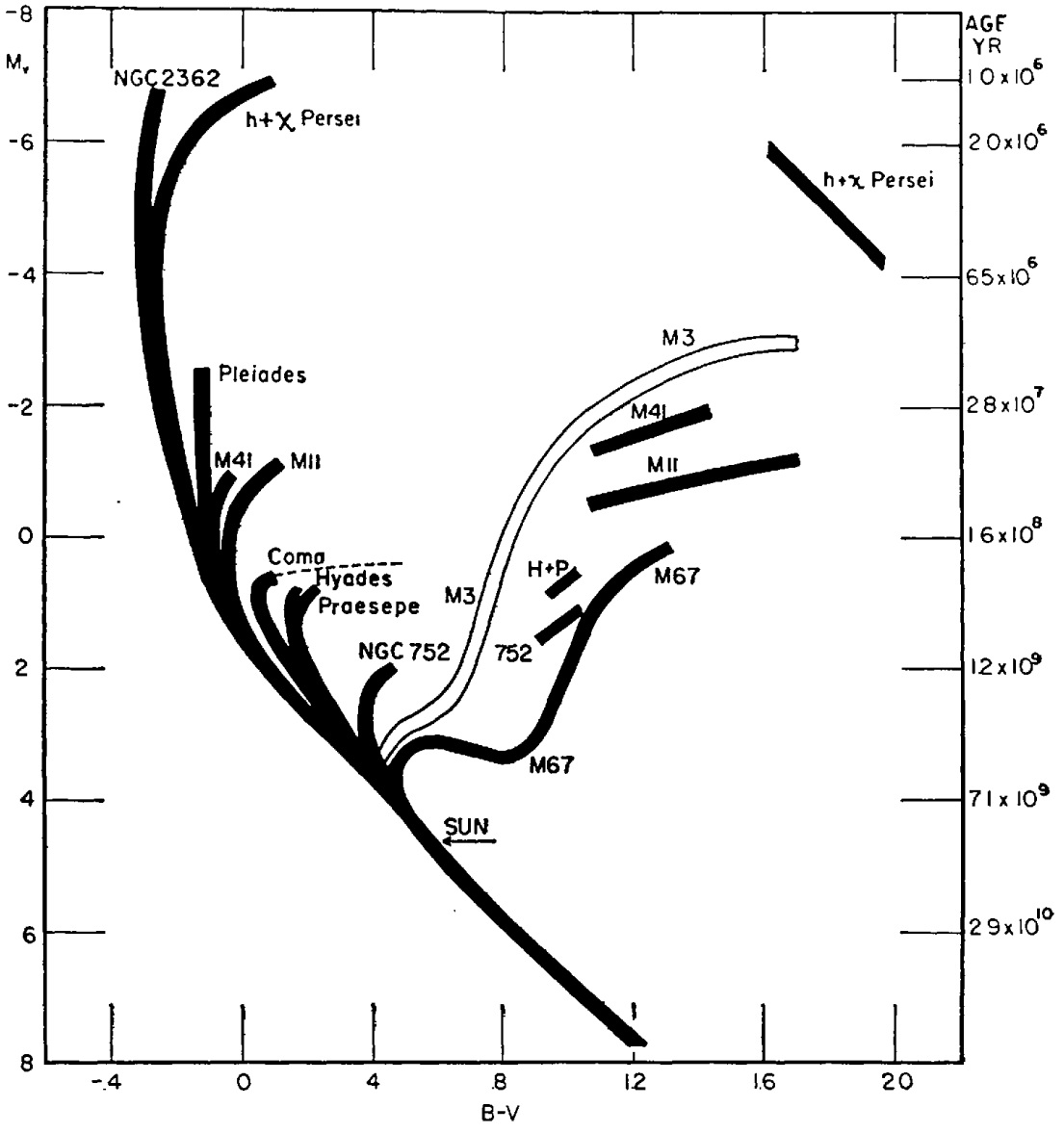

Figure 1.5: Cluster sequences – The sequences of several clusters of different ages are shown in the colour-magnitude diagram with absolute V-band magnitude M_V vs. colour index $B-V$. The low-mass stars all reside at the faint cool end (lower right) of the main sequence. Massive stars finish their main sequence phase earlier and turn off to the subgiant and giant branches at higher luminosities. The position of this *turn-off* is a function of the age of the cluster. The figure is taken from Sandage (1956).

Montes (2001) analysed the relation of young nearby moving groups with young nearby clusters and the Gould Belt by comparing their galactic space velocities. The study gave rise to the speculation that the Gould Belt could be the origin of young moving groups.

1.1.4 The nature of the UMa group – cluster or association, or something else?

On the one hand, there is this concentration of stars in the Big Dipper constellation, the UMa cluster or often called *UMa nucleus* (Roman 1949; King et al. 2003). It is gravitationally bound indicated by the small vertex deviations. Probably it is the remainder of an almost evaporated cluster (Wielen 1978). It represents the closest open cluster at a distance of ≈25 pc with the five bright members of spectral type A constituting the Big Dipper constellation. The cluster is situated in an otherwise quite empty region of the sky off the galactic plane and forms a complete constellation (Fig. 1.3). Hence its appearance is quite different from other open clusters perceived as local concentrations of stars like the Pleiades and Hyades open clusters.

On the other hand, there are many widely spread co-moving stars which form the *UMa stream* or moving group. In contrast to the cluster, they are associated only by motion and not by concentration on the sky. The relation of the stream members to the cluster is not yet clear. Wielen (1978) advocated a separate formation of stream members and cluster members still within the same association. Following Eggen (1994), the UMa cluster is part of the so-called *Sirius supercluster*.

The UMa group is young with a canonically quoted age of ≈300 Myrs which has already been given by von Hoerner (1957) (cf. Giannuzzi 1979; Duncan 1981; Soderblom & Mayor 1993). It is still under discussion and the reader is referred to Sect. 1.3.5 for details. If we assumed that the UMa group was a large open cluster, its age would equal the time-scale of dissolution (≈200 Myrs, Wielen 1971).

The term “UMa group” will be used throughout this thesis. Fuhrmann (2004) rather suggested to use the term “UMa association”[6] by comparing to the properties of recently discovered young nearby groups and associations. An additional argument is the scope of the UMa group which may exceed the size of open clusters by far (see Sect. 1.2.3).

1.2 Why is the UMa group interesting?

1.2.1 A snapshot in stellar evolution

Due to the common age, the UMa group members are an ideal sample for stellar evolutional studies. The properties of stars of different mass can be compared to equal-mass members of other groups with different age like the Hyades and the Pleiades. Then stellar properties are analysed in terms of evolution. An example is given by chromospheric

[6] or even more simpler “UMa stars”

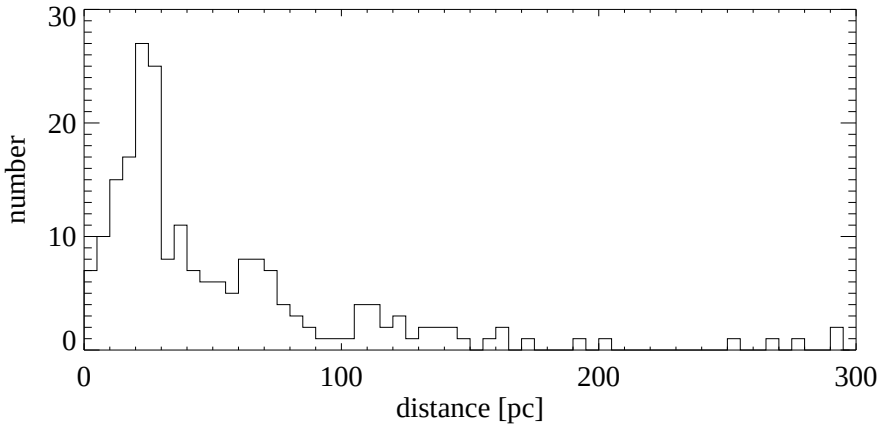

Figure 1.6: Distribution of distances of UMa group members – The distance distribution of all UMa group members and candidates with known distances (mostly from *Hipparcos*) is shown. While few stars are more distant than 200 pc, most are closer than 100 pc with a strong peak between 20 and 30 pc (supposedly contributions by the UMa open cluster).

emission or lithium abundance which can be studied precisely at an age of some 10^8 years (Fuhrmann 2004).

1.2.2 A laboratory in front of the door

Most known UMa group members are very nearby (Fig. 1.6) making the UMa group a homogeneous laboratory for many sorts of studies. Astrometric, photometric and spectroscopic studies can be done with high resolution and high signal-to-noise ratio. Most distances were derived precisely from *Hipparcos* data (ESA 1997; Perryman et al. 1997) so that luminosities are well-known. Due to the proximity, photometric measurements do not suffer from interstellar extinction.

Substellar companions (brown dwarfs and extrasolar planets) can be imaged at small separations from the host stars. The proper motions are high (Fig. 1.7) but not only due to the small distance. Another reason is the large angular distance of the UMa cluster – including a large part of the UMa group members – from the radiant and the convergent point (Fig. 1.2). Hence the positions of the stars change measurably within months and further co-moving objects are found quickly, i.e. additional UMa group members or gravitationally bound companions. The UMa group member ε Eri, for example, shows a very high proper motion of almost 1”/yr. The known age of about $3 \cdot 10^8$ years allows to estimate the mass of a faint companion from observed luminosities when using evolutionary models (e.g. Burrows et al. 1997) and puts constraints on the time scale of formation. Previous direct imaging campaigns revealed multiple brown dwarf companions of Gl 569 (e.g. Forrest, Shure, & Skrutskie 1988; Kenworthy et al. 2001) and HD 130948 (Potter et al. 2002). König et al. (2002) confirmed a low-mass stellar companion of χ^1 Ori.

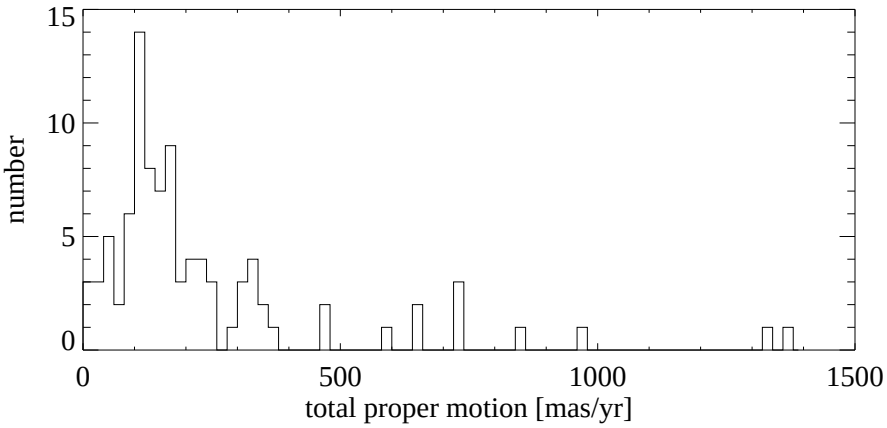

Figure 1.7: Distribution of total proper motions of UMa group members – The distribution of proper motions of very nearby UMa group members and candidates within 30 pc is displayed. Most of the stars have relatively high proper motion clustering between 100 and 200 mas/year.

Most known UMa group members are bright so that searches for radial velocity planets can be easily done with telescopes of intermediate size[7]. ε Eri is an example for an UMa group members harbouring a radial velocity planet (e.g. Campbell, Walker, & Yang 1988).

1.2.3 The census of the solar neighbourhood

How is the Sun embedded in its galactic neighbourhood? The census of the solar vicinity is incomplete and the UMa group may contribute a large part.

Proxima Centauri's distance of only 1.3 pc is eponymous. Yet it is a faint star with spectral type M5 and an apparent V-band magnitude of 11 mag. Therefore Proxima Centauri cannot be seen with the naked eye. How many more faint stars lurk in the nearby space?

The *initial mass function* (e.g. Kroupa 2002), i.e. the mass distribution of newly formed stars after one star formation event, gives a clue. Only a few high-mass stars are formed while there are up to thousands of low-mass stars. Eggen (1998) compared the number of bright UMa group stars with the initial mass function of field stars:

> ".. either most of the small proper-motion stars near the Sun remain to be identified or the luminosity function of the supercluster is drastically different from that of the field stars."

The stars might be outnumbered by brown dwarfs even by a factor of two (Kirkpatrick 2001) so that one can only guess on the true scope of the UMa group. Fuhrmann (2004) gave an account of faint UMa group members in the solar vicinity.

[7] apertures of 2 m-4 m

1.3 Constraining the UMa group – previous approaches

Several approaches were undertaken over the past 150 years in order to establish membership lists of the UMa group. Roman (1949) presented a good account of the research on the UMa group before the middle of the last century. A historical overview of the pre-*Hipparcos* era was given by Eggen (1992) and Soderblom & Mayor (1993). The relation of moving groups and open clusters suggests to identify members by spatial concentration (Sect. 1.3.1). Though kinematic approaches are more promising. Traditionally the mean space velocity or the convergent point of the motion are derived from a list of "canonical members", usually the UMa nucleus. Kinematic criteria then decide on the membership of further stars (Sect. 1.3.2). Rather than adopting a "canonical" member list, moving groups can be recovered as concentrations in the total kinematic space (Sect. 1.3.3). Table 1.1 lists kinematic parameters of the UMa group derived in recent studies. The existence of moving groups has been rather controversial considering the lack of precise distances – before the *Hipparcos* mission – and radial velocities.

Table 1.1: The UMa group kinematic parameters compiled frome some recent studies – The comments in the last column specify details with respect to the given source.

reference	conv. point		space velocity [km/s]			comments
	A (2000.0)	D (2000.0)	*U*	*V*	*W*	
Chereul et al. (1999)			14.0	1.0	-7.8	scale 3
Chupina et al. (2001)	$300.^\circ6864$	$-29.^\circ74465$	13.5	3.0	-7.5	UMa nuc.
Asiain et al. (1999)			8.7	2.8	-6.9	group A
Montes et al. (2001a)	$20.^h55$	$-38.^\circ10$	14.9	1.0	-10.7	
King et al. (2003)			13.9	2.9	-8.4	UMa nuc.

The kinematic criteria alone turned out to be weak constraints so that additional criteria are necessary. Previous spectroscopic determinations of stellar parameters and abundances are either inhomogeneous or based on small samples (Sect. 1.3.4). The use of age constraints from photometry and spectroscopy turned out to be challenging (Sect. 1.3.5 and 1.3.6). Some advance has been achieved by combining several criteria (Sect. 1.3.7).

1.3.1 Spatial clustering

Spatial clustering can be perceived as long as the density of cluster stars in the considered region of the celestial sphere is similar or higher than the density of field stars. This is not the case for the UMa cluster although it coincides with a quite sparsely populated region on the celestial sphere – in the region of the Big Dipper, close to the celestial pole. The situation turns out to be different when taking into account the distances. Chereul et al. (1999) looked for inhomogeneities in the spatial distribution of a volume-complete and

magnitude-limited sample of the solar neighbourhood. Wavelet analysis of *Hipparcos* data recovered the UMa cluster at a distance of 25 pc.

1.3.2 Kinematic criteria – derived from a "canonical" member list

As noted above, Proctor (1869) and Huggins (1871) discovered the first indications for the existence of the UMa cluster considering the common space motions of five bright central stars in the Big Dipper (bottom panel of Fig. 1.1). The determination of the convergent point turned out to be difficult. The common method of Klinkerfues (1873) and Bohlin (1905) was based on the following principle: The convergent point is the pole of the circle made up by the poles of the great circles of stellar proper motions (top panel of Fig. 1.4). Unfortunately the five Big Dipper stars are clustered closely on exactly this circle (Fig. 1.2) so that the resulting convergent point is not well determined.

The work of Haas (1931) was the first systematic search for more members in the region of the UMa cluster. Hertzsprung (1909) has realised well before that co-moving stars reside outside of the cluster, too. Both analyses were hampered by the still very uncertain distances.

In further searches, many stars were classified as members by comparing the space velocities of the stars with the cluster velocity. However it turned out to be difficult to define a proper limit for the residuals. Being more critical, Smart (1939a,b) put constraints on the individual observables (position angles of proper motion, radial velocities and parallaxes) retaining only 42 definite members out of 135.

In the 1990's, precise *Hipparcos* distances became available. A more recent approach similar to Smart (1939a,b) was the study of the UMa nucleus region by Chupina et al. (2001). Proper motions and radial velocities were treated separately in order to retain the high proper motion precision achieved with *Hipparcos*.

The explanations now concentrate on the most recent UMa group member lists presented by Montes et al. (2001a) and King et al. (2003) which will form the basis for this thesis. The definition of the kinematic membership criterion by King et al. (2003) followed Soderblom & Mayor (1993) but was based on precise *Hipparcos* distances and new radial velocity data. Their candidates were mostly taken from Soderblom & Mayor (1993) and Montes et al. (2001a). Using a list of canonical members, the UMa nucleus, they calculated the weighted means of their galactical U,V, and W velocities and the corresponding standard deviations. The kinematic membership criterion then required that the kinematics of a candidate deviates by less than 3σ from the nucleus' mean in the $U-V$ and the $W-V$ plane.

Most studies of the UMa group are dedicated to bright early-type stars. In contrast, Montes et al. (2001a) comprehensively selected late-type members of young moving groups from a large sample of candidates taken from various sources. According to Montes et al. (2001a), the kinematic properties of the UMa group are given by the galactic space velocities $(U,V,W) = (14.9, 1.0, -10.7)$ km/s, the total space velocity $V_{\mathrm{T}} = 18.4$ km/s, the right ascension of the convergence point $\alpha_{\mathrm{C.P.}} = 20\overset{h}{.}55$ and its declination $\delta_{\mathrm{C.P.}} = -38\overset{\circ}{.}10$ (Eggen 1992). The selection proceeded in several steps:

1. Selection of young disc stars ($-50\,\mathrm{km/s} < U < 20\,\mathrm{km/s}$, $-30\,\mathrm{km/s} < V < 0\,\mathrm{km/s}$, $-25\,\mathrm{km/s} < W < 10\,\mathrm{km/s}$) following Eggen (1989).

2. Selection of *possible* moving group members with small V dispersion following Eggen. However a large dispersion of U and V of $\lesssim 8\,\mathrm{km/s}$ with respect to the moving group velocities was allowed for. A deviation of the same amount in the W component led to the exclusion of a candidate.

3. The application of the peculiar (V_{pec}) and the radial velocity criterion (ρ_{c}) following Eggen (1958, 1995) led to the decision on UMa group membership. For details see Appendix A.

The kinematic membership assignments of Montes et al. (2001a) and King et al. (2003) are compared in Table 1.2 which will form the basis for this thesis described later. The list comprises 56 stars of all spectral types and is composed of all 33 sure kinematic members presented by King et al. (2003) (denoted by kinematic membership status 'Y' in their table 5) and the 28 late-type UMa group members from Montes et al. (2001a) which fulfil both Eggen's criteria (denoted by 'Y' in their table 4). Only seven of the twenty stars in common are classified as kinematic members by both King et al. (2003) and Montes et al. (2001a): HD 59747, HD 75605, HD 109647, HD 110463, HD 115043, HD 238224, and HD 129798 A. For six common stars, the membership assignments are contradicting: HD 13594 A, HD 24916 A, HD 81659, HD 199951 A, HD 167389, HD 134083. Fig. 1.8 shows the positions of these stars in the U-V diagram and the W-V diagram, respectively. Obviously the criterion of King et al. (2003) is much tighter than that of Montes et al. (2001a) giving a sample with a very homogeneous space motion. However the kinematic boundary of King et al. (2003) was chosen quite arbitrarily as was the tolerance limit of Eggen's criteria in Montes et al. (2001a). Furthermore the difference in the adopted cluster's space velocity (see Table 1.1), i.e. the adopted convergent point, is visible in Fig. 1.8.

Table 1.2: The kinematic sample – space velocities and membership. The galactic space velocity components of the kinematic sample of Fig. 1.8. The column *ref* gives the origin of the values: 1=Montes et al. (2001a), 2=King et al. (2003). If stars are common to both, space velocities were taken from the former.

object	U [km/s]	V [km/s]	W [km/s]	ref	kin. mem.	V_{pec}	ρ_{c}
HD 11131	19.31± 1.86	2.07± 0.29	-2.59± 0.70	1	?	Y	Y
HD 11171	18.74± 0.66	1.91± 0.18	-5.95± 1.40	1	?/Y?	Y	Y
HD 13594 A	15.75± 1.17	0.42± 1.06	-12.62± 0.79	1	N?	Y	Y
HD 18778	12.99± 2.63	3.30± 3.12	-6.71± 1.96	2	Y		
HD 24160	19.74± 0.89	0.38± 0.57	-11.19± 0.87	1	?	Y	Y
HD 24916 A	7.40± 0.79	0.34± 0.17	-16.16± 0.73	1	N?	Y	Y
HD 26923	14.02± 0.23	-0.29± 0.18	-9.60± 0.35	1	Y?	Y	Y

Table 1.2 continued next page

Table 1.2 continued

object	U [km/s]	V [km/s]	W [km/s]	ref	kin. mem.	V_{pec}	ρ_c
HD 28495	14.44± 0.35	2.99± 0.43	-6.38± 0.31	1	Y	N	Y
HD 33111	14.02± 1.24	2.63± 0.58	-10.75± 0.71	2	Y		
HD 38393	18.35± 0.57	4.59± 0.60	-11.68± 0.38	1	?/Y?	Y	Y
HD 39587	13.01± 0.20	2.58± 0.10	-7.97± 0.12	2	Y		
HD 41593	10.55± 0.10	0.25± 0.10	-10.91± 0.20	1	N?/?	Y	Y
HD 59747	13.07± 0.37	2.70± 0.17	-10.33± 0.24	1	Y	Y	Y
HD 71974 A	12.03± 0.50	4.03± 0.24	-9.06± 0.38	1	Y	Y	N
HD 71974 B					Y		
HD 75605	13.78± 1.18	3.18± 1.49	-10.74± 0.97	1	Y	Y	Y
HD 81659	25.68± 0.86	0.57± 0.69	-16.53± 0.50	1	N?	Y	Y
HD 87696	13.64± 0.90	1.92± 0.77	-7.16± 0.95	2	Y		
HD 91480	12.40± 0.30	3.25± 0.18	-5.77± 0.40	1	Y	Y	N
HD 95418	13.69± 0.42	2.82± 0.26	-7.35± 0.65	2	Y		
HD 95650	12.43± 0.68	3.51± 0.54	-9.76± 1.81	1	Y	N	Y
HD 103287	13.94± 0.34	2.73± 0.27	-8.20± 0.70	2	Y		
HD 238087	15.79± 3.65	1.92± 3.99	-10.96± 8.43	1	Y?	Y	Y
HD 109011	14.11± 0.88	2.45± 0.68	-10.26± 0.57	2	Y		
HD 109647	14.16± 0.40	3.64± 0.28	-7.14± 0.28	1	Y	Y	Y
HD 109799	16.12± 0.77	0.18± 1.07	-12.28± 0.94	1	?	Y	Y
HD 110463	14.45± 0.29	2.87± 0.23	-7.71± 0.27	1	Y	Y	Y
HD 111456	14.17± 0.96	1.15± 0.88	-9.84± 1.26	1	?	Y	Y
HD 112185	13.96± 0.19	2.50± 0.14	-8.77± 0.18	2	Y		
HD 112196	9.61± 0.61	0.59± 0.17	-8.56± 0.04	1	N?/?	Y	Y
HD 113139 A	12.88± 0.22	3.25± 0.25	-9.16± 0.44	1	Y	N	Y
HD 113139 B					(Y)		
HD 115043	14.52± 0.26	2.19± 0.21	-8.08± 0.27	1	Y	Y	Y
HD 116656	13.34± 0.21	4.19± 0.24	-5.62± 0.44	2	Y		
HD 116657	14.03± 0.42	2.57± 0.88	-8.87± 1.76	2	Y		
HD 116842	13.17± 0.68	3.44± 0.62	-9.25± 0.46	2	Y		
HD 238224	13.98± 1.20	3.71± 2.38	-6.21± 4.27	1	Y	Y	Y
HD 129798 A	15.73± 0.50	3.08± 0.68	-8.51± 0.81	1	Y	Y	Y
HD 129798 B					(Y)		
HD 134083	17.70± 0.89	-1.17± 0.61	-16.46± 1.73	1	N?	Y	Y
HD 139006	14.26± 0.92	3.15± 0.79	-7.58± 1.62	2	Y		
HD 141003 A	13.74± 1.32	3.07± 0.61	-11.04± 1.56	2	Y	N	Y
HD 141003 B	13.63± 0.57	4.06± 0.30	-10.80± 0.57	1	(Y)		
HD 147584	13.30± 1.11	4.58± 0.95	-6.28± 0.38	2	Y		
HD 152863 A	13.30± 1.45	1.37± 0.77	-12.14± 1.44	1	?	Y	Y
HD 155674 A	12.50± 0.52	5.32± 0.17	-4.39± 0.29	1	?	Y	Y

Table 1.2 continued next page

Table 1.2 continued

object	U [km/s]	V [km/s]	W [km/s]	ref	kin. mem.	V_{pec}	ρ_c
HD 155674 B	11.78± 0.78	5.22± 0.25	-4.97± 0.45	1	?	Y	Y
HD 165185	14.42± 0.20	3.73± 0.14	-9.33± 0.17	1	Y	N	Y
HD 167389	17.20± 0.94	-3.75± 2.21	-13.33± 1.11	1	N?	Y	Y
HD 171746 A	11.90± 0.41	3.23± 0.26	-10.14± 0.73	1	Y	N	Y
HD 171746 B					Y		
HD 180777	13.89± 0.39	4.03± 0.63	-10.21± 0.37	2	Y		
HD 184960	19.13± 0.28	1.07± 0.20	-12.86± 0.21	1	?/Y?	Y	Y
HD 199951 A	13.75± 0.69	3.47± 0.27	-10.50± 0.62	1	Y	N	N
HD 205435	14.92± 0.36	6.31± 0.90	-10.07± 0.27	1	?/Y?	Y	Y
HD 211575	16.53± 0.55	2.80± 0.31	-10.85± 0.15	1	Y?	Y	Y

End of Table 1.2

King et al. (2003) markedly summarise the problem of finding accurate cluster parameters for the selection of further members:

> "... many stars are deemed to have uncertain membership status, and the necessity of adopting a priori kinematic definitions of the UMa group (based on the sparse nucleus) biases the resulting kinematic statistics".

1.3.3 Kinematic parameters – derived from kinematic clustering

Dziewulski (1916) suggested a statistical approach in order to isolate moving groups. At first, intersections of the great circles of stellar motion (top panel of Fig. 1.4) were expected to be distributed homogeneously on the celestial sphere. This expectation was based on the assumption that stellar proper motions were completely stochastical. Then concentrations of intersections would indicate moving groups. Based on the catalogue of Boss, the density of intersections of an UMa group sample indeed exceeded the density for stochastic motion. According to Dziewulski (1916), this was only true for a small segment around the convergent point of the UMa group. The probability to include spurious members strongly increased if the segment was increased.

Gliese (1941) defined moving groups (*UMa* and *Taurus streams*) by detecting concentrations of space velocities in the FK3 catalogue. Delhaye (1948) studied space motions of 2000 bright stars and encountered a concentration of space motions towards the UMa nucleus.

The Taurus and UMa streams were identified with *Kapteyn's streams I and II*, respectively. These are directed in opposite directions and result from galactic rotation. Following Roman (1949), "it has become important to decide whether the Ursa Major stream can be distinguished from [Kapteyn's] stream II". The kinematic analysis of the UMa group became revived after the advent of the precise *Hipparcos* data and put Eggen's groups on more firm grounds. Asiain et al. (1999) presented a review. They analysed

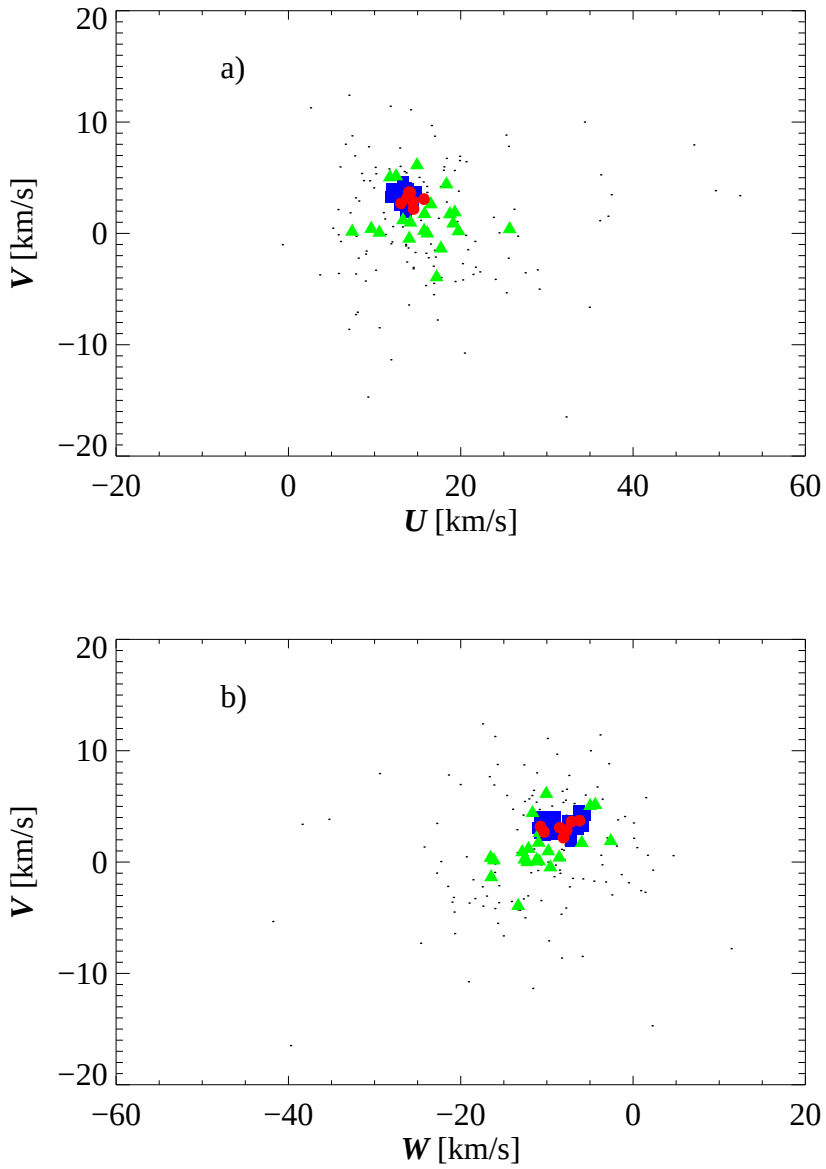

Figure 1.8: Space velocities of the kinematic sample – **(a)** The galactic space velocities U and V of kinematic members and further UMa group candidates are displayed. Triangles denote the stars fulfilling both membership criteria in Montes et al. (2001a). Squares denote the stars which fulfil the kinematic criterion of King et al. (2003). Circles are the seven stars which fulfil the criteria of both Montes et al. (2001a) and King et al. (2003). Dots are further candidates whose kinematic membership status is still under discussion. **(b)** Same as top, now for *W* and *V*. Note that the dots do not fulfil both *UV* and *WV* constraints simultaneously. If space velocities are given by both Montes et al. (2001a) and King et al. (2003), then they are taken from the former. See Table 1.2 for the velocities of the kinematic members.

the distribution of space velocities of ≈2000 nearby early-type stars adding as fourth dimension the photometric age. A concentration at $(U, V, W) = (8.7, 2.8, -6.9)$ km/s could be identified with Eggen's Sirius supercluster although some substructure was found, too. Chereul et al. (1999) used wavelet analyses to study clustering in the velocity space. While tangential velocities were well-known from *Hipparcos*, the available radial velocities were incomplete and biased. Therefore they first considered every possible convergent point (similar to Dziewulski 1916) by forming all possible pairs of stars. Then, in contrast to Dziewulski (1916), they assumed that these velocities were strictly parallel and reconstructed the total space velocities of each pair. The candidate convergent point is only kept if the amounts of the reconstructed space velocities differ by less than 0.5 %. Clusters of the retained velocities in the space velocity distribution were detected by wavelet analysis and indicated the presence of moving groups. Similarly to Asiain et al. (1999), Chereul et al. (1999) recovered the Sirius supercluster with mean velocity components $(U, V, W) = (+14.0, +1.0, -7.8)$ km/s and isolated some substructure at $(U, V, W) = (12.4, +0.7, -7.7)$ km/s and $(U, V, W) = (12.4, +4.2, -9.0)$ km/s.

On the one hand, these methods of kinematic clustering yielded unbiased cluster parameters in contrast to the determinations which are based on selected stars. On the other hand, the results from kinematic clustering showed all the more that the definition of kinematic membership criteria remains difficult.

1.3.4 Stellar parameters and abundances

The UMa group members are expected to have similar abundances if they formed coevally in the same region. Only a few studies were dedicated to the UMa group as a whole although exhaustive data on nearby stars is catalogued multiply in the recent literature. Boesgaard & Friel (1990) derived an UMa group mean value of [Fe/H]=-0.085 but a large spread over 0.2 dex seems realistic (Soderblom & Mayor 1993; Gaidos & Gonzalez 2002).

King et al. (2003) realised the inhomogeneity of compiled literature values. Their following statement clearly indicates the necessity of a *homogeneous* abundance analysis:

> "We acknowledge that the tabulated values [for the iron abundance] are probably inhomogeneous, and no attempt has been made to rectify this. Such an attempt is not practically accomplished either empirically (because of lack of overlap between different studies) or fundamentally (because of implicit differing assumptions in the analyses, such as choice of model atmospheres, temperature scales, atomic data, solar normalization, etc., which are impossible to calibrate)."

This is exemplified by the clearly comprehensive compilation of iron abundances for stars of spectral types F, G, and K by Cayrel de Strobel, Soubiran, & Ralite (2001). The entry for the kinematic UMa group member HD 39587 illustrates the present situation (Table 1.3). Several determinations can be found for some UMa group members while hardly any are available for other members. The measurements are based on different

Table 1.3: The literature data – Example: HD 39587 – The entry for the UMa group member HD 39587 in the catalogue of Cayrel de Strobel et al. (2001). While the effective temperatures agree well, the surface gravities and abundances scatter widely.

$T_{\rm eff}$ [K]	$\log(g\,[\frac{\rm cm}{\rm s^2}])$	[Fe/H]	source
5929		-0.05	Boesgaard, Budge, & Burck (1988)
5929		-0.05	Boesgaard (1989)
5929	4.50	-0.05	Boesgaard & Friel (1990)
5900	4.21	-0.05	Friel & Boesgaard (1992)
5953	4.46	-0.03	Edvardsson et al. (1993)
5895	4.21	-0.04	Gratton, Carretta, & Castelli (1996)
5950	4.46	+0.11	Mallik (1998)
5929 70	4.49 0.10	-0.02 0.12	Castro, Porto de Mello, & da Silva (1999)
5805 70	4.29 0.10	-0.18 0.10	Chen et al. (2000)

methods and different data. Large scatter is introduced especially in surface gravities and abundances. This scatter is beyond the error bars that can be achieved from spectra with high resolution and high signal-to-noise ratio. Considering this situation, it does not seem realistic to draw a homogeneous and reliable data set from the literature for a larger sample of UMa group members.

The situation has improved only partly in the past few years although new data sets have become available. Gray et al. (2003) and Nordström et al. (2004) presented large scale surveys based on spectra with intermediate resolution and Strömgren photometry, respectively. Stellar parameters and metallicities for many UMa group members can be found within these surveys. The situation is not satisfying for iron abundances and photometric gravities while effective temperatures agree in a statistical sense with spectroscopic determinations. See Luck & Heiter (2005) who compared spectroscopic parameters with Nordström et al. (2004) and other photometric measurements. Emphasis is put here on the fact that the photometric studies of Nordström et al. (2004) and Gray et al. (2003) do not aim at precise abundance measurements but at accurate radial velocities and spectral types, respectively. The use of effective temperature calibrations – as done by Nordström et al. (2004) – is only valid in a statistical sense and does not allow to determine precise effective temperatures of individual stars (Fuhrmann 1993; Fuhrmann, Axer, & Gehren 1994). For these tasks, high-resolution spectroscopy is clearly preferable.

The homogeneous analysis of Castro et al. (1999) showed that the UMa group abundance pattern is different from that of the field, particularly considering barium and copper. However this study was restricted to only seven UMa group members.

Recent magnitude-limited spectroscopic surveys were undertaken by Luck & Heiter (2005) and Allende Prieto et al. (2004) for stars within 15 pc and by Fuhrmann (2004, and preceeding papers) within 25 pc. Most stars of the UMa group are beyond 15 pc so that only the survey of Fuhrmann (2004) comprised homogeneous spectroscopic analyses of a larger sample of UMa group members.

1.3.5 The age of the UMa group – photometric criteria

As pointed out in Sect. 1.1.3, the alignment of cluster members along sequences in the Hertzsprung-Russell and the colour-magnitude diagram is interpreted in terms of age and thus advocates the use of photometry as a membership criterion. Eggen (1998) compared the colour $B-V$ and the absolute $V-$band magnitude $M_{\rm V}$ of Sirius supercluster members from the Bright Star catalogue to *theoretical isochrones* of Castellani, Chieffi, & Straniero (1992) and derived an age of 400 Myrs. In a similar way, King et al. (2003) compared UMa nucleus stars with isochrones of Yi et al. (2001) but separately for the colours $B-V$ and $V-I$, respectively. Similar to Eggen (1998), isochrones of 600 Myrs and 400 Myrs, respectively, matched the UMa nucleus sequences. King et al. (2003) derived a *photometric membership criterion* from this finding. Correspondingly photometric members were required to reside between the 400 Myrs and the 600 Myrs isochrone. King & Schuler (2005) readdressed the photometric age of the UMa group but based on the final members of King et al. (2003). The new photometric age was ≈600 Myrs. King et al. (2003) pointed out that the photometric membership criterion is only sensitive close to the turn-off, i.e. at early spectral types (compare Fig. 1.5).

In contrast to King et al., König et al. (2002) advocated a much younger age of 200 Myrs. Based on astrometry, they detected a companion of the UMa group member χ^1 *Ori* (HD 39587) with a mass of only $M = 0.15 \pm 0.02\,M_{\odot}$. The comparison with evolutionary models of Baraffe et al. (1998) clearly places the faint object on the pre-main sequence. The corresponding age is substantially younger than even the canonical value of 300 Myrs (see König et al. 2002 for a discussion). The problem could be easily solved by simply excluding χ^1 *Ori* from the UMa group. However the membership of this star is assured by kinematics and enforced by spectroscopic signatures common to UMa group members. See the next section.

1.3.6 Spectroscopic indicators for age and activity

The coupling of the convective envelope to stellar rotation generates magnetic fields by means of a *stellar dynamo*. The dissipation of the magnetic fields induces phenomena of stellar activity, e.g. coronal X-ray emission and chromospheric emission which fills-in, i.e. adds intensity to the cores of strong absorption lines (see Stix 1989 and Mestel 1999 and references therein). The filling-in of the Hα line is a common tracer of chromospheric emission (see Herbig 1985; Pasquini & Pallavicini 1991; Montes et al. 2001b; Fuhrmann 2004; Biazzo et al. 2006, and references therein). Activity in the UMa group already has been noted by Roman (1949):

> "It is interesting to note that, of the four stars later than G0, three show emission at H and K."

Walter et al. (1984) addressed the X-ray emission of UMa group members. Activity signatures in the UMa group were studied comprehensively by Soderblom & Mayor (1993). These address their applicability as membership criteria, motivated by the young age of the UMa group of only ≈300 Myrs. They distinguished probable spectroscopic

members, possible spectroscopic members, and probable non-members. Interestingly they concluded that

> "... stars that meet the spectroscopic criteria also have kinematics that agree better with the space motions of the nucleus of UMaG [UMa group] than does the starting sample as a whole."

King et al. (2003) concluded that chromospheric activity can be used to exclude non-members.

Activity measures are indirect age indicators whereas absorption lines of lithium are directly related to the age of late-type stars. Their large convective envelopes transport lithium to the hot central parts where the temperature is high enough to burn lithium ($\gtrsim 2.5 \times 10^6$ K). This *lithium depletion* is faster for cooler stars having deeper convective envelopes.

The lithium abundances of Hyades members with spectral type G are tightly correlated with effective temperature (Thorburn et al. 1993). In contrast, Pleiades members show substantial scatter (Soderblom et al. 1993b) which might be due to different rotation rates or an age spread. According to standard evolutionary models, the amount of lithium depletion depends only on mass, age, and metallicity. Yet convection is the only mixing mechanism taken into account by these models while mixing due to rotation, diffusion, mass loss, and gravitational waves is not implemented (see Pinsonneault 1997). Sestito & Randich (2005) emphasised the necessity of a homogeneous analysis. See Carlsson et al. (1994) for a good review on the use of lithium as age indicator.

Montes et al. (2001b) applied chromospheric activity and lithium absorption as membership criteria. For three stars, they derived the chromospheric flux from the filling-in of the Balmer lines and Ca II H&K lines as well as the Ca II infrared triplet (λ8498 Å, λ8542 Å, and λ8662 Å) and detected moderate chromospheric activity according to the age of the UMa group. Furthermore they compared the equivalent widths of the Li I λ6707.8 Å absorption line of their three UMa group candidates with the equivalent widths of several open clusters having different age. These equivalent widths were in between the values found in the Pleiades and the Hyades and corroborated UMa group membership. Similarly the lithium abundances found by King & Schuler (2005, see their fig. 6) were higher than these of the Hyades at effective temperatures cooler than the Sun. Following Montes et al. (2001b), this would support the young age of the UMa group. Yet the reasoning of King & Schuler (2005) was different. They approved an age similar to the Hyades based on the lithium absorption of the hotter stars. Referring to the literature quoted above, the present work follows the reasoning of Montes et al. (2001b) and relies on the age sensitivity at spectral types mid- and late-G.

Within his spectroscopic analysis of nearby stars within 25 pc, Fuhrmann (2004) isolated UMa group members – including HD 39587 discussed in the previous section – by the following distinct spectral properties:

- homogeneous filling-in of the cores of Hα and the Ca II infrared triplet as well as Na D and Mg Ib (Fuhrmann 2000),

- faster rotation compared to other main sequence stars, and
- strong lithium absorption except for the coolest members.

The stars isolated by Fuhrmann (2004) happened to have space velocities similar to these of the UMa cluster core. In this respect, the main advance of Fuhrmann (2004) is the underlying volume-complete and magnitude-limited sample.

1.3.7 Combining kinematic, spectroscopic, and photometric criteria

Montes et al. (2001b) added their spectroscopic criteria mentioned above to the kinematic membership criteria in Montes et al. (2001a) and confirmed the UMa group membership of three stars.

King et al. (2003) followed the work of Soderblom & Mayor (1993) and additionally assigned photometric membership to the stars which were enclosed by the 400 and 600 Myr isochrones in the colour-magnitude diagram as discussed above. Combining kinematic, photometric and spectroscopic criteria, they presented a list of nearly 60 assured members out of 220 candidates. They used the same kinematic criterion as Soderblom & Mayor (1993) though now based on well-known distances from *Hipparcos* and new radial velocities. Photometry and iron abundance are only used to exclude non-members and not to confirm membership of candidates. King et al. (2003) stated that:

> "... photometric membership and abundance-based membership are necessary but far from sufficient conditions to guarantee UMa membership."

1.4 A new homogeneous spectroscopic study

I summarise the problems encountered in the research on the UMa group:

1. Kinematic membership criteria are not sufficient to decide on the membership of further candidates.
2. At mid and late spectral types, photometric and spectroscopic criteria can presently only be used to exclude candidates.
3. Up to now, there is no homogeneous set of precise stellar parameters and abundances of a large sample of late-type UMa group members. The homogeneous work of Fuhrmann (2004) does not include any UMa group members beyond 25 pc.
4. Previous age determinations range widely from 200 Myrs to 600 Myrs.

Therefore, in the present work, I select a sample of UMa group members (Sect. 1.4.1). These stars then are analysed homogeneously following the method of Fuhrmann (1998) (Sect. 1.4.2) so that the work of Fuhrmann (2004) on the UMa group is extended beyond 25 pc.

1.4.1 Defining the sample

King et al. (2003) and Montes et al. (2001a) presented the most recent listings of UMa group members, accounting for the *Hipparcos* astrometry. Their member lists are still discrepant due to different membership criteria. A member list defining these criteria is missing although there is some agreement on spectroscopic and photometric properties. Yet this set of properties rather describes something that one would call a class of objects. What actually supports the reality of the UMa group as an entity of related stars? This question points back to the original evidence of the UMa group. This evidence is given by the very central part, the UMa cluster which has ever been the kinematically most coherent part of the UMa group. For this thesis, the UMa cluster and all assuredly co-moving stars will be the member list for the derivation of the spectroscopic properties. These properties may be the basis for future membership criteria.

For this thesis, I selected the assured kinematic members from King et al. (2003) and Montes et al. (2001a) (Tables 1.4 and 1.2). Considering the need for a sufficiently large sample, a compromise is made and the two selections are simply joined. The result is still a list of stars which can be called the certain kinematic members in contrast to the bulk of ≈200 UMa group candidates. It's worth noting that the most prominent member of the UMa group, Sirius (HD 48915 A), is not found in this kinematic list.

Table 1.4: The kinematic sample – stellar names and positions. The last column gives the reference for the distances: 1=Perryman et al. (1997), 2=Fuhrmann (2004), 3=Gliese & Jahreiß (1991)

HD	name	HR	GJ	HIP	α (2000)	δ (2000)	d [pc]	ref
11131	χ Cet B		9061 B	8486	01 49 23.36	- 10 42 12.8	23.61± 0.49	2
11171	χ Cet	531	9061 A	8497	01 49 35.10	- 10 41 11.1	23.61± 0.49	1
13594 A		647		10403	02 14 02.46	+ 47 29 03.2	41.55± 1.66	1
18778		906		14844	03 11 42.67	+ 81 28 14.6	62.00± 2.04	1
24160	g Eri	1195		17874	03 49 27.25	- 36 12 00.9	64.35± 2.40	1
24916 A			157 A	18512	03 57 28.70	- 01 09 34.0	15.77± 0.50	1
26923		1322		19859	04 15 28.80	+ 06 11 12.7	21.19± 0.48	1
28495			3295	21276	04 33 54.27	+ 64 37 59.7	27.53± 0.81	1
33111	67 Eri	1666	9175	23875	05 07 50.99	- 05 05 11.2	27.24± 0.56	1
38393	γ Lep	1983	216 A	27072	05 44 27.79	- 22 26 54.2	08.97± 0.05	1
39587	54 Ori	2047	222 B	27913	05 54 22.98	+ 20 16 34.2	08.66± 0.08	1
41593			227	28954	06 06 40.48	+ 15 32 31.6	15.45± 0.22	1
59747				36704	07 33 00.58	+ 37 01 47.4	19.69± 0.50	1
71974 A				41820	08 31 35.02	+ 34 57 58.4	28.71± 1.13	1
71974 B								
75605		3512		43352	08 49 51.50	- 32 46 49.9	70.13± 6.15	1
81659				46324	09 26 42.83	- 14 29 26.7	39.89± 1.59	1
87696	21 LMi	3974	9314	49593	10 07 25.76	+ 35 14 40.9	27.95± 0.66	1
91480	37 UMa	4141		51814	10 35 09.69	+ 57 04 57.5	26.46± 0.43	1

Table 1.4 continued next page

Table 1.4 continued

HD	name	HR	GJ	HIP	α (2000)	δ (2000)	d [pc]	ref
95418	β UMa	4295	9343	53910	11 01 50.47	+ 56 22 56.7	24.35± 0.36	1
95650			410	53985	11 02 38.34	+ 21 58 01.7	11.66± 0.18	1
103287	γ UMa	4554		58001	11 53 49.84	+ 53 41 41.1	25.65± 0.45	1
238087			457	59496	12 12 05.22	+ 58 55 35.2	28.38± 1.00	1
109011			1160	61100	12 31 18.91	+ 55 07 07.7	23.74± 1.75	1
109647				61481	12 35 51.29	+ 51 13 17.3	26.26± 0.77	1
109799		4803		61621	12 37 42.28	- 27 08 20.0	34.59± 0.90	1
110463			3743	61946	12 41 44.52	+ 55 43 28.8	23.22± 0.44	1
111456		4867	9417	62512	12 48 39.46	+ 60 19 11.4	24.16± 1.87	1
112185	ϵ UMa	4905		62956	12 54 01.74	+ 55 57 35	24.81± 0.38	1
112196				63008	12 54 40.02	+ 22 06 28.6	34.26± 1.88	1
113139 A	78 UMa	4931		63503	13 00 43.70	+ 56 21 58.8	24.96± 0.37	1
113139 B								
115043			503.2	64532	13 13 37.01	+ 56 42 29.8	25.69± 0.44	1
116656	ζ UMa	5054	3783 A	65378	13 23 55.54	+ 54 55 31.3	23.96± 0.35	1
116657		5055	3784 B		13 23 56.41	+ 54 55 18.1	24.15± 3.56	3
116842	80 UMa	5062	3785	65477	13 25 13.53	+ 54 59 16.6	24.88± 0.35	1
238224			509.1	65327	13 23 23.30	+ 57 54 22.1	25.10± 0.91	1
129798 A		5492		71876	14 42 03.25	+ 61 15 42.9	42.61± 1.03	1
129798 B								
134083	45 Boo	5634	578	73996	15 07 18.07	+ 24 52 09.1	19.72± 0.30	1
139006	α CrB	5793	9524	76267	15 34 41.27	+ 26 42 52.9	22.91± 0.41	1
141003 A	β Ser	5867		77233	15 46 11.26	+ 15 25 18.6	46.93± 1.89	1
141003 B								
147584	ζ TrA	6098	GJ 624	80686	16 28 28.14	- 70 05 03.8	12.11± 0.08	1
152863 A	56 Her	6292		82780	16 55 02.16	+ 25 43 50.5	140.06±13.14	1
155674 A			659 A	83988	17 10 10.51	+ 54 29 39.8	21.21± 0.85	1
155674 B			659 B	83996	17 10 12.36	+ 54 29 24.5	20.89	
165185		6748	702.1	88694	18 06 23.72	- 36 01 11.2	17.37± 0.23	1
167389				89282	18 13 07.23	+ 41 28 31.3	33.43± 0.66	1
171746 A		6981		91159	18 35 53.22	+ 16 58 32.5	34.21± 1.80	1
171746 B								
180777	59 Dra	7312	748.1	94083	19 09 09.88	+ 76 33 37.8	27.29± 0.36	1
184960		7451	4116	96258	19 34 19.79	+ 51 14 11.8	25.59± 0.31	1
199951 A	γ Mic	8039		103738	21 01 17.46	- 32 15 28.0	68.54± 3.71	1
205435	ρ Cyg	8252		106481	21 33 58.85	+ 45 35 30.6	38.17± 0.74	1
211575		8507		110091	22 18 04.27	- 00 14 15.6	41.48± 1.58	1

End of Table 1.4

1.4.2 How to obtain precise stellar parameters?

What is the best spectroscopic approach for a homogeneous analysis of the UMa group? Allende Prieto et al. (2004) derived effective temperatures from calibrations and surface

gravities from evolutionary isochrones while only the abundances were derived from spectra. They encountered discrepancies in the iron abundance when derived from lines of neutral and ionised iron separately; in contrast to Fuhrmann (2004) and Luck & Heiter (2005) who obtained all parameters consistently from the spectra only (see Luck & Heiter 2005 for a discussion). It is important to note here that King & Schuler (2005) – a work dedicated to the UMa group – derived the stellar parameters similarly to Allende Prieto et al. (2004) and encountered the same problems with the ionisation equilibrium.

For this thesis, the extension of the work of Fuhrmann (2004) right into the UMa cluster still is favourable since he already has analysed homogeneously a good account of late-type UMa group members closer than 25 pc. Fuhrmann's quantitative spectral analysis is differential with respect to the Sun and proved of value in his comprehensive work on nearby dwarfs, sub-giants, and young stars including UMa group members among others (see e.g. Fuhrmann 1998, 2000, 2004). Details are explained in Chapter 3. Effective temperatures are derived from the wings of the Balmer lines (cf. Barklem et al. 2002). Surface gravities are derived from the iron ionisation equilibrium (cf. Luck & Heiter 2005) or from the wings of the Mg Ib triplet. Iron abundance is derived from some ten lines of ionised iron. Microturbulence is found consistently from the spectra by the following requirement: Iron abundance derived from individual lines of the same star must not vary with equivalent width.

The obtained spectra not only allow to derive the stellar parameters but also to measure lithium equivalent widths and the chromospheric filling-in of the Hα line.

2 Observations, reduction and calibration

The requested spectroscopic features define how the stellar light has to be collected and measured: the wings and cores of Balmer lines and Mg Ib lines, the equivalent widths and profiles of lines of neutral and singly ionised iron and the Li I λ6708 Å absorption line (Sect. 2.1). *FOCES* on Calar Alto, Spain, and the Coudé-Échelle spectrograph in Tautenburg, Germany, are valuable instruments providing the desired spectra with high quality (Sect. 2.2). Using these instruments, spectra of ≈100 UMa group members and candidates were taken in 2002-2004 (Sect. 2.3). The observed spectra are arranged on CCD frames, forming arrays of many spectral orders. The process of data reduction (Sect. 2.4) transforms these raw data to data products which can be used in the subsequent analysis.

2.1 Required data

The aim of spectral analysis is to derive the stellar properties from various spectral features. The properties of interest for the present work are encoded in the following lines:

- Well-sampled wings of the Balmer lines Hα λ6562.81 Å and Hβ λ4861.34 Å yield the effective temperature while filling-in of the Hα line core allows to estimate chromospheric activity.

- Equivalent widths of many iron lines of neutral (Fe I) and singly ionised (Fe II) iron are used to determine surface gravity and iron abundance. These equivalent widths as well as microturbulence and rotational velocity are obtained precisely by fitting synthetic lines to the observed lines.

- Several lines of neutral magnesium (Mg I), especially the *Mg Ib triplet* (λ5167.33 Å, λ5172.70 Å, and λ5183.62 Å), provide an additional constraint on the surface gravity and for some stars even the only constraint. The weak Mg I lines λ4571.10 Å and λ5711.09 Å are needed in order to estimate the magnesium abundance.

- The equivalent width of the Li I line at λ6707.8 Å allows a relative age estimate. It is a blend of the ^{7}*Li I resonance doublet* comprised of components at λ6707.761 Å and λ6707.912 Å (Pavlenko 1995).

These spectral lines are located over wide parts of the optical spectrum and are best recorded simultaneously by spectroscopic observations covering the whole optical wavelength range. Aiming at a precise analysis, spectra with a high spectral resolution of $\frac{\lambda}{\Delta\lambda} \gtrsim 40000$ and with a high signal-to-noise ratio of $S/N > 200$ are indispensable.

2.2 Instruments

The constraints of wide wavelength coverage, high signal-to-noise ratio and high resolution are fulfilled with the Coudé-Échelle spectrograph of the *Alfred-Jentsch-Teleskop* located at the *Thüringer Landessternwarte Tautenburg* in Germany and *FOCES*[1] at the German-Spanish observatory on Calar Alto in Andalusia, Spain. For specific information on *FOCES*, refer to Pfeiffer et al. (1998) and Grupp (2003) as well as the unfinished PhD thesis of M. Pfeiffer which is attached to Grupp (2004). Also see the *FOCES* web page[2]. For details on the Tautenburg Coudé-Échelle spectrograph, refer to König (2003). For further information, consider the institute's web pages[3].

Both spectrographs are *Échelle spectrographs*. In Tautenburg, the light enters the spectrograph in the Coudé[4] focus while in the case of *FOCES* the light is collected in the Cassegrain focus and guided through the fibre to the spectrograph. In both spectrographs, the stellar light is expanded by an Échelle grating into high spectral orders. The orders overlap so that they have to be separated by a grism (Tautenburg)[5], or prisms (*FOCES*)[6] vertical to the direction of dispersion, i.e. in the direction of *cross-dispersion*. Eventually the orders are imaged onto a CCD[7]. Fig. 2.1 shows spectra of calibration light sources with flat spectral energy distributions, so-called *flat-fields*. Solid lines roughly mark central cuts along the direction of cross-dispersion.

For the configuration of both spectrographs, see Table 2.1. In the case of *FOCES*, I referred closely to the configuration used by Klaus Fuhrmann in recent years. The configuration of the Coudé-Échelle spectrograph in Tautenburg is the same as for the radial velocity planet search program (*TOPS*, Hatzes et al. 2005), of course without the iodine cell. See also König (2003) for a description of the setup.

2.3 Observations

Observations with *FOCES* on Calar Alto were applied for in collaboration with Klaus Fuhrmann, Brigitte König, and Ralph Neuhäuser. Four campaigns in 2003 and 2004 were granted. In collaboration with Eike Guenther, observations were carried out in

[1] Fibre Optics Cassegrain Échelle Spectrograph
[2] *http://www.usm.uni-muenchen.de/people/gehren/foces.html*
[3] *http://www.tls-tautenburg.de/telesc.html*, *http://www.tls-tautenburg.de/coude/echelle_spectrograph.html*
[4] See Kitchin (1998) for basics on telescope designs.
[5] Three grisms covering different wavelength ranges can be moved into the light path: *UV*, *VIS*, and *IR*. The *VIS grism* is used for this work covering the wavelength range $\lambda 4700 - 7400$ Å.
[6] Two prisms are used simultaneously in tandem mounting.
[7] Charge-Coupled Device

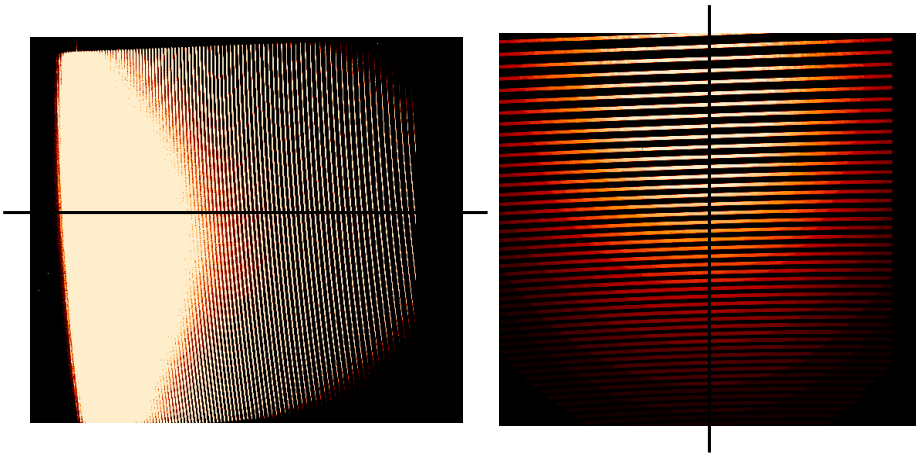

Figure 2.1: Spectral layout of frames of *FOCES* (left) and of the Tautenburg Coudé spectrograph (right) – Flat-field frames are shown. The direction of cross-dispersion is indicated by solid lines. Red wavelengths are to the left on the *FOCES* frame and on top on the Tautenburg frame.

Table 2.1: Properties and configuration of telescopes and instruments

	Coudé-Échelle Tautenburg (Germany)	*FOCES* Calar Alto (Spain)
telescope		
latitude (North)	50° 58′ 48.4″	37°13′ 23.8″
longitude (East)	11° 42′ 40.2″	02°32′ 45.7″
altitude [m] (sea level)	341	2168
telescope aperture [m]	2.0	2.2
focus	Coudé	Cassegrain
spectrograph		
Échelle orders (extracted)	78-121	69-137
wavelength range [Å]	4700-7400	4100-8200
slit width [μm]	520	120
CCD	2048^2 pixel	Loral#11i, 2048^2 pixels
nominal 2 pixel resolving power	67000	65000
pixel distance [μm]	15	15
readout noise [#e^-]	4.16	8.5
sensitivity [#e^-/ADU]	2.6	1.7

Table 2.2: Overview over the observing runs in chronological order – In total, more than 100 UMa group members and candidates were observed and more than 500 spectra were obtained. Only a part of these spectra is included in this thesis. See Table B.1 for these exposures.

run identifier	period	observatory (instrument)
Jun02	24.06.-01.07.2002	Tautenburg (Coudé Échelle)
Jul02	17.07.-29.07.2002	Tautenburg (Coudé Échelle)
Aug02	26.08.-02.09.2002	Tautenburg (Coudé Échelle)
Mar03	11.03.-18.03.2003	Tautenburg (Coudé Échelle)
Jul03	14.07.-21.07.2003	Tautenburg (Coudé Échelle)
Aug03	11.08.-13.08.2003	Calar Alto (*FOCES*), 2.2m #16, PI Ammler
Oct03	07.10.-10.10.2003	Calar Alto (*FOCES*), 2.2m #16, PI Ammler
Feb04	06.02.-09.02.2004	Calar Alto (*FOCES*), 2.2m #12, PI Ammler
Mar04	06.03.-15.03.2004	Tautenburg (Coudé Échelle)
May04	28.05.-02.06.2004	Calar Alto (*FOCES*), 2.2m #12, PI Ammler
Sep04	27.09.-05.10.2004	Tautenburg (Coudé Échelle)

seven campaigns during 2002-2004 with the Coudé-Échelle spectrograph in Tautenburg. Table 2.2 shows an overview introducing identifiers for each run. In particular, the Calar Alto runs were very successful because only one night out of 17 was lost due to weather. See Table 2.3 for details. Table B.1 lists the spectra used for this thesis together with the signal-to-noise ratio. For HD 95650, HD 109647, HD 115043, HD 155674 A, HD 171746 B, HD 238087, and HD 238224, single spectra with high signal-to-noise ratio ($\gtrsim$200) could not be obtained. Except of HD 171746 B and HD 109647, two spectra each were available and added by means of the program *coad.pro* of Andreas Korn. The addition of subsequently obtained spectra is possible for the analyses done within this thesis but not for measurements of precise radial velocities.
The measured signal not only is a response to the stellar properties which are encoded in the incoming stellar light but also to the properties of the telescope and the instrument. Therefore in addition to the scientific stellar observations, several calibration frames were taken in order to remove these imprints from the scientific frames and to recover the requested stellar signal:

- **Bias frames:** In order to avoid negative signals due to the read-out noise, a constant offset is applied to the CCD signal, the so-called *bias level*. In order to subtract this signal from the exposures, it has to be determined from *bias frames*. These frames are obtained by mere read-out, i.e. zero exposure time, with the camera shutter being closed. They further allow to estimate the read-out noise which modulates the bias level. See McLean (1997) for details.

Table 2.3: Completeness of the observations of kinematic members – The last column refers to the following comments: **(1), (3)** These stars have already been analysed by Fuhrmann (2004) and Fuhrmann (2000), respectively, with the same methods. **(2)** HD 24916 A was analysed by König et al. (2006) with the same method as Fuhrmann (2000, 2004). **(4)** These stars could be observed within the campaigns described in Table 2.2. **(5)** The complete stellar atmosphere analysis according to Fuhrmann (1998) with iron and magnesium lines is not possible for these stars. Either they are early-type stars (A - mid F), very late-type stars (K2 - M), giants or close binaries, or simply to faint. **(6)** These stars of the southern sky could not be observed from Calar Alto and Tautenburg.

name	α (2000)	δ (2000)	spec. type	V	comment
HD 7804	01 17 47.96	+03 36 52.1	A3V	5.140	5
HD 11131	01 49 23.36	-10 42 12.8	G1V	6.721	1
HD 11171	01 49 35.10	-10 41 11.1	F3III	4.664	4,5
HD 13594 A	02 14 2.46	+47 29 3.2	F4V	6.080	4,5
HD 18778	03 11 42.67	+81 28 14.6	A7III-IV	5.910	5
HD 24160	03 49 27.25	-36 12 0.9	G9II-III	4.172	5,6
HD 24916 A	03 57 28.70	-01 09 34.0	K4V	8.000	2,5
HD 26923	04 15 28.80	+06 11 12.7	G0IV	6.330	1
HD 28495	04 33 54.27	+64 37 59.7	K3V	7.748	4
HD 33111	05 07 50.99	-05 05 11.2	A3III	2.790	5
HD 38393	05 44 27.79	-22 26 54.2	F7V	3.586	4
HD 39587	05 54 22.98	+20 16 34.2	G0V	4.410	1
HD 41593	06 06 40.48	+15 32 31.6	K0V	6.767	1
HD 59747	07 33 0.58	+37 01 47.4	G5V	7.710	1
HD 71974 A	08 31 35.02	+34 57 58.4	G5V	7.300	4,5
HD 71974 B					4,5
HD 75605	08 49 51.50	-32 46 49.9	G5III	5.204	5,6
HD 81659	09 26 42.83	-14 29 26.7	G6/G8V	7.900	6
HD 87696	10 07 25.76	+35 14 40.9	A7V	4.490	4,5
HD 91480	10 35 9.69	+57 04 57.5	F1V	5.161	4,5
HD 95418	11 01 50.47	+56 22 56.7	A1V	2.346	4,5
HD 95650	11 02 38.34	+21 58 1.7	M0	9.690	4,5
HD 103287	11 53 49.84	+53 41 41.1	A0V	2.427	4,5
HD 238087	12 12 5.22	+58 55 35.2	K5	9.980	4,5
HD 109011	12 31 18.91	+55 07 7.7	K2V	8.100	4,5
HD 109647	12 35 51.29	+51 13 17.3	K0V	8.503	4
HD 109799	12 37 42.28	-27 08 20.0	F1IV	5.416	5,6
HD 110463	12 41 44.52	+55 43 28.8	K3V	8.256	4
HD 111456	12 48 39.46	+60 19 11.4	F5V	5.845	3,4,5
HD 112185	12 54 1.74	+55 57 35.3	A0	1.760	4,5

Table 2.3 continued next page

Table 2.3 continued

name	α (2000)	δ (2000)	spec. type	V	comment
HD 112196	12 54 40.02	+22 06 28.6	F8V	6.985	4
HD 113139 A	13 00 43.70	+56 21 58.8	F2V	4.930	4,5
HD 115043	13 13 37.01	+56 42 29.8	G1Va	6.814	4
HD 116656	13 23 55.54	+54 55 31.3	A2V	2.270	4,5
HD 116657	13 23 56.41	+54 55 18.1	A1m	3.950	4,5
HD 116842	13 25 13.53	+54 59 16.6	A5V	4.005	4,5
HD 238224	13 23 23.30	+57 54 22.1	K5	9.730	4,5
HD 129798 A	14 42 3.25	+61 15 42.9	F2V	6.250	4,5
HD 134083	15 07 18.07	+24 52 9.1	F5V	4.930	3,4,5
HD 139006	15 34 41.27	+26 42 52.9	A0V	2.210	4,5
HD 141003 A	15 46 11.26	+15 25 18.6	A2IV	3.660	4,5
HD 147584	16 28 28.14	-70 05 3.8	F9V	4.910	6
HD 152863 A	16 55 2.16	+25 43 50.5	G5III	6.073	4,5
HD 155674 A	17 10 10.51	+54 29 39.8	K0	8.800	4
HD 155674 B	17 10 12.36	+54 29 24.5	K8	9.290	4,5
HD 165185	18 06 23.72	-36 01 11.2	G5V	5.949	6
HD 167389	18 13 7.23	+41 28 31.3	F8	7.380	4
HD 171746 A	18 35 53.22	+16 58 32.5	G2V	6.924	4
HD 171746 B	18 35 53.22	+16 58 32.5	G2V	7.009	4
HD 180777	19 09 9.88	+76 33 37.8	A9V	5.120	4,5
HD 184960	19 34 19.79	+51 14 11.8	F7V	5.714	4
HD 199951 A	21 01 17.46	-32 15 28.0	G4III	4.677	5,6
HD 205435	21 33 58.85	+45 35 30.6	G8III	3.986	4,5
HD 211575	22 18 4.27	-00 14 15.6	F3V	6.398	4,5

End of Table 2.3

- **Flat-field frames:** The sensitivity varies across the CCD and strongly depends on the wavelength. Furthermore the measured light depends on the wavelength-dependent efficiency of the instrument. In order to correct for these effects, the exposures are divided by so-called *flat-field frames*. These are obtained by illuminating the instrument with a light source having a continuous spectrum. Samples of flat-field frames are shown in Fig. 2.1. In Tautenburg, the flat-fields are obtained by pointing the telescope at a homogeneously illuminated screen inside the dome. *FOCES* uses an internal lamp which is moved into the light-path in front of the fibre. The intensity of the *FOCES* flat-fields rapidly decreases towards the blue Échelle orders. Therefore, flat-fields with three different exposure times are obtained (Fig. 2.2) in order to maintain high signal-to-noise ratio when calibrating the object exposures while in Tautenburg, two different exposure times are sufficient in order to have all orders well-exposed (see Fig. 2.3).

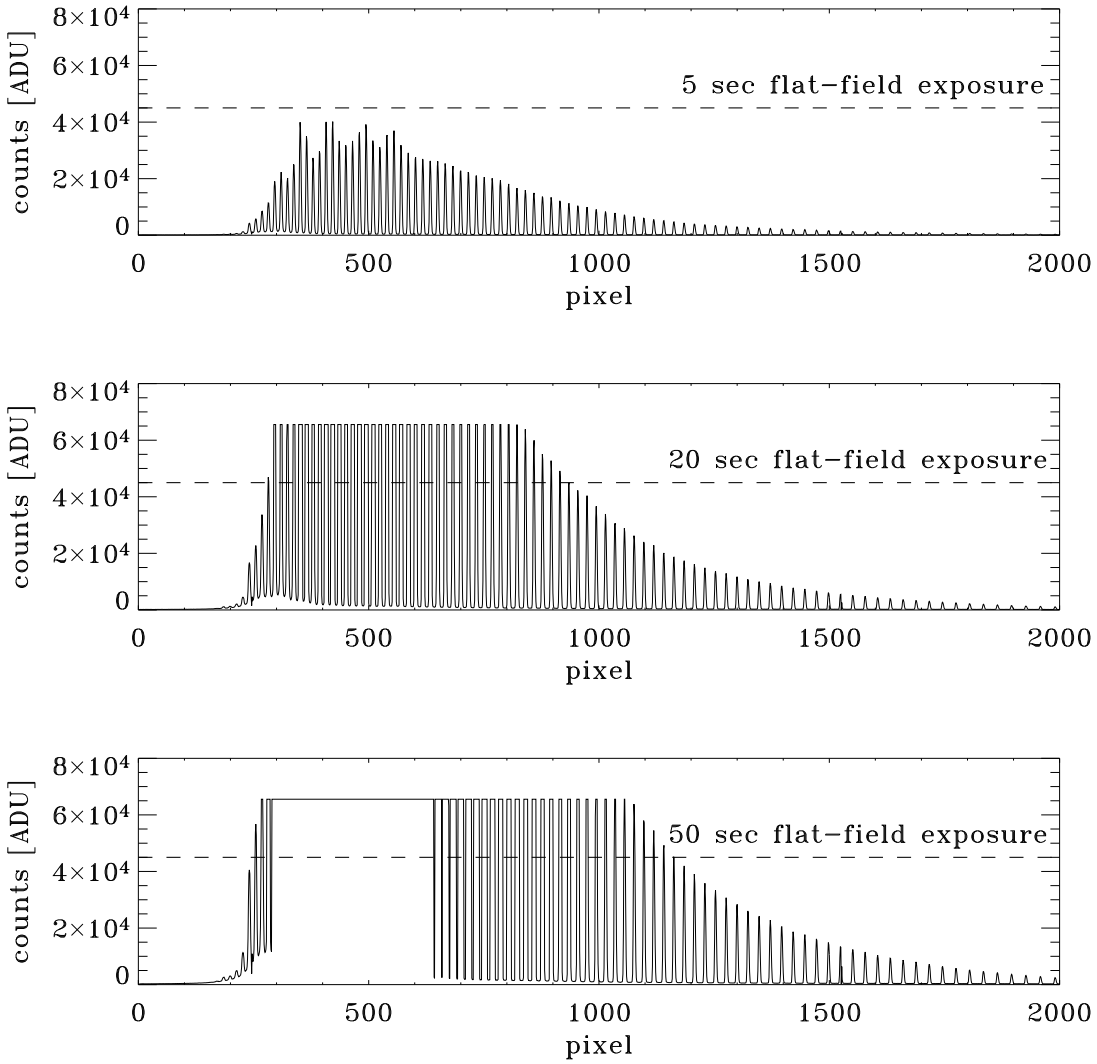

Figure 2.2: Types of flat-fields taken with *FOCES* – Cuts through raw flat-field frames in the direction of cross-dispersion (approximately along the lines in Fig. 2.1) are shown. The intensity decreases rapidly from the red (left) to the blue (right) orders. Therefore the exposure times were adjusted to have each the blue, green and red regimes well-exposed. Several Échelle orders are saturated in the lower two cases and cannot be used. Therefore, only the orders below a certain intensity limit (dashed line) are included.

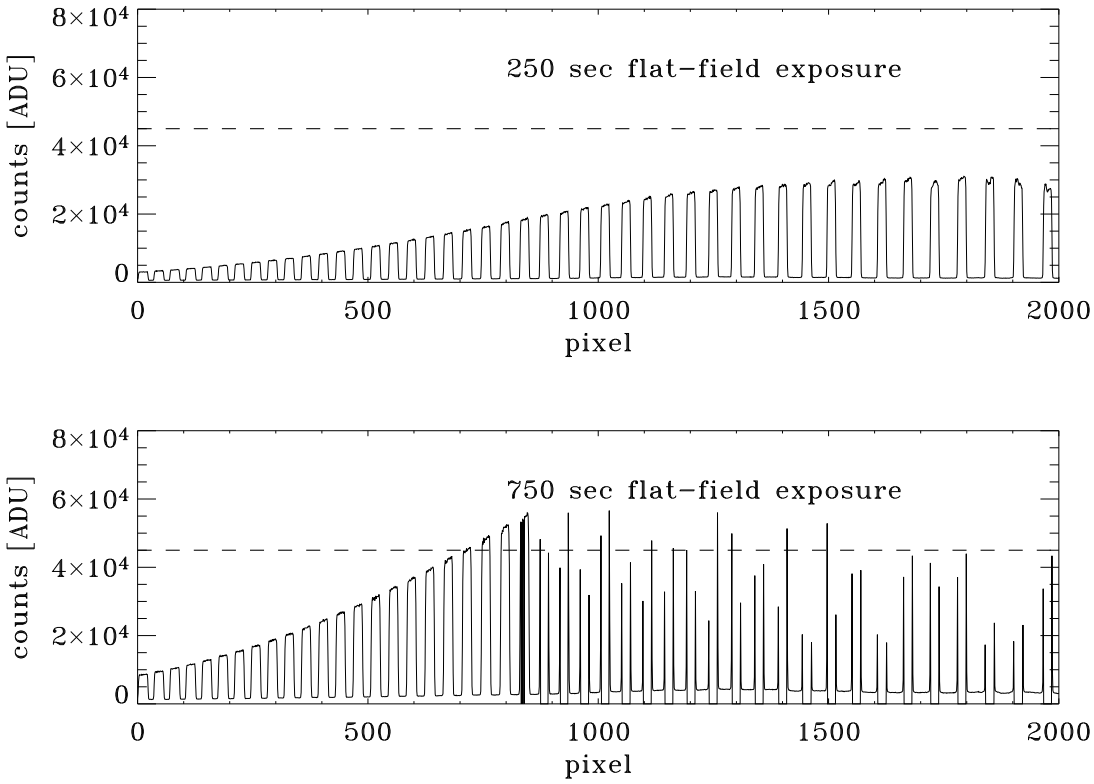

Figure 2.3: Types of flat-fields taken in Tautenburg – Same as Fig. 2.2 but with Tautenburg flat-fields. The blue wavelength range is to the left and the red to the right. The intensity slope from red to blue is not as steep as the slope of *FOCES* flat-fields so that two different exposure times are sufficient. Note that the saturated parts are set to zero automatically within the CCD readout.

Table 2.4: The layout of the observations with typical exposure times.

	Calar Alto		Tautenburg	
type of exposure	number of exposures	exposure time	number of exposures	exposure time
daytime calibrations				
bias frames	5	0 s	10	0 s
flat-field frames	10	5 s	3	250 s
	10	20 s	1	750 s
	10	50 s		
Th-Ar frames	6	10-60 s	2	15 s
scientific observations				
each target	2	40 s-60 min	2	20 s-45 min
end of night calibrations				
bias frames	5	0 s	3	0 s
Th-Ar frames			2	15 s

- **Wavelength calibration:** The identification of the pixel position on the CCD frame with the wavelength of the incoming light, i.e. the *dispersion relation*, is best found by means of a calibration lamp. Stellar spectral lines are affected by *Doppler shift* due to stellar radial velocities, macroscopic velocity fields, and by Earth's motion itself. Therefore, the absolute laboratory wavelength scale of the spectra is determined by taking a spectrum of a thorium-argon (Th-Ar) calibration lamp which provides sharp emission lines at well-known wavelengths.

All calibration frames are taken during daytime so that the nighttime can be devoted to the science observations. The typical observing schedule follows the scheme in Table 2.4.

The observations are spread over several campaigns so that slight differences in the instrumental setup or the ambient conditions might introduce variations in the observed spectra. These influences were monitored by obtaining solar spectra during each campaign. The Sun is too bright so that the telescope was pointed towards the Moon yielding spectra of the reflected light of the Sun. Section 4.1.1 shows that consistent solar parameters werde derived from all these spectra.

2.4 Reduction and calibrations

The data reduction extracts the requested information from the observed CCD frames. It follows the common scheme (cf. Horne 1986, McLean 1997) and is carried out with the *FOCES EDRS*[8] (Pfeiffer et al. 1998) for both spectrographs.

- **Bias subtraction:** The bias is a constant offset which is subtracted from all frames, i.e. flat-field frames, Th-Ar frames and science frames.
- **Order detection:** The reduction software detects the Échelle orders by following the order ridges. Fig. 2.1 shows the spectral layout of both spectrographs and indicates the difficulty to detect the Échelle orders automatically. Note that *FOCES* is a fibre spectrograph producing narrow orders with well-defined intensity ridges, so that the Échelle orders can be detected automatically by following the order ridges. In contrast, the Tautenburg spectrograph has no additional pre-slit optics and the incoming light fully covers the slit producing much broader orders. Hence Klaus Fuhrmann adjusted the order detection algorithm to the Tautenburg spectrograph.
- **Wavelength calibration:** The Th-Ar Échelle orders are extracted and used to derive the wavelength scale.
- **Master flat-field:** The useful Échelle orders of all flat-field frames (cf. Figs. 2.2 and 2.3) are combined to have one master flat-field for all spectral orders .
- **Background subtraction:** The pollution by scattered light is measured between the Échelle orders in all frames and subtracted.
- **Flat-field division:** The extracted science orders are divided by the master flat-field orders.

The simple order extraction algorithm[9] integrates all light along the direction of cross-dispersion at each position of the Échelle order and ignores the exact order profile.

An absolute flux calibration is difficult and not necessary in this thesis. The spectral analysis described later requires the line profiles only, given with respect to the relative continuum. Therefore the relative continuum itself has to be found by considering the parts of the spectrum which are apparently free of line absorption. This process, the *rectification of the continuum*, is most critical for the proper measurement of effective temperature. The principle is shown in Fig. 2.4. First, several points of the relative continuum are fixed manually. Spline interpolation then recovers the approximate relative continuum. The division by this curve finally *normalises* the spectral order.

In some cases, the continuum is masked by strong lines (Balmer lines, Mg Ib triplet, Na D doublet) or telluric bands. Since the continua change monotonically with order number for all spectra (cf. Fig. 2.6 and 2.7), the relative continuum can still be recovered

[8] Échelle Data Reduction Software
[9] The optimal extraction scheme as described in Horne (1986) is not used here.

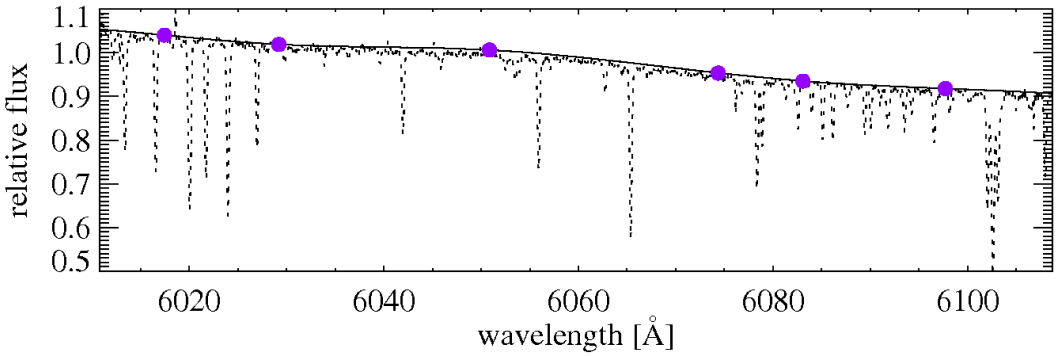

Figure 2.4: Normalisation of an order with a clearly perceivable relative continuum – A reduced, extracted, and calibrated spectral order of HD 115043 obtained in Tautenburg is shown (dotted line). It is affected neither by broad lines nor by strong blends. Several continuum points are fixed manually (dots) and used to recover the complete continuum by spline interpolation (solid).

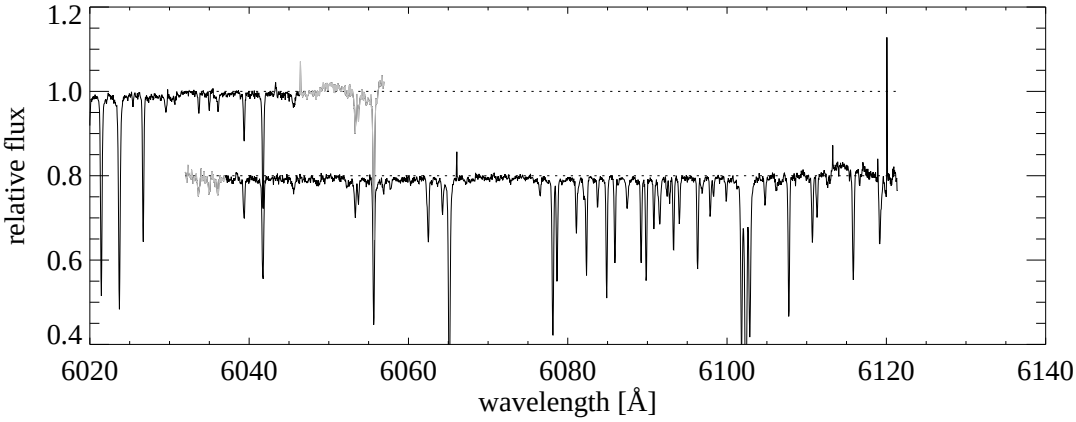

Figure 2.5: Merging of two Échelle orders. – The overlaps of order 94 (top) and order 93 (offset by −0.2 for clarity) of a *FOCES* spectrum of HD 28495 are compared. The order ends usually suffer from high noise as well as bad rectification and normalisation (grey parts). The merging allows to remove these parts and to average the remaining good parts.

in most cases by interpolation with unaffected neighbouring orders. This is essential for the Balmer lines used in the determination of effective temperature. In Fig. 2.6, especially the green orders look quite similar in each set corroborating normalisation with interpolated splines. In contrast, the continua of blue orders are veiled by countless stellar lines and some red orders are strongly affected by Earth's atmosphere. Therefore the normalisation is not well determined in these spectral regions. While *FOCES* is known for its flat orders (Korn 2002; here the green and red parts), the centres of the Tautenburg orders show a wide bump. The red *FOCES* order ends are strongly affected by oscillations. However, these parts overlap with other orders and can usually be removed within the merging described below.

For the analysis, the orders are merged in order to have one spectrum running from blue to red wavelengths continuously. In the optical, the Échelle orders mostly overlap conveniently in wavelength so that the overlapping parts can be used to "glue" the order ends. These parts are compared so that discrepancies in the rectification can be seen and removed (Fig. 2.5). Overlapping parts with good quality are averaged and therefore improve locally the signal-to-noise ratio. Bad redundant parts on the edges of the orders are removed.

The positions of the spectral features do not yet agree with the corresponding laboratory wavelengths. They are shifted by the Doppler effect due to the radial velocity of the star and the motion of the observer caused by Earth's motion and rotation. The correction for these line shifts, i.e. the *radial velocity correction*, is derived by correlating the observed spectrum with a synthetic solar-like spectrum provided by Brigitte König.

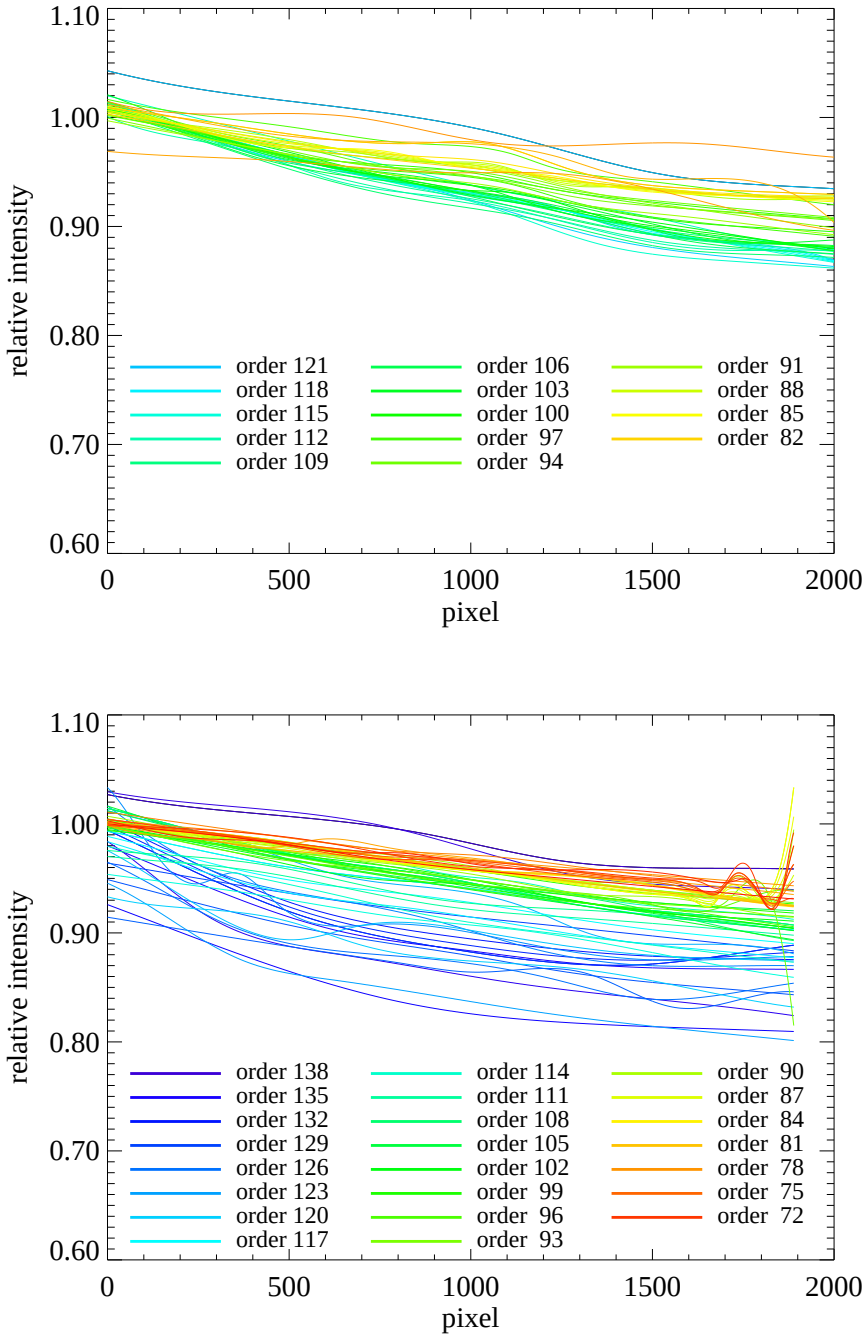

Figure 2.6: Rectification splines of Tautenburg and *FOCES* Échelle orders – Relative intensity is plotted versus pixel position. The spline sets are obtained from Tautenburg **(top)** and *FOCES* **(bottom)** spectra of HD 217813. The colours indicate the number of the rectified Échelle order.

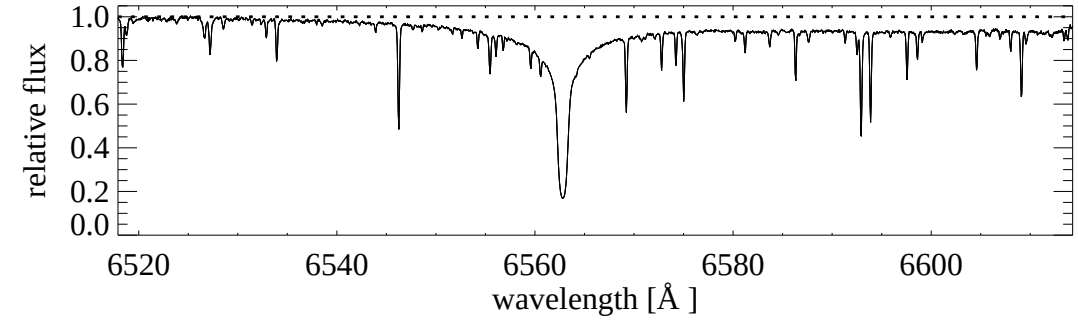

(a) raw order

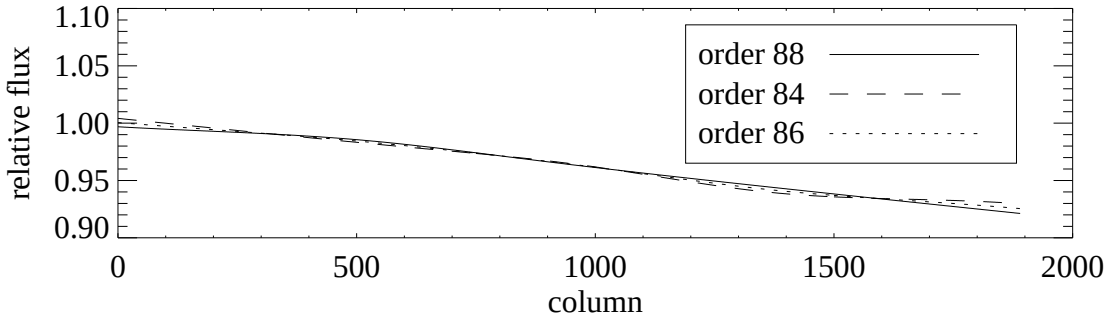

(b) interpolation of rectification spline with neighbouring orders

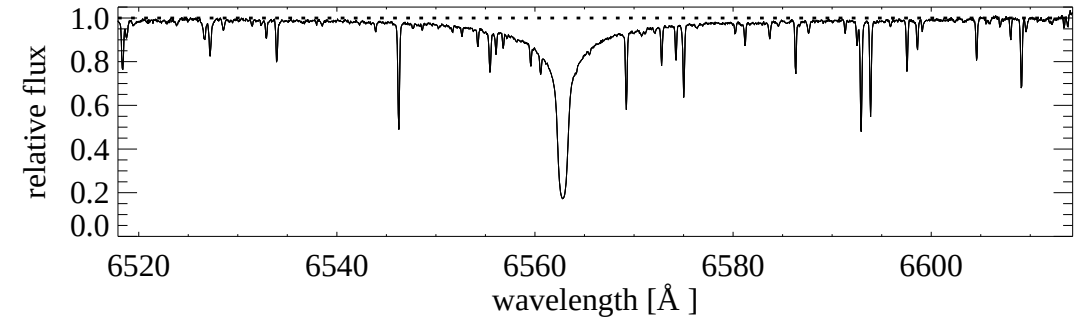

(c) normalised order with rectified continuum

Figure 2.7: Normalisation of an order with a masked relative continuum – **(a)** Order 86 with the Hα line before rectification of the continua (Moon exposure obtained with *FOCES*). **(b)** The spline curves for the neighbouring orders 84 and 88 are unaffected by the Hα wings and used to find an interpolated spline curve for the affected orders 85-87 (only order 86 is shown in this example). **(c)** The Hα line after rectification and normalisation of the continuum.

3 Deriving the stellar parameters – Methods

A wealth of information is accessible by spectral analysis of the integrated stellar light. The higher the spectral resolution and the stronger the signal, the more information we can obtain. The stellar parameters, e.g. effective temperature, surface gravity and metallicity, leave their traces in the stellar spectrum and it is the task of stellar atmosphere analysis to disentangle their influence on a set of spectral absorption lines. I was instructed by Klaus Fuhrmann in the use of his spectral analysis package (cf. Fuhrmann 1998) which works strictly differential with respect to the Sun (Sect. 3.1) and is based on the use of model atmospheres and synthetic line formation (Sect. 3.2). The application of these theoretical tools to the derivation of stellar parameters is described in Sect. 3.3.

3.1 Differential analysis

The presented analysis is strictly differential with respect to the Sun. Hence it is instructive to relate the stellar to the solar parameters. Mass, radius, and luminosity are given in units of the solar values, i.e. $M_\odot = 1.9891 \cdot 10^{30}\,\mathrm{kg}$ and $R_\odot = 6.9598 \cdot 10^{8}\,\mathrm{m}$, and $L_\odot = 3.845 \cdot 10^{26}\,\mathrm{W}$, respectively. Similarly the abundance $\log \varepsilon(\mathrm{X}) = \log \frac{N_\mathrm{X}}{N_\mathrm{H}} + 12$ of an element X with respect to hydrogen H, where N is the number of particles, is related to the solar value by :

$$[\mathrm{X/H}] \equiv \log \frac{\varepsilon}{\varepsilon_\odot} \tag{3.1}$$

The differential analysis works for stars with stellar parameters only slightly different from the Sun. Model atmospheres calibrated to match the Sun can still be used (Sect. 3.2). Oscillator strengths which usually are not well-known can be calibrated to match the spectrum of the Sun (Sect. 3.2.6). Furthermore the assumption of *local thermodynamic equilibrium* (LTE) (Sect. 3.2.4) is valid for weak lines and for the far wings of strong lines. The assumptions of LTE and plane-parallel atmospheres (Sect. 3.2.2) will certainly break down for giants while they are still valid for any star with spectral type G0 or G5 on the main sequence. Certainly an exact definition of the limits of the differential approach is difficult. However it proved of value for dwarf and subgiant stars with spectral types late-F to early-K (Fuhrmann 1998, 2000, 2004).

3.2 Model atmospheres and synthetic line formation

I derive the parameters of the stellar atmospheres by analysing observed spectral absorption lines. Therefore the radiative transfer problem has to be solved which couples the emerging light to the properties of the absorbing and emitting stellar material. The *FORTRAN77* codes *MAFAGS*[1] and *LINFOR* are used to model the stellar atmospheres and the line formation, respectively. *MAFAGS* is an unpublished model atmosphere code which was developed by T. Gehren and revised by Reile (1987). The line formation code *LINFOR* by T. Gehren, C. Reile, K. Fuhrmann, and J. Reetz is based on *MAFAGS*.

The stellar parameters in a differential analysis cannot be decoupled from the underlying models. Results of the present work will only be useful in the future if the circumstances of their origin are well-known. Therefore a specification of the used models is indispensable. The last comprehensive documentation for *MAFAGS* is given by Reile (1987). Furthermore some basics are needed in order to discuss the application of *MAFAGS* and *LINFOR* to the young UMa group stars and to understand the methods for the determination of the stellar parameters (Sect. 3.3). The following presentation is formally close to Mihalas (1978), Gray (1992), and Gray (2005). See these publications for more details on general topics. Some details on the algorithm in *MAFAGS* for the construction of model atmospheres are not of immediate importance for this thesis. They are outlined in Appendix D.

In Sect. 3.2.9, the onedimensional hydrostatic modelling is confronted with recent results of multidimensional hydrodynamic approaches and methods of *statistical equilibrium*, often called *non-LTE*. Consequences are discussed with respect to the differential analysis.

3.2.1 Radiative transfer

The properties of radiation are described by the *specific intensity* :

$$I_\nu = \frac{\mathrm{d}E}{\cos\theta\,\mathrm{d}A\,\mathrm{d}\omega\,\mathrm{d}t\,\mathrm{d}\nu} \tag{3.2}$$

where $\mathrm{d}E$, $\mathrm{d}A$, $\mathrm{d}\omega$, $\mathrm{d}t$, $\mathrm{d}\nu$ are the increments of energy, area, solid angle, time, and frequency, respectively. The directional average of the specific intensity is given by the *mean intensity*:

$$J_\nu = \oint I_\nu \frac{\mathrm{d}\omega}{4\pi} \tag{3.3}$$

Consider a radiation field which interacts with a plasma of density ρ. Think of a stellar plasma which consists of atoms, ions, molecules and ionic molecules. Then the change of intensity along a path with an increment $\mathrm{d}s$ is composed of losses and gains

$$\mathrm{d}I_\nu = -\kappa_\nu \rho I_\nu \mathrm{d}s + j_\nu \rho \mathrm{d}s$$

where κ_ν is the *absorption coefficient* and j_ν the *emission coefficient*.

[1] Model Atmospheres for F- And G-Stars

The *optical depth* $\mathrm{d}\tau_\nu = \kappa_\nu \rho \mathrm{d}s$ relates the path increment to the absorption. It is a measure for the depth an observer can look into the medium. Then the intensity fulfils the *equation of radiative transfer*:

$$\frac{\mathrm{d}I_\nu}{\mathrm{d}\tau_\nu} = -I_\nu + S_\nu \tag{3.4}$$

where $S_\nu = \frac{j_\nu}{\kappa_\nu}$ is the *source function*. In contrast to absorption, it adds up to the radiation field along $\mathrm{d}\tau_\nu$.

The equation of radiative transfer can be written in integral form

$$I_\nu(\tau_\nu) = \int_0^{\tau_\nu} S_\nu(t_\nu) e^{-(\tau_\nu - t_\nu)\sec\theta} \mathrm{d}t_\nu + I_\nu(0) e^{-\tau_\nu} \tag{3.5}$$

(Gray 1992, p. 111) where the integration constant $I_\nu(0)$ represents some external incident radiation.

3.2.2 Radiative transfer in solar-like stars – defining the geometry

The atmosphere is considered to be homogeneous so that the atmospheric parameters (effective temperature, gas pressure, electron pressure) only depend on the depth. Of course, real photospheres are by far more complicated than suggested by the presented model. Integral effects of inhomogeneity have to be taken into account for absolute abundance analyses while homogeneity can still be assumed within the presented framework of differential analysis (see Sect. 3.2.9 for some discussion). The study of surface structures is challenging (e.g. Doppler imaging or interferometry). Only the surface of the Sun can be analysed precisely.

In spherical symmetry (coordinates r, θ, ϕ), the radiation quantities can be written independently of the azimuthal angle ϕ so that the radiative transfer equation is expressed by:

$$\frac{\partial I_\nu}{\partial r}\frac{\cos\theta}{\kappa_\nu \rho} - \frac{\partial I_\nu}{\partial \theta}\frac{\sin\theta}{\kappa_\nu \rho r} = -I_\nu + S_\nu \tag{3.6}$$

Assuming that close to or on the main-sequence the photosphere is thin compared to the stellar radius, a *plane-parallel approximation* is applied. The thickness of the solar photosphere, for example, amounts to only $\approx 1\,\%$ of the solar radius. Furthermore the direction is reversed and follows the line of sight from the observer back into the deep photospheric layers:

$$\cos\theta \frac{\mathrm{d}I_\nu}{\mathrm{d}\tau_\nu} = I_\nu - S_\nu \tag{3.7}$$

where $\mathrm{d}\tau_\nu = \kappa_\nu \rho \mathrm{d}z$ is the *optical depth* along an axis z.

The flux is the quantity relevant for the analysis of the integrated stellar light. It is related to intensity by:

$$F_\nu = 2\pi \int_0^\pi I_\nu \cos\theta \sin\theta \, \mathrm{d}\theta \, \mathrm{d}\phi$$

Separation into incoming and outgoing radiation gives:

$$F_\nu = 2\pi \int_0^{\frac{\pi}{2}} I_\nu^{\text{in}} \cos\theta \sin\theta \, \mathrm{d}\theta + 2\pi \int_{\frac{\pi}{2}}^{\pi} I_\nu^{\text{out}} \cos\theta \sin\theta \, \mathrm{d}\theta \tag{3.8}$$

The insertion of I_ν at a certain optical depth τ_ν for incoming and outgoing radiation corresponding to Eq. 3.5 yields (Gray 1992, p. 115):

$$F_\nu = 2\pi \int_{\tau_\nu}^{\infty} S_\nu \int_0^{\frac{\pi}{2}} \mathrm{e}^{-(t_\nu - \tau_\nu)\sec\theta} \sin\theta \, \mathrm{d}\theta \, \mathrm{d}t_\nu - 2\pi \int_0^{\tau_\nu} S_\nu \int_{\frac{\pi}{2}}^{\pi} \mathrm{e}^{-(t_\nu - \tau_\nu)\sec\theta} \sin\theta \, \mathrm{d}\theta \, \mathrm{d}t_\nu \tag{3.9}$$

The innermost integrals can be expressed in terms of *exponential integrals*:

$$\int_0^{\frac{\pi}{2}} \mathrm{e}^{-(t_\nu - \tau_\nu)\sec\theta} \sin\theta \, \mathrm{d}\theta = \int_1^{\infty} \frac{\mathrm{e}^{-xw}}{w^2} \mathrm{d}w \equiv E_2(x) \tag{3.10}$$

3.2.3 Thermodynamic equilibrium

Information on the occupation of atomic and molecular states as well as ionic states is necessary in order to quantify the gains and losses of the radiation field. In thermodynamic equilibrium, the population ratio of an atomic upper level N_u and a lower level N_l with energy levels χ_u and χ_l, respectively, can be described by providing the equilibrium temperature T only:

$$\frac{N_\mathrm{u}}{N_\mathrm{l}} = \frac{g_\mathrm{u}}{g_\mathrm{l}} e^{-\frac{\chi_\mathrm{u} - \chi_\mathrm{l}}{kT}} \tag{3.11}$$

where g_u and g_l are the corresponding statistical weights and $k = 1.380650 \cdot 10^{-16}$ erg/K is the *Boltzmann constant*. The population of a level n with respect to the total number N of a species is then given by the *Boltzmann equation*:

$$\frac{N_n}{N} = \frac{g_n}{U(T)} e^{\frac{-\chi_n}{kT}}, \tag{3.12}$$

where

$$U(T) = \sum_i g_i e^{\frac{-\chi_i}{kT}}$$

is the *partition function*.

In thermal equilibrium, the fraction of $N_{r+1,m}$ particles at an ionisation stage $r+1$ to $N_{r,m}$ particles at an ionisation stage r of a species m with an ionisation energy $I_{r,m}$ can be expressed in terms of temperature, too – by the *Saha equation*:

$$\frac{N_{r+1,m}}{N_{r,m}} P_\mathrm{e} = \frac{(2\pi m)^{\frac{3}{2}} (kT)^{\frac{5}{2}}}{h^3} \frac{2U_{r+1,m}(T)}{U_{r,m}(T)} e^{-\frac{I_{r,m}}{kT}} \tag{3.13}$$

where P_e is the electron pressure.

Thermal equilibrium of radiation is modelled by the black body. Its radiation field $B_\nu(T)$ is described by:

$$B_\nu(T) = \frac{2h\nu^3}{c^2} \frac{1}{e^{\frac{h\nu}{kT}} - 1} \tag{3.14}$$

The law is based on quantum mechanics as is shown by the appearance of Planck's constant h (see Gray 1992 for further discussion).

3.2.4 Local thermodynamic equilibrium (LTE)

Thermal equilibrium is not globally valid in a stellar photosphere. An important property of a black body is the little loss of radiation. In the upper photospheric layers, by contrast, radiation escapes freely. Yet thermal equilibrium is still maintained as a local concept in the deeper photospheric layers where excitation and de-excitation are dominated by collisions. Thus most photons cannot escape so that thermal equilibrium is still valid locally. Then a single temperature, i.e. the local equilibrium temperature T at each depth point τ, is sufficient to describe the atmosphere (Eqs. 3.12, 3.13).

The temperatures and densities of solar-like atmospheres justify the assumption of ideal gas so that the thermodynamic state of the photospheric layers is fully described in *MAFAGS* by providing the temperature and the gas pressure stratification, $T(\tau)$ and $P_\mathrm{g}(\tau)$, respectively.

For the young main-sequence stars analysed in this work, LTE is valid for weak absorption lines (formed in deep photospheric layers) of abundant species and the wings of strong lines. It is not valid for transitions of rare species like Fe I in stars hotter than the Sun or in the cores of strong lines formed in the upper photospheric layers or even in the chromosphere (see Fig. 3.1). In these cases, the methods of *statistical equilibrium/ non-LTE* apply which are not implemented in *MAFAGS* and *LINFOR*. See Mihalas (1978) for a textbook.

If we consider a spectral line formed under LTE conditions, the source function is given by the *Kirchhoff-Planck relation* $S_\nu = B_\nu(T)$ and the outcoming flux is expressed following Eq. 3.9 and Eq. 3.10 by (Gray 1992, p. 275):

$$F_\nu = 2\pi \int_0^\infty B_\nu(T)\, E_2(\tau_\nu)\, \mathrm{d}\tau_\nu \tag{3.15}$$

3.2.5 Contributions to absorption and emission

Pure absorption and scattering

Radiation is attenuated along its path by "true" absorption (χ_ν, e.g. atomic line absorption) or by just scattering photons into other directions (σ_ν). Therefore the total absorption coefficient or *opacity* is given by:

$$\kappa_\nu = \chi_\nu + \sigma_\nu \tag{3.16}$$

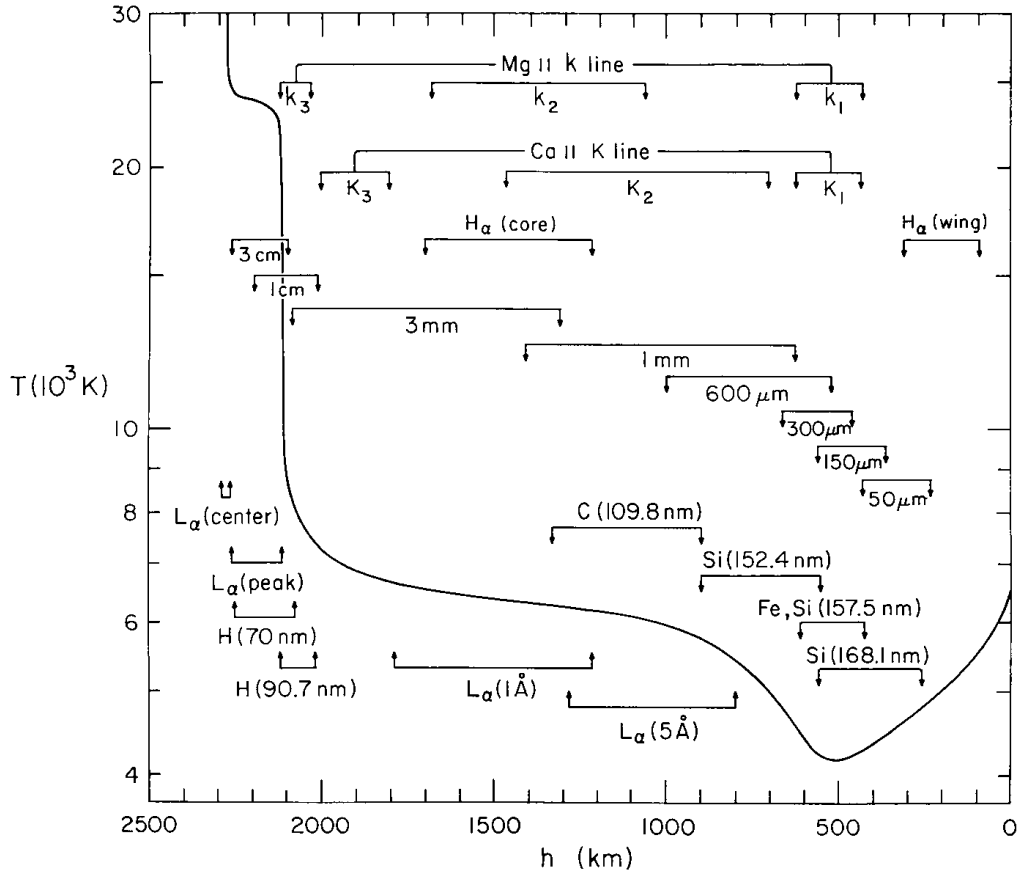

Figure 3.1: Depths of line formation – The formation heights of several spectral lines are indicated. The continuous line traces the temperature stratification of the quiet Sun derived by Vernazza et al. (1981). The transition from the photosphere to the chromosphere is at ≈500 km, from the chromosphere to the corona at ≳2000 km. Note that the Hα core is formed in the chromosphere while the wings are still formed in the photosphere. LTE line formation is not valid in the Hα core. The figure is taken from Vernazza et al. (1981).

Similarly light may be scattered into the light path and adds up to the intensity, described by the coefficient j_ν^{S}. This again merely is redistributed light while emission from de-excited atoms, for example, adds energy to the thermal pool of the radiation field (j_ν^{T}):

$$j_\nu = j_\nu^{\mathrm{T}} + j_\nu^{\mathrm{S}} \tag{3.17}$$

In the case of *pure absorption*, photons are absorbed completely and all emitted photons are newly created with a distribution governed by the physical state of the material. Hence the source function for pure absorption S_ν^{p} is given by the Planck function $B_\nu(T)$ (Eq. 3.14), and the law of Kirchhoff-Planck relates the absorption and emission coefficients:

$$S_\nu^{\mathrm{p}}(T) = B_\nu(T) = \frac{j_\nu^{\mathrm{T}}}{\kappa_\nu} \tag{3.18}$$

Furthermore the scattering coefficient j_ν^{S} is given by:

$$j_\nu^{\mathrm{S}} = \sigma_\nu J_\nu, \tag{3.19}$$

where J_ν is the mean intensity (Eq. 3.3). Solving Eq. 3.18 for j_ν^{T} and using Eqs. 3.4, the definition of the source function, and the components of opacity and emissivity (Eqs. 3.16 and 3.17), the total source function is expressed by:

$$S_\nu = \gamma_\nu B_\nu + (1 - \gamma_\nu) J_\nu \tag{3.20}$$

(Gray 1992, p. 98) where $\gamma_\nu \equiv \frac{\chi_\nu}{\kappa_\nu}$. Obviously the specification of χ_ν and σ_ν is sufficient under LTE conditions (Eq. 3.16).

Eqs. 3.3, 3.4, and 3.20 further illustrate that the problem of radiative transfer is not described by a simple differential equation. In the equation of radiative transfer, the specific intensity I_ν is related to the source function S_ν which partly depends on the mean intensity J_ν and thus again on I_ν. Hence the equation of radiative transfer is an inhomogeneous, non-linear *integro-differential equation* which cannot be solved analytically.

3.2.6 Line profiles

The absorption coefficient χ_ν is comprised of contributions from bound-free and free-free (continuous absorption) as well as bound-bound transitions (line absorption):

$$\chi_\nu = \chi_\nu^{\mathrm{bb}} + \chi_\nu^{\mathrm{bf}} + \chi_\nu^{\mathrm{ff}} \tag{3.21}$$

MAFAGS and *LINFOR* include the bound-free transitions of H and He^+, the bound-free and free-free transitions of H^-, the free-free transitions of H_2^-, absorption by H_2^+ and H_2, bound-free transitions of He, free-free transitions of He^-, bound free transitions of the neutral species of C, N, O, Si, Fe, Al, Mg, and Ca, and free-free transitions of all positive ions (Reile 1987). In *MAFAGS*, the time expensive direct calculation of opacities can be avoided by optionally using *ODF* (see below). For the present work, I am specifically interested in the bound-bound transition, i.e. the formation of spectral lines. The line absorption coefficient of bound-bound transitions between a level *n* and a level *i* with

energy levels $E_i > E_n$ of an element m in an ionisation stage r under the assumption of total redistribution and LTE is given by (Fuhrmann 1993; Reile 1987):

$$\chi_\nu = \frac{\pi e^2}{m_\mathrm{e} c} \frac{1}{\rho k T} \frac{P_\mathrm{r,m}}{U_\mathrm{r,m}(T)} g_\mathrm{n} f_\mathrm{ni} \Phi_\mathrm{ni}(\nu) e^{-\frac{E_\mathrm{n}}{kT}} E(\nu, T) \tag{3.22}$$

$\Phi_\mathrm{ni}(\nu)$ is the profile function, $P_{r,m}$ the partial pressure of an element m at the ionisation stage r, f_ni the oscillator strength for the transition (see below), m_e the electron mass, and $E(\lambda, T)$ is the correction for stimulated emission $E(\nu, T) = 1 - e^{-\frac{hc}{\nu k T}}$. In *MAFAGS* and *LINFOR*, all quantities are used in terms of wavelength instead of frequency.

$$\chi_\lambda = \frac{\pi e^2}{m_\mathrm{e} c^2} \frac{1}{\rho k T} \frac{P_\mathrm{r,m}}{U_\mathrm{r,m}(T)} g_\mathrm{n} f_\mathrm{ni} \lambda_\mathrm{ni}^2 \Phi_\mathrm{ni}(\lambda) e^{-\frac{E_\mathrm{n}}{kT}} E(\lambda, T) \tag{3.23}$$

The *line profiles* Φ_λ are subject to a variety of line broadening mechanisms: radiation damping, pressure broadening and Doppler broadening.

Radiative damping and natural line broadening

A simple model for absorption of light by matter is the absorption of a plane electromagnetic wave by a dipole. Following Gray (2005, p. 234 et seq.), the atomic absorption coefficient in this case is given by:

$$\alpha(\lambda) = \frac{e^2}{mc} \frac{\lambda^2}{c} \frac{\gamma \lambda^2 / 4\pi c}{\Delta\lambda^2 + (\gamma \lambda^2 / 4\pi c)^2} \tag{3.24}$$

where $\Delta\lambda$ is the distance from the line centre. The damping constant in the classical treatment has to be adopted in cases where damping constants are not available from the literature:

$$\gamma_\mathrm{rad} = \frac{a}{\lambda^2} \tag{3.25}$$

LINFOR adopts the constant $a = 0.221$ as given in Fuhrmann (1993, p. 167).
Integration over wavelengths yields:

$$\int_0^\infty \alpha \mathrm{d}\lambda = \frac{\pi e^2}{mc} \frac{\lambda^2}{c}$$

A quantum mechanical treatment gives rise to the *oscillator strength* f:

$$\int_0^\infty \alpha \mathrm{d}\lambda = \frac{\pi e^2}{mc} \frac{\lambda^2}{c} f$$

The oscillator strength can be defined for both emission and absorption. These cases are related by:

$$g_\mathrm{u} f_{em} = g_\mathrm{l} f_{abs} \tag{3.26}$$

where g_u is the statistical weight of the upper level of the transition and g_l of the lower level. Therefore, oscillator strengths are unambiguously given by gf values.

Collisional or pressure broadening

Collisions of the absorber with other particles change the energy levels involved in the transition. This results in additional line broadening when averaged along the line of sight. The energy change depends on the distance R of the colliding particles and can be approximated by:

$$\Delta E \propto R^{-n}$$

The exponent n depends on the type of interaction:

n	type	source of perturbation
2	Linear Stark effect	ions and electrons
3	Resonance broadening	dipole coupling with same species
4	Quadratic Stark effect	electrons
6	Van der Waals broadening	neutral particles

The damping constant γ_4 for the quadratic Stark effect is related to the Stark interaction constant $\log C_4$ taken from the literature (Gray 1992, p. 215):

$$\log\gamma_4 = K + \frac{2}{3}\log C_4 + \log P_\mathrm{e} - \frac{5}{6}\log T$$

The electron pressure P_e and the temperature T are given by the model atmosphere calculated with *MAFAGS*. The exact value of K is uncertain and is 19.4 in *LINFOR*.

The van der Waals broadening in cool stars is mostly due to interaction with neutral helium and hydrogen atoms. Similar to the quadratic Stark effect, the van der Waals damping constant γ_6 is related to the van der Waals interaction constant $\log C_6$ by (Gray 1992, p. 217):

$$\log\gamma_6 \approx 19.6 + 0.4\log C_6(\mathrm{H}) + \log P_\mathrm{g} - 0.7\log T \tag{3.27}$$

The gas pressure P_g and the temperature T are given by the model atmosphere. Equation 3.27 is only an approximation giving the general behaviour while the implementation in *LINFOR* is more complicated.

Thermal broadening

Thermal broadening is due to the thermal movement of the absorbers and emitters. The line of sight velocity v_r results in a wavelength shift:

$$\frac{\Delta\lambda}{\lambda} = \frac{v_\mathrm{r}}{c}$$

where c is the speed of light. Thus the distribution of wavelength shifts is proportional to the Maxwellian distribution of velocities with a width of $v_0 = \sqrt{\frac{2kT}{m}}$ where k is Boltzmann's constant, T the local temperature and m the mass of the species. We get for the width of the wavelength distribution:

$$\Delta\lambda_\mathrm{D} = \frac{v_0}{c}\lambda$$

The total line profile is given for a transition between the levels n and i by:

$$\Phi_{\mathrm{ni}} = \frac{H(a,u)}{\sqrt{\pi}\Delta\lambda_{\mathrm{D}}} \tag{3.28}$$

with $a = \frac{\gamma_{\mathrm{ni}}}{4\pi c}\frac{\lambda_{\mathrm{ni}}^2}{\Delta\lambda_{\mathrm{D}}}$ and $u = \frac{\Delta\lambda}{\Delta\lambda_{\mathrm{D}}}$ (Reile 1987, p. 98). $H(a,u)$ is the *Hjerting function* which is related to the *Voigt function* (Gray 1992):

$$V(a,u) = \frac{\lambda^2}{c\sqrt{\pi}\Delta\lambda_{\mathrm{D}}} H(a,u) \tag{3.29}$$

In *LINFOR* and *MAFAGS*, this function is evaluated by means of approximations and series expansions[2].

The damping constant γ_{ni} is composed of the natural damping constant γ_{rad}, the Stark damping constant γ_4, and the van der Waals damping constant γ_6:

$$\gamma = \gamma_{\mathrm{rad}} + \gamma_4 + \gamma_6 \tag{3.30}$$

Curve of growth and microturbulence

The microturbulence is a free parameter introduced in the analysis of *curves of growth* and describes the monotonic increase of line equivalent width with increasing abundance of the absorbing species. The shape changes with equivalent width. The equivalent width of *weak lines* ($W_\lambda \lesssim 80\,\mathrm{m\AA}$) is proportional to the abundance. The line width is dominated by the thermal broadening $\Delta\lambda_{\mathrm{D}}$. The line saturates with increasing abundance and starts to form strong wings. The Doppler profile is still present in the very central part of the line, the *Doppler core*. In this part of the curve of growth, the equivalent width increases with the square root of the abundance. The microturbulence ξ accounts for the observed fact that the equivalent widths of saturated lines are larger than predicted from thermal and damping broadening alone.

The effects of turbulent motion are regarded in two limits within the line synthesis, the microturbulence and the macroturbulence limit. In the microturbulence limit, turbulent cells are small compared to the optical depth and effectively increase the thermal velocity in the absorption process. They are approximated by a Gaussian velocity distribution with the width ξ [km/s]:

$$N(v)\mathrm{d}v = \frac{1}{\pi^{\frac{1}{2}}\xi} e^{-(\frac{v}{\xi})^2}$$

This distribution is formally convolved with the absorption coefficient. The convolution of Gaussians gives a new Gaussian so that the total line broadening is implemented by:

$$\Delta\lambda_{\mathrm{D}} = \frac{\lambda}{c}\left(v_0^2 + \xi^2\right)^{\frac{1}{2}}$$

[2] cf. Gray (1992, p. 227 et seq.) and Mihalas (1978, p. 280 et seq.).

Accounting for macroturbulence, rotation and instrumental profile

In the macroturbulence limit, turbulent cells are large compared to the optical depth. The radiative transfer is unchanged and only the non-thermal velocity broadening is increased. In consequence, the macroturbulence parameter ζ [km/s] conserves the equivalent width. The *radial-tangential* model postulates Gaussian distributed velocities with a parameter ζ_{RT} either along stellar radii or tangent to the surface as is suggested by the motion of convective cells.

The macroturbulence is taken into account by convolving the theoretical spectrum after synthesis with *LINFOR*. Additionally the synthetic spectrum is convolved with the non-thermal broadening due to stellar rotation and due to the *instrumental profile* which incorporates the limited resolution of the spectrograph.

Opacity distribution functions (*ODF*)

Instead of calculating the absorption of individual lines, so-called opacity distribution functions can be optionally used in *MAFAGS*. Following Kurucz (1979), these are created by dividing the whole wavelength scale in small intervals with widths of typically 10 Å. In each of these wavelength intervals i, the wavelengths are rearranged and mapped with a function f_i onto the interval $[0; 1]$ in a way that the opacities $\kappa_i(\lambda)$ become monotonic increasing distributions $\kappa_i(f_i(\lambda))$. The argument behind this method is that the atmospheric structure depends only on wavelength integrals of the radiation quantities and not on monochromatic quantities. Therefore, the integrals can be obtained from these distribution functions as well. The distribution functions are pre-calculated on a grid of electron and gas pressure, temperature, and abundances, saving much time in the actual calculation of the model atmospheres. *ODF* are sufficient for the calculation of the atmospheric stratification.

Fuhrmann et al. (1997a) argue that the solar abundance most probably equals the meteoritc value of $\log\varepsilon(\mathrm{Fe}) = 7.51$ which is considerably lower than the value of $\log\varepsilon(\mathrm{Fe}) = 7.67$ adopted by Kurucz (1992). Therefore, instead of using the original Kurucz *ODF* (see Kurucz 1995), *MAFAGS* adopts interpolated *ODF* scaled by -0.16 dex. For more details and a discussion, see Fuhrmann et al. (1997a) and (Fuhrmann 1993, p. 157-161, 164). .

Line profiles with *MAFAGS* and *LINFOR*

The following paragraphs outline the treatment of line absorption and compile the references for the line data. A discussion is not included. Instead the reader is referred to the quoted literature.

The treatment of the Balmer and Lyman series in *MAFAGS* neglects Doppler broadening, radiation damping and resonance damping. Only the linear Stark effect according to Edmonds, Schlüter, & Wells (1967) is accounted for. Correction for stimulated emission is not included. In the present implementation of *LINFOR*, the unified theory by Vidal, Cooper, & Smith (1970) is used. Instead of applying the tables of Vidal, Cooper, & Smith

(1973), the Stark profiles were interpolated in the recalculated tables of T. Schöning and K. Butler (Fuhrmann 1993; Fuhrmann, Axer, & Gehren 1993). This profile is convolved with resonance broadening (Ali & Griem 1965, 1966) including radiation damping for Hα-Hδ.

The profiles of metallic lines in *MAFAGS* account for Doppler, radiation, and van der Waals broadening according to the theory of Unsöld (1955) with empirical corrections of Holweger (1972) and O'Mara (1976). In *LINFOR*, *astrophysical* van der Waals broadening constants γ_6 are used, i.e. the constants were not obtained from laboratory measurements but fitted to match the solar flux atlas of Kurucz, Furenlid, & Brault (1984) (Fuhrmann 1993; Fuhrmann et al. 1997a). Radiation damping constants for magnesium were taken from Chang (1990). The radiation damping constants for iron were obtained from a line list of Kurucz if available and otherwise calculated from the classical formula Eq. 3.25 (Fuhrmann 1993). The damping due to the Stark effect γ_4 is taken into account only for Mg I λ5172, 5183 and 5528 Å (Fuhrmann et al. 1997a). loggf values for the list of Fe I and Fe II lines are again derived from the solar flux atlas of Kurucz et al. (1984) (Fuhrmann et al. 1997a). An average of literature values was adopted for the oscillator strengths of the Mg Ib triplet (Fuhrmann 1993, table 7.2). The oscillator strengths of the remaining magnesium lines were determined in the same way as these of iron. See Axer, Fuhrmann, & Gehren (1994) for the derivation of astrophysical oscillator strengths and van der Waals damping constants. They emphasised the importance of the fact that these atomic data were derived with the same model atmospheres used in their subsequent stellar analyses. See Table C.1 for the adopted line data.

The absorption and emission processes are further controlled by the exact abundance pattern. The solar abundance pattern of *MAFAGS* and *LINFOR* is mostly based on Holweger (1979) (see Table 3.1).

3.2.7 Hydrostatic equilibrium

Hydrostatic equilibrium is assumed for solar-like stars on the main sequence. The gas pressure is the dominant pressure component:

$$\frac{\mathrm{d}P}{\mathrm{d}\tau_\lambda} = \frac{g}{\kappa_\lambda} \tag{3.31}$$

The mass of a thin photosphere is regarded negligible compared to the total mass of the star. Hence the surface gravity g is approximately constant throughout the atmosphere.

3.2.8 Convection

The *mixing-length theory* (Böhm-Vitense 1958) is a common approach to implement convection. Convection is modelled by rising warm cells which dissolve after a certain height l_{mix} and release their excess energy into the surrounding material. The efficiency of convection is thereby related to a free parameter $\alpha = l_{\mathrm{mix}}/H_{\mathrm{P}}$ where H_{P} is the pressure scale height. Analysing the temperature dependent wings of the Balmer lines, Fuhrmann (1993) concluded that the convective efficiency significantly influences the temperature

Table 3.1: The adopted solar elemental abundance pattern – Almost all abundances are taken from Holweger (1979). The few exceptions are indicated. The last column lists the number of ionisation stages accounted for in the synthetic line formation.

Z	element	$\varepsilon_\odot$	weight [u]	$N_{\rm ion}$
1	H	12.00	1.008	3
2	He	11.00	4.003	2
3	Li	3.28	6.939	2
6	C	8.58[1]	12.011	2
7	N	7.99[2]	14.007	2
8	O	8.92[3]	15.999	2
10	Ne	7.73	20.179	2
11	Na	6.28	22.990	2
12	Mg	7.53	24.305	3
13	Al	6.43	26.982	3
14	Si	7.50	28.086	3
15	P	5.35	30.974	3
16	S	7.20	32.060	3
17	Cl	5.26	35.453	2
18	Ar	6.83	39.948	2
19	K	5.05	39.100	2
20	Ca	6.36	40.080	3
21	Sc	2.99	44.958	3
22	Ti	4.88	47.900	3
23	V	3.91	50.944	3
24	Cr	5.61	51.996	3
25	Mn	5.47	54.938	3
26	Fe	7.51[4]	55.847	3
27	Co	4.85	58.940	3
28	Ni	6.18	58.710	3
29	Cu	4.24	63.550	3
30	Zn	4.60	65.370	3
38	Sr	2.93	87.630	3
39	Y	2.18	88.908	3
40	Zr	2.46	91.220	3
56	Ba	2.18	137.350	3
57	La	1.07	138.920	3
58	Ce	1.58	140.130	3
60	Nd	1.40	144.250	3
62	Sm	0.88	150.360	3
63	Eu	0.48	151.960	3

[1]Stürenburg & Holweger (1990); Biemont et al. (1993) [2]Biemont et al. (1993) [3]Lambert (1978) [4]Biemont et al. (1991)

stratification of the *MAFAGS* atmospheres. He was able to derive consistent temperatures when setting α to 0.5. This value is adopted for all stars in the present work within the scope of the differential analysis.

3.2.9 Three-dimensional hydrodynamics versus one-dimensional hydrostatics

Looking at the Sun, we find photospheric features like the granules[3] and spots. They have an effect onto the integrated stellar light, too, as can be seen from shifts and asymmetries of spectral lines (Asplund 2005, fig. 3). Within this context, the solar metallicity has recently been subject to a substantial revision (see Asplund 2005 for a review). Steffen & Holweger (2002) encountered a substantial increase of line strength when modelling the convective solar surface layers by two-dimensional hydrodynamics, and derived "granulation abundance corrections". Asplund, Grevesse, & Sauval (2005) presented a relative solar metal abundance lower by almost a factor of two than previously adopted. Their analysis is based on non-LTE calculations and a three-dimensional hydrodynamic solar model atmosphere. At first, the differential analysis is not affected by these results since abundances are measured relative to the Sun.

Ludwig & Kučinskas (2005) stated that the microturbulence and macroturbulence parameters as well as the mixing-length parameter of convection have become obsolete with the advent of three-dimenionsal hydrodynamical models. Yet they admitted that a grid of such models has not yet been available.

3.3 The stellar parameters

After specifying the theoretical tools, we can turn to the determination of the stellar parameters. Synthesised Hα and Hβ lines are compared to the observed profiles in order to infer effective temperature (Sect. 3.3.1). Sect. 3.3.2 describes the derivation of surface gravities. Iron lines further allow to determine the iron abundance, the microturbulence, and the projected rotational velocity (Sect. 3.3.3). It is mostly the effective temperature which indicates the mass of the star in the Hertzsprung-Russell (HR) diagram (Sect. 3.3.5).

3.3.1 Effective temperature

The effective temperature $T_{\rm eff}$ characterises the radiative flux emitted from the stellar photosphere connecting the stellar luminosity L to the stellar radius R by the *Stefan-Boltzmann* law:

$$L = 4\pi\sigma R^2 T_{\rm eff}^4 \tag{3.32}$$

[3]The granulation pattern results from the overshooting of convective cells from the solar convection zone into convectively stable layers. See Stix (1989) for details.

with the *Stefan-Boltzmann constant* $\sigma = 5.67{\cdot}10^{-5}\frac{\mathrm{erg}}{\mathrm{cm^2 s K^4}}$. Accordingly the most obvious way to derive effective temperature relates photometric measurements ($\rightarrow L$) to measured apparent diameters ($\rightarrow R$). This method works only for certain stars with resolved angular diameters (Perrin et al. 1998, Hanbury Brown et al. 1974, Richichi et al. 1998). The infrared flux method is a modification which partly relies on model atmospheres (Blackwell & Shallis 1977). Most conveniently, effective temperatures are derived from colours or spectral types by using calibrations based on direct measurements. Yet these are only valid in a statistical sense (Fuhrmann 1993; Fuhrmann et al. 1994).

Precise effective temperatures have been derived from the Balmer lines since the early 1980's although the temperature sensitivity of the Balmer lines of F and G stars has already been realised in the 1950's. The advance is due to improvements in spectroscopic observations, atmosphere modelling, and line modelling (see Fuhrmann 1993 for a historical account). Fuhrmann (1993) and Fuhrmann et al. (1994) concluded that the Balmer lines allow to derive more precise effective temperatures than photometric methods[4].

Figure 3.2 shows an example. The solar temperature is derived from an observation of the lunar disk which reflects the light of the Sun. The adopted effective temperature $T_{\mathrm{eff}} = 5780{\pm}60\,\mathrm{K}$ is consistent with the literature value for the Sun and with the value derived from the Hβ line. The wings are considered at their strongest curvature because the sensitivity to effective temperature is highest there. The LTE modelling is insufficient at a relative flux lower than 0.7 (see Sect. 3.2.4 and Appendix E) but these parts of the line core are not used in any case.

In the case of stars with spectral types F, G and K, the curvature of the Balmer line wings strongly depends on effective temperature but hardly on other parameters (surface gravity, metallicity). Hence the effective temperature can be derived first with rough main-sequence estimates for surface gravity and iron abundance.

The stars of the present sample are still young so that the Balmer lines may be effected by chromospheric emission. In the case of UMa group stars, the consistency of the temperatures from Hα and Hβ gives support that at least the Hα wings are unaffected by chromospheric activity (Fuhrmann 2004; Cayrel, Cayrel de Strobel, & Campbell 1988). Chromospheric activity mostly affects the line cores which are not considered in the analysis. In the case of even younger stars, the determination of effective temperatures from the Hα wing may be sincerely affected by activity, e.g. EK Dra (König et al. 2005).

3.3.2 Surface gravity

The following sections describe the methods for the derivation of surface gravities. Two methods were also applied by Fuhrmann (1998): firstly the iron ionisation equilibrium and secondly the strong line method using the Mg Ib triplet. Neither the iron ionisation equilibrium nor the Mg Ib triplet can be used for some of the hotter stars so that surface gravities are determined from *Hipparcos* distance in these cases.

[4] At first, the Balmer line temperatures do not reflect the true effective temperature in the sense of the definition Eq. 3.32 but are only valid in the context of the used model atmospheres. Comparing with other temperature determinations, Fuhrmann showed that these temperatures are accurate indeed.

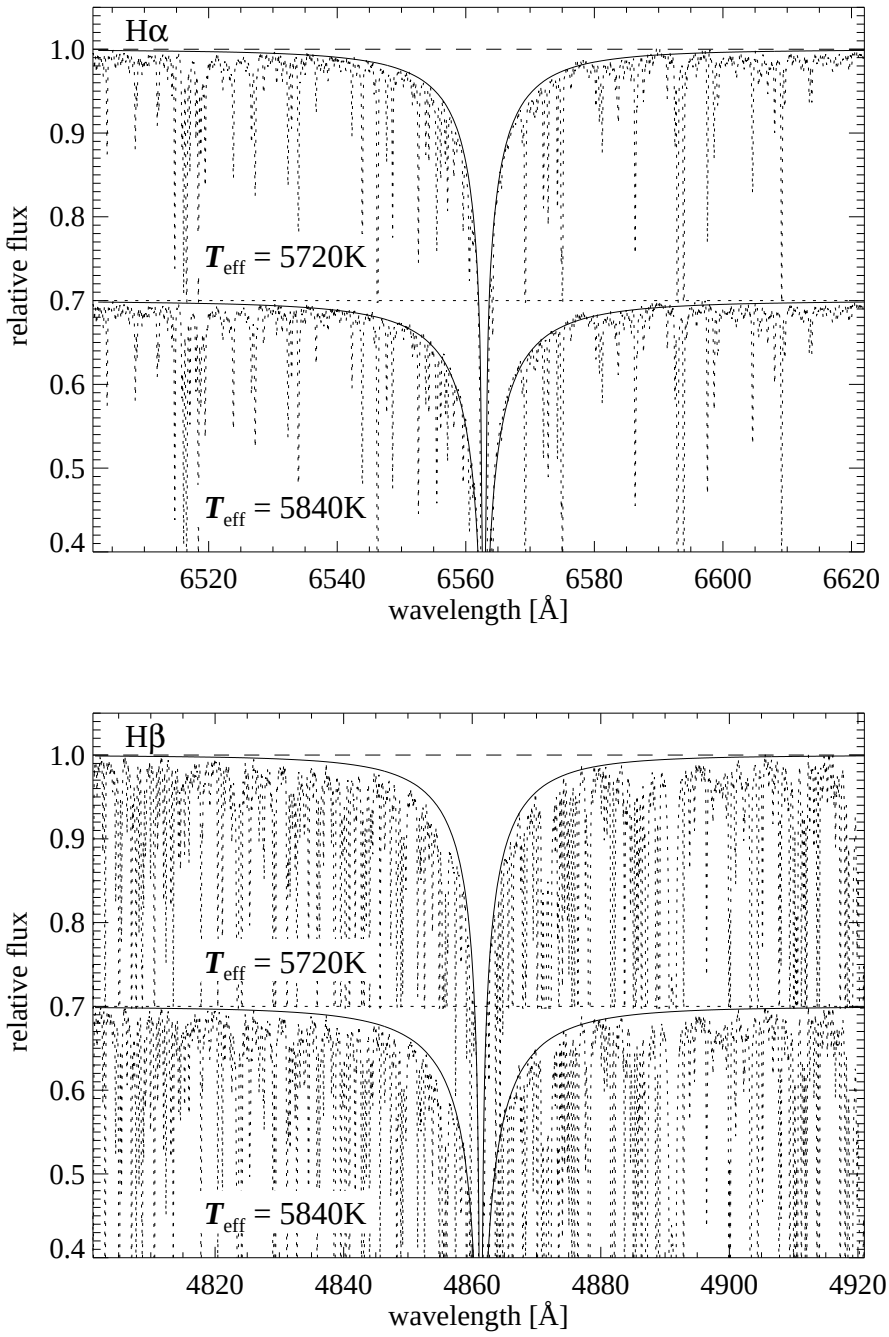

Figure 3.2: Fitting the Balmer lines of a moon spectrum in order to derive the effective temperature – top: Two theoretical fits (solid line) for different temperatures (top and bottom panel) constrain the observed Hα profile (dots) which is blended by other lines (cf. Fuhrmann et al. 1997a). **bottom:** Same as the upper figure but for the Hβ line. The profile can be recovered similarly although it is heavily blended by many lines.

Surface gravity from the iron ionisation equilibrium

The absorption of weak lines of two ionisation stages of an element is compared, in this case the neutral and the singly ionised states of iron, Fe I and Fe II, respectively. The surface gravity follows from the requirement that the absorption of both ionisation stages is related to the same elemental abundance. The physical background for the different behaviour of Fe I and Fe II lines can be retraced by following the reasoning in Gray (1992). The *Eddington approximation* is used for spectral lines in order to obtain estimates. Then the source function $S_\nu(\tau_\nu) \approx \frac{3}{4\pi}F_\nu(0)(\tau_\nu + \frac{2}{3})$ equals the flux $F_\nu(0)$ at an optical depth of ≈3.5 and the line profile is approximated by:

$$\frac{F_\mathrm{c} - F_\nu}{F_\mathrm{c}} \approx \frac{S_\nu(\tau_\mathrm{c} = 3.5) - S_\nu(\tau_\nu = 3.5)}{S_\nu(\tau_\mathrm{c} = 3.5)} \tag{3.33}$$

F_ν is the flux in the line and F_c is the continuum flux. After several further steps[5], we get

$$\frac{F_\mathrm{c} - F_\nu}{F_\mathrm{c}} \propto \frac{l_\nu}{\kappa_\nu} \tag{3.34}$$

κ_ν varies hardly across the line. In consequence, the profile of a weak line in LTE has approximately the shape of the line absorption coefficient l_ν (Gray 1992, p. 275 et seq.).

Electron and gas pressure in photospheres with spectral types F, G, and K are related to surface gravity g by (Gray 1992):

$$P_\mathrm{e} \propto g^{\frac{2}{3}} \tag{3.35}$$

$$P_\mathrm{g} \propto g^{\frac{1}{3}} \tag{3.36}$$

In solar-like photospheres, most of the iron is found in the singly ionised stage. Hence the occupation of the upper level N_{r+1} in the Saha equation (Eq. 3.13) is approximately given by the total number of iron absorbers. Consequently the pressure dependence of the numbers of neutral absorbers in Eq. 3.13 reduces to $N_r \propto P_\mathrm{e}$. The line absorption coefficient l_ν is proportional to N_r while the continuous absorption coefficient κ_ν is dominated by H^- and thus proportional to P_e . Therefore $\frac{l_\nu}{\kappa_\nu}$ does not change with pressure and gravity in the case of Fe I lines.

The number of Fe II ions approximately equals the constant total number of iron absorbers in Eq. 3.13 as stated above so that l_ν does not change with pressure. Considering the pressure dependence of κ_ν, we get:

$$\frac{l_\nu}{\kappa_\nu} \propto \frac{1}{P_\mathrm{e}} \tag{3.37}$$

i.e. the dependence on surface gravity enters indirectly by the dependence of the ionic stage on electron pressure. This qualitative behaviour is nicely illustrated by Fig. 3.3.

[5] Gray (1992, p. 276 et seq.)

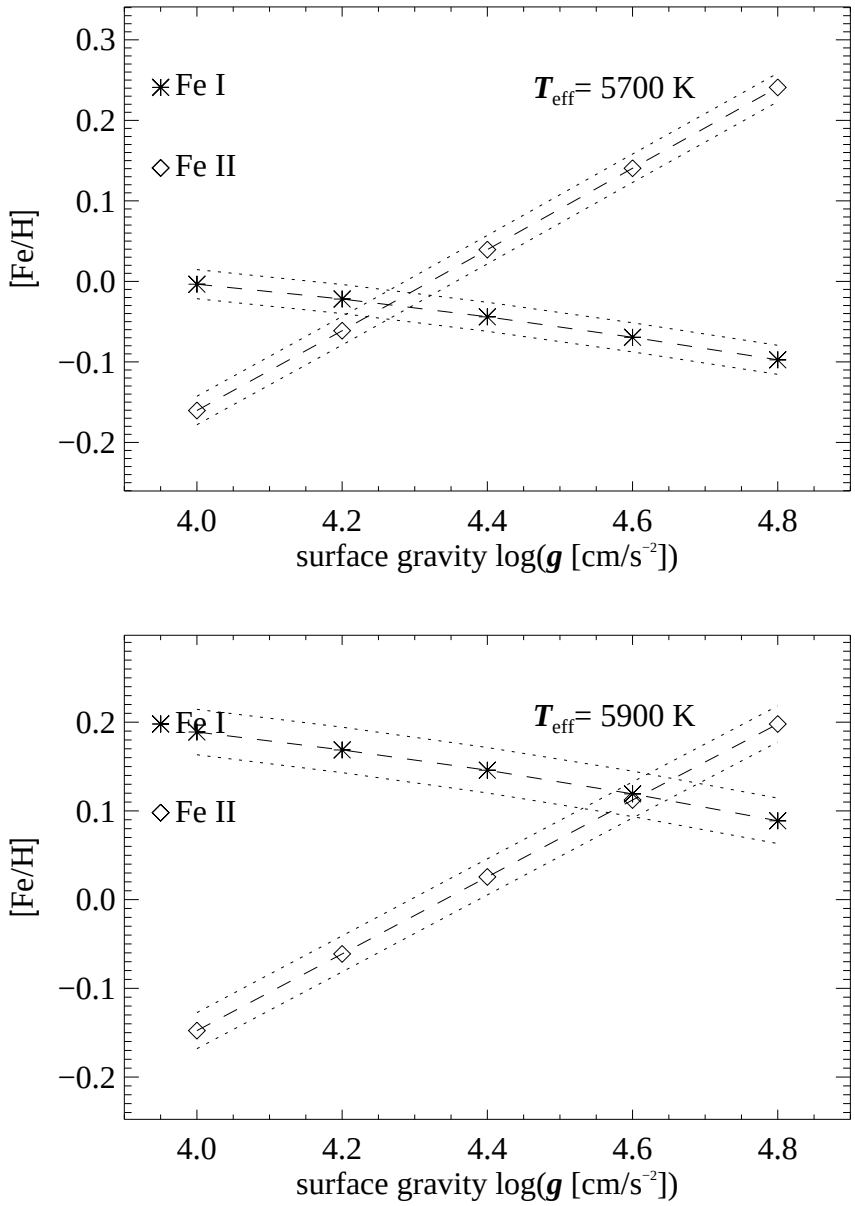

Figure 3.3: The solar surface gravity derived from the iron ionisation equilibrium – Abundances were derived from 27 Fe I and 11 Fe II lines of a spectrum of the lunar disk. The diagrams show the variation of derived abundance [Fe/H] with changing surface gravity log$g$, separately for Fe I and II and for different effective temperatures: 5700 K **(top)** and 5900 K **(bottom)**. The dotted lines indicate the 1 σ-scatter of the values from the individual lines. The abundance determined from Fe II strongly varies with surface gravity while the value derived from Fe I does not (see text). The analysis of both species has to yield the same Fe abundance so that the intersection of both curves determines the surface gravity. In this case, the Balmer lines support an effective temperature of 5780±60 K so that interpolation gives log$g$ = 4.43±0.09.

The measured quantities are the equivalent widths[6] of Fe I and Fe II lines. Iron abundances are derived from these equivalent widths on a grid of surface gravities. The correct surface gravity is then found by requiring that both species yield the same total iron abundance (see Fig. 3.3). The error of the surface gravities is estimated by repeating the derivation with the limits of the effective temperatures. The sensitivity of surface gravity to effective temperature is pronounced: $\partial_{\mathrm{T}} \log g \approx \frac{0.15\,\mathrm{dex}}{100\,\mathrm{K}}$.

The ionisation equilibrium is controlled by both effective temperature and surface gravity, in contrast to the Balmer line wings. The effective temperature is fixed independently by the Balmer lines.

Some more words have to be said on the calculation of iron abundance for the iron ionisation equilibrium. Instead of applying curves of growth, theoretical spectra for a dense grid of atmospheric parameters (T_{eff}, log$g$, [Fe/H], ξ_{t}) are used. Theoretical equivalent widths for all iron lines are calculated from these spectra and compared to the observed equivalent widths. The microturbulence ξ_{t} is accounted for by an initial estimate, usually the solar value[7], and is constrained iteratively.

The coolest stars in the stellar atmosphere analysis, HD 110463 and HD 109647 ($T_{\mathrm{eff}} \approx 5000\,\mathrm{K}$), are at the limits of the grid of theoretical spectra[8]. In these cases the stellar parameters are found by directly fitting the observed lines and requiring following constraints:

- The microturbulence is adjusted until the abundances derived from each Fe I and Fe II line do not show any trend with the equivalent widths.
- The surface gravity is changed until the difference between the average abundances of Fe I and Fe II becomes smaller than 0.05 dex. According to Luck & Heiter (2005), such a difference adds an error of 0.10 dex in the surface gravity. The use of a stricter constraint does not improve the overall uncertainty which is governed by the large scatter of the few useful Fe II lines.

At effective temperatures of ≈5000 K, the analysis is complicated by severe line blends. Furthermore the number of suitable Fe II lines is strongly reduced. The few available Fe II lines were checked for blends using the *extract stellar* feature of *VALD*[9] (Kupka et al. 2000, 1999; Ryabchikova et al. 1997; Piskunov et al. 1995) with a sensitivity limit of 0.05.

The UMa group members are chromospherically active. In order to avoid influence of chromospherical effects, only iron lines with equivalent widths $\lesssim$60 mÅ are used according to Fuhrmann (2004) because these form in the deeper layers of the photosphere.

[6] These equivalent widths do not originate from direct integrations of the observed line profiles because these are subject to corruptions like blends with lines of other species rendering erroneous equivalent widths. Such problems are avoided for the most part by using the equivalent widths of synthetic lines calculated with *LINFOR* and fitted to match the observed spectrum.

[7] Fuhrmann (1998) derived a value of $\xi_{\mathrm{t}} = 0.95 \pm 0.15$ km/s for the Sun pointing out that the precise value depends on the quality of the modelling, on the spectrum, and on the model atmospheres.

[8] An extension of the grid to lower effective temperatures requires a substantial programming effort not done within the present work (see App. D for details).

[9] Vienna Astrophysical Line Data-Base

This value had to be compromised repeatedly due to the sparseness of weak lines so that a limit of $\lesssim 80$ mÅ was applied mostly.

Surface gravity from strong lines

The surface gravities of the hotter stars ($\gtrsim$6000 K) are underestimated when derived with the iron ionisation equilibrium (cf. Fuhrmann et al. 1997a, fig. 4). The discrepancies probably arise from the Fe I lines. Most iron is ionised in hotter stars so that the lines of neutral iron depend on the details of the temperature structure described insufficiently by the LTE model atmospheres (Fuhrmann et al. 1997a).

Surface gravities of stars hotter than the Sun can still be determined from strong lines since their pressure broadened wings indicate surface gravity (see Sect. 3.2.6). Fuhrmann et al. (1997a) recommended the strong Mg Ib triplet because oscillator strengths and the collisional damping are well-known. Furthermore, the continuum can be placed accurately in this spectral region (cf. Sect. 2.4). The Mg I λ5167 Å line suffers from severe blends whereas the other two triplet lines Mg I λ5172 Å and λ5183 Å provide redundant information on the surface gravity. Figure 3.4 shows synthetic lines fitted to match the solar Mg Ib triplet.

Of course, the depth of the Mg Ib triplet also depends on the magnesium abundance and the microturbulence. The microturbulence is derived from iron lines (see Sect. 3.3.3).

Fuhrmann et al. (1997a) pointed out that the ionisation potential and the cosmic abundance of magnesium were similar to that of iron. Consequently, weak Mg I lines are found (e.g. Mg I λ4571 Å and λ5711 Å) which are independent of surface gravity and can be used to fix the magnesium abundance. Yet this abundance is only valid as an intrinsic parameter of *LINFOR*. Similar to the iron abundance derived from Fe I lines, it is presumably not very accurate for hotter stars.

Fuhrmann (2004) encountered problems with the magnesium line wings of hotter UMa group members. Possibly the line cores of stronger Mg I lines were affected by chromospheric activity. Moreover large projected rotational velocities of $v\sin i \gtrsim 40$ km/s smeared out the weak Fe II lines and inhibited the proper derivation of abundances. Consequently Fuhrmann (2004) recommended to use surface gravities which are derived from the *Hipparcos* distance. On the other side, all hot stars in the present sample show sufficiently low $v\sin i$ probably due to different inclination angles so that weak lines can still be used. In the end, substantially raised Mg Ib wings hamper the derivation of surface gravities of several sample stars hotter than $\approx$ 5900 K.

Surface gravity from distance

The surface gravity of some of the hotter stars of the sample can be neither derived from the iron ionisation equilibrium nor from the wings of strong lines. In these cases, the only way is to calculate surface gravities from the well-known *Hipparcos* distances and magnitudes. The distance modulus is:

$$V - M_V = 5 \cdot \log d - 5 + A_V \tag{3.38}$$

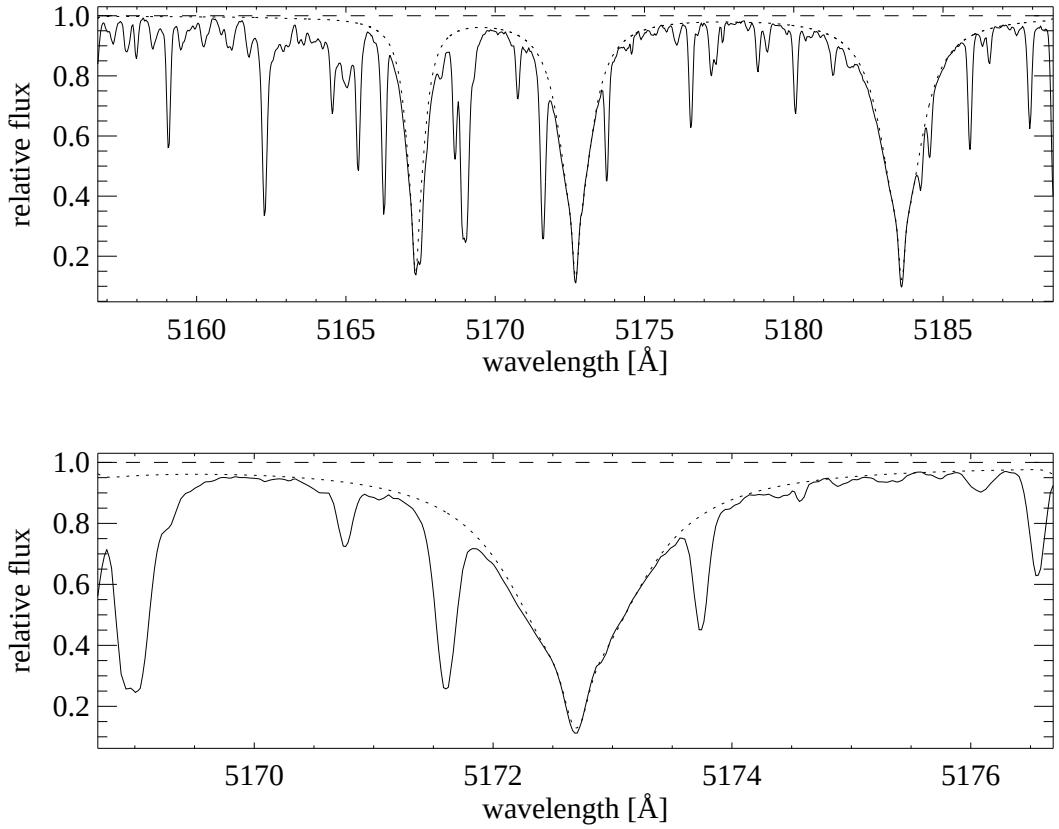

Figure 3.4: The solar Mg Ib triplet – Top: A fit of a synthetic spectrum (dots) with log$g$ = 4.40 to the observed solar Mg Ib triplet (solid) is shown. The spectrum originates from an observation of the bright lunar disk. **Bottom:** The region centred on λ5172 Å is enlarged.

with the apparent V-band magnitude V, the corresponding absolute magnitude M_V, the interstellar absorption A_V, and the distance d. The absolute magnitude is connected to the luminosity by:

$$M_V = M_{\rm bol} + B.C._{\rm V} = M_{\rm bol,\odot} - 2.5 \cdot \log \frac{L}{L_\odot} + B.C._{\rm V}$$

with the *bolometric correction* $B.C._{\rm V}$. The luminosity in turn is expressed in terms of the stellar parameters derived in the analysis, i.e the mass M, the surface gravity g, and the effective temperature $T_{\rm eff}$:

$$L \propto R^2 T_{\rm eff}^4 \propto \frac{M}{g} T_{\rm eff}^4 \Longrightarrow \frac{L}{L_\odot} = \frac{M \cdot T_{\rm eff}^4 \cdot g_\odot}{M_\odot \cdot T_{\rm eff,\odot}^4 \cdot g}$$

Insertion into the equation of distance modulus (Eq. 3.38) gives after some rearrangements (cf. Fuhrmann et al. 1997b):

$$\log g = -2\log d + 4.44 + \log M + 4\log \frac{T_{\rm eff}}{5780\,{\rm K}} + \frac{2}{5}(V - A_{\rm V} - B.C._{\rm V} + 5 - M_{\rm bol,\odot}) \quad (3.39)$$

Obviously, some additional information is required:

- Distances d are calculated directly from precise *Hipparcos* parallaxes π by $d\,[{\rm pc}] = \frac{1}{\pi\,[''']}$.
- The apparent visual magnitude V is derived from the precise *Hipparcos* $H_{\rm P}$ magnitude using the conversion tables of Bessell (2000).
- The bolometric corrections $B.C._{\rm V}$ are taken from Alonso, Arribas, & Martínez-Roger (1995)[10].
- The interstellar extinction $A_{\rm V}$ can be neglected since all stars of the sample are nearby.
- The derivation of the mass M is described in Sect. 3.3.5.

Errors of surface gravities are calculated from Eq. 3.39 by error propagation. Photometric variability may strongly increase the errors but is expected to be low for the considered hotter stars of the sample (cf. Adelman, Coursey, & Harris 2000).

3.3.3 Abundances and microturbulence

The effects of abundances and microturbulence on the spectrum are intertwined. The same constraint as in Sect. 3.3.2 is applied: The abundances derived from each line must not correlate with equivalent width (cf. Gray 1992)! The microturbulence is usually

[10] They use another definition of $B.C._{\rm V}$ with opposite sign!

derived from the Fe II lines only because these are least affected by inadequacies in the model atmospheres. If the correct microturbulence is established, the measured iron abundance does not change with equivalent width and thus is known, too. Limits on the iron abundance are determined by repeating the analysis with the upper and lower limits on effective temperature. An adoption of abundance errors as small as 0.05 or lower hardly seems realistic. The accuracy of the analysis is entangled with the accuracy of the solar abundances and even these are not known to better than 0.04 dex (Asplund et al. 2005).

The value of the microturbulence and its scatter is finally confirmed by fitting several selected Fe II lines keeping the other parameters fixed at the determined values.

3.3.4 Instrumental profile, rotation, and macroturbulence

In contrast to the microturbulence, the projected rotational velocity does not change the equivalent width and thus is determined simultaneously. Instrumental profile and macroturbulence result in non-thermal broadening (cf. Sect. 3.2.6). In order to measure the rotational velocity, the rotational broadening has to be disentangled from the instrumental broadening and the broadening by macroturbulence.

The *instrumental broadening* is due to the finite resolution of the spectrograph and is approximately constant within each observing run. Eleven spectral windows with widths of 20 Å of an observed moon spectrum are used. These are convolved with the high resolution Kitt Peak solar flux atlas of Kurucz et al. (1984). The instrumental broadening is well described by a Gaussian. In the present work, it is quantified by the width of this Gaussian ranging within ≈3-5 km/s for the typical resolving power of ≈60000. The derived values are insofar insufficient as they are derived from some spectral windows only. In contrast, the instrumental profile may vary strongly along each Échelle order being largest at the order ends.

According to Fuhrmann (2000), the macroturbulence parameter is calculated from the linear fit given by Gray (1984):

$$\zeta_{\mathrm{RT}}[\mathrm{km/s}] = 3.95 \cdot T_{\mathrm{eff}}[10^3\mathrm{K}] - 19.25 \tag{3.40}$$

Then the projected rotational velocity is derived by fitting individual weak Fe II lines. The scatter of these values usually is below 0.50 km/s. An error of 1.0 km/s seems more realistic regarding the uncertainties in the instrumental broadening and the macroturbulence parameter.

3.3.5 Estimating the stellar mass

Evolutionary models for post-main (e.g. VandenBerg et al. 2000) or pre-main sequence stars (e.g. Baraffe et al. 1998) predict the evolution of the stellar parameters at a certain stellar mass. In the Hertzsprung-Russell diagram, the stars follow *evolutionary tracks* (Fig. 3.5). Stars with same age but different mass are aligned along *isochrones* (cf. Fig. 1.5). Estimates of the mass are obtained by comparing the measured values to

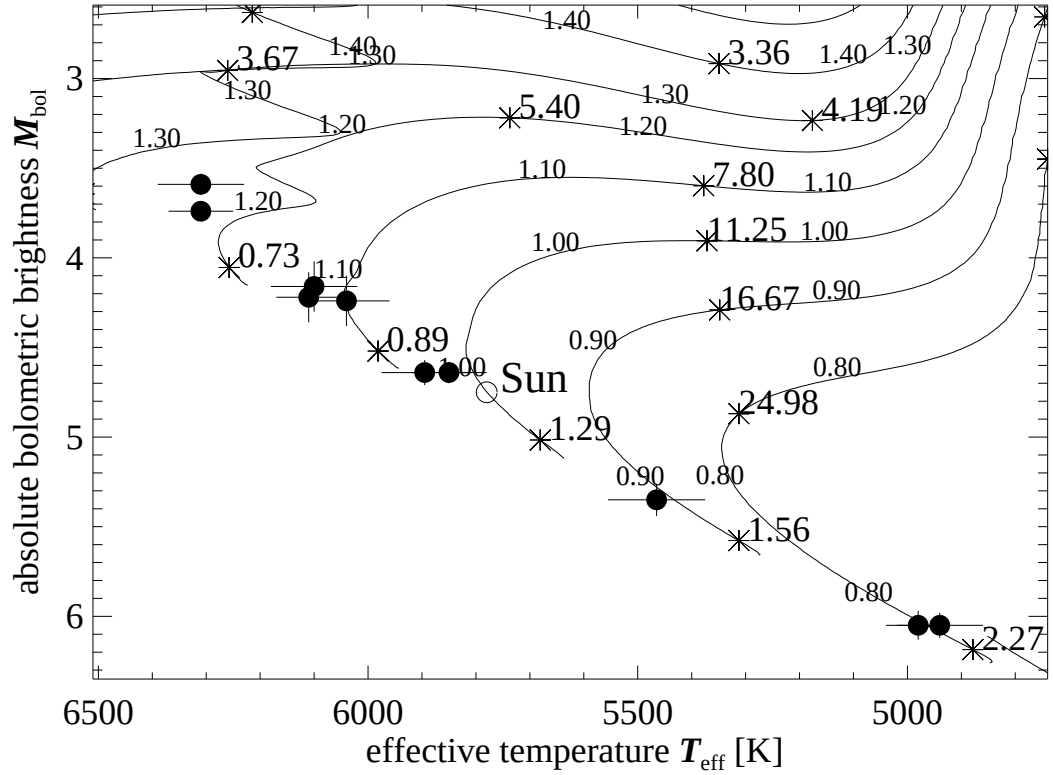

Figure 3.5: Estimation of mass in the Hertzsprung-Russell diagram – Filled circles denote the stars analysed in this work. The open circle indicates the position of the Sun. Furthermore, evolutionary tracks of VandenBerg et al. (2000) ([Fe/H] = 0.00, [α/Fe] = 0.0) for different mass (small labels, [$M_{\odot}$]) are shown. Ages are indicated at the positions of the asterisks (large labels, [Gyrs]).

the predicted values. Previous age estimates for the UMa group range from 100 Myrs (König et al. 2002) to 600 Myrs (King & Schuler 2005) and place stars with spectral types late-F to early-K onto the zero-age main sequence (*ZAMS*) at the lower boundary of the main sequence.

Masses for the present sample are derived from the post-main sequence models by VandenBerg et al. (2000) with solar abundance pattern ([Fe/H]=0.00, [α/Fe]=0.00[11]). These proved of value in the work of Fuhrmann (2004). In this thesis, their use in a Hertzsprung-Russell diagram assures methodical consistency with Fuhrmann (2004). The mass of each star is estimated directly from Fig. 3.5.

[11]The *α-element abundance* [α/Fe] gives the abundance of elements enriched by the α process (O, Ne, Mg, Si, S, Ca). Stars with low metallicities tend to be overabundant in the α elements.

4 Results and implications for the UMa group

The spectral analysis provided precise values for effective temperatures, surface gravities and metallicities. However, precision does not imply accuracy. How sure can one be about the accuracy of these parameters (Sect. 4.1)? In Sect. 4.2, all information obtained in the present work is collected and interpreted in order to constrain the properties of the UMa group. Finally all results are discussed especially in terms of age and membership criteria (Sect. 4.3 and 4.4).

4.1 How accurate are the resulting stellar parameters?

Several steps are undertaken. First of all, one has to assess the overall reliability of the analysis. The analysis was done differentially with respect to the Sun. Therefore the analysis has to reproduce the solar parameters from the Moon spectra obtained in each observing run (Sect. 4.1.1). The next step is to reproduce Fuhrmann (2004) in the analysis of a star similar to the stars in the UMa group (Sect. 4.1.2). After these general tests, the sample of this work is addressed as a whole. The precise *Hipparcos* parallaxes allow a crucial test of the spectroscopic surface gravities (Sect. 4.1.3). Finally the parameters of individual stars are compared to previous determinations. One question is of particular interest: How do discrepancies affect the parameters which are used to characterise the UMa group members, e.g. iron abundance?

The data derived for assured kinematic members – composed of the results of this thesis, of Fuhrmann (2000, 2004), and of König et al. (2006) – are compiled and compared to other previous work (Sect. 4.1.5). Table 4.1 lists the stellar parameters of these stars and presents a homogeneous though not complete set of stellar parameters of UMa group stars selected by kinematic criteria only.

In this work, the effective temperature of each star was derived from the Hα and Hβ line. Iron abundances are based on Fe II lines only, as was discussed in Sect. 3. The surface gravity of HD 28495, HD 109647, HD 110463, and HD 115043 was derived from the iron ionisation equilibrium and from the Mg Ib line wings for HD 167389 and HD 184960. The surface gravity of HD 38393, HD 112196, HD 171746 A and HD 171746 B could not be determined with either method and had to be calculated from *Hipparcos* distances. The Balmer lines of HD 155674 A indicate an effective temperature

Table 4.1: The set of homogeneous stellar parameters – The stellar parameters of the sample stars which were studied following the method of Fuhrmann (1998). The columns list the following quantities: **(2)** effective temperature, **(3)** surface gravity, **(4)** iron abundance, **(5)** magnesium overabundance, **(6)** microturbulence, **(7)** macroturbulence, **(8)** projected rotational velocity. The second line provides the corresponding errors for each object. The last column gives the references for the given parameters: 1=this work, 2=Fuhrmann (2004), 3=König et al. (2006), 4=Fuhrmann (2000)

object	$T_{\rm eff}$ [K]	log$g$ [$\frac{\rm cm}{\rm s^2}$]	[Fe/H]	[Mg/Fe]	$\xi_{\rm t}$ [km/s]	$\zeta_{\rm RT}$ [km/s]	$v\sin i$ [km/s]	ref.
HD 11131	5796	4.43	-0.10	0.00	0.97	3.70	1.5	2
	60	0.10	0.07	0.05	0.20		1.0	
HD 24916 A	4600	4.60	-0.03				2.1	3
	100	0.20	0.07				2.0	
HD 26923	5975	4.41	-0.06	-0.01	0.99	4.40	0.0	2
	70	0.10	0.07	0.05	0.20			
HD 28495	5465	4.45	-0.05	0.00	0.93	2.34	4.5	1
	90	0.12	0.05	0.05	0.20		1.0	
HD 38393	6310	4.28	-0.05	0.01	1.30	5.70	8.1	1
	60	0.03	0.05	0.06	0.20		1.0	
HD 39587	5920	4.39	-0.07	-0.01	0.95	4.20	8.7	2
	70	0.10	0.07	0.05	0.20		0.8	
HD 41593	5278	4.54	0.02	-0.01	1.12	1.70	4.3	2
	80	0.10	0.07	0.05	0.20		1.0	
HD 59747	5094	4.55	-0.03	-0.01	1.00	0.90	1.5	2
	90	0.10	0.07	0.05	0.20		1.0	
HD 109647	4980	4.70	0.05	-0.07	0.80	0.40	3.1	1
	60	0.15	0.15	0.15	0.20		1.0	
HD 110463	4940	4.68	0.00	-0.02	0.86	0.40	3.1	1
	80	0.18	0.10	0.10	0.20		1.0	
HD 111456	6300	4.32				5.70	41.0	4
HD 112196	6110	4.39	0.01	0.02	1.31	4.90	12.0	1
	60	0.06	0.05	0.05	0.20		1.0	
HD 115043	5850	4.36	-0.10	0.05	1.26	3.90	7.5	1
	70	0.13	0.07	0.05	0.20		1.0	
HD 134083	6480	4.30				6.40	45.0	4
HD 167389	5895	4.37	-0.02	-0.03	0.99	4.00	3.3	1
	80	0.15	0.07	0.05	0.20		1.0	
HD 171746 A	6100	4.36	-0.04	0.03	1.50	4.80	8.3	1
	80	0.06	0.06	0.05	0.20		1.0	
HD 171746 B	6040	4.37	0.02	-0.04	1.51	4.60	7.3	1
	80	0.06	0.05	0.05	0.20		1.0	
HD 184960	6310	4.22	-0.08	-0.01	1.55	5.70	8.0	1
	80	0.10	0.05	0.05	0.20		1.0	

Table 4.2: Parameters of the Sun are listed derived for the observing runs. The results of two Moon spectra each are averaged. The rows with the parameters (uncertainties below) are led by the run identifier as introduced in Table 2.2. Effective temperatures and surface gravities agree well with the literature values from Gray (2005).

run	$T_{\rm eff}$ [K]	$\log(g\,[\frac{\rm cm}{\rm s^2}])$	[Fe/H]	[Mg/Fe]	$\xi_{\rm t}$ [km/s]	$\zeta_{\rm RT}$ [km/s]
Jul03	5792	4.41	0.04	0.00	0.81	3.58
	90	0.20	0.10	0.05	0.20	
Oct03	5780	4.42	0.03	0.02	0.91	3.62
	40	0.10	0.05	0.05	0.20	
Feb04	5771	4.40	0.02	0.01	0.84	3.52
	72	0.13	0.06	0.06	0.20	
May04	5791	4.43	-0.01	0.02	0.94	3.62
	60	0.11	0.06	0.06	0.20	
Gray (2005)	5777	4.438				

much lower than previous estimates and than expectations from its spectral type K 0[1].

Two spectra of each star were analysed if available. The values in Table 4.1 are the means of the results from the individual spectra.

HD 134083 and HD 111456 were analysed by Fuhrmann (2000). Due to their high projected rotational velocities, weak lines are smeared out and the abundance analysis is not possible. This lack of stellar parameters of UMa group members at effective temperatures beyond 6000 K is now filled by the analyses of HD 38393, HD 112196, HD 171746 A, HD 171746 B, and HD 184960.

4.1.1 The Moon spectra and the solar parameters

As discussed in Chapter 3, the spectral analysis is differential with respect to the Sun and should reproduce the solar parameters from Moon spectra which primarily are spectra of the reflected Sun light. Table 4.2 testifies the good agreement of the derived parameters between the different observing runs and with the literature values.

4.1.2 Consistency with Fuhrmann (2004)

The previous section showed that following the method of Fuhrmann (1998), I was able to reproduce the parameters of the Sun. But how do things look like for younger stars at the age of the UMa group? Table 4.3 shows that the analysis of the young probable UMa group member (though not a kinematically certain member) HD 217813 agrees well with the analysis of Fuhrmann (2004).

[1]The Balmer lines only give an upper limit of 4800 K and an analysis is not possible within the frame of this thesis. The companion HD 155674 B has a wide separation of $\approx 0\farcs5$ and does not pollute the measured light of the primary.

Table 4.3: The stellar parameters of the probable UMa group member HD 217813 (Ammler et al. 2005) compared to the results of Fuhrmann (2004).

	this work	Fuhrmann (2004)
$T_{\rm eff}$	5900 ± 80 K	5866 ± 70 K
log$g$	4.44 ± 0.14	4.43 ± 0.10
[Fe/H]	0.01 ± 0.10	0.01 ± 0.07
$v$sin$i$	2.1 ± 1.0 km/s	2.0 ± 1.0 km/s
$\langle \xi_{\rm t} \rangle$	1.1 ± 0.2 km/s	1.0 ± 0.2 km/s
$M_{\rm sp}$	$1.10 \pm 0.05\ M_{\odot}$	$1.05\ M_{\odot}$[1]
$d_{\rm sp}$	24.88 ± 4.15 pc	24.28 ± 3.32 pc

[1] Fuhrmann (2004) does not provide uncertainties in mass but expects errors to be less than 10 %.

4.1.3 Comparison of spectroscopic distance with *Hipparcos* distance

The derived stellar parameters are a clue to the distance of the star. All necessary relations already have been given in Sect. 3.3.2. Rearrangement of Eq. 3.39 gives:

$$\log d_{\rm sp} = -\frac{1}{2}(\log g - 4.44 - \log M) + 2\log\frac{T_{\rm eff}}{5780\,{\rm K}} + \frac{1}{5}(V - A_{\rm V} - B.C._{\rm V} + 5 - M_{\rm bol,\odot}) \quad (4.1)$$

The spectroscopic distances are calculated from the data in Table 4.1 and 4.4 and compared to the astrometric distance precisely known for all stars in the sample from the *Hipparcos* mission (ESA 1997) (see Fig. 4.1). The spectroscopic distance is mostly sensitive to the derived surface gravity so that the comparison with *Hipparcos* results represents a crucial test for this quantity. Of course, the spectroscopic distances of HD 38393, HD 112196, HD 171746 A, and HD 171746 B are not included since their surface gravities were calculated from the *Hipparcos* distances. They will be placed on the line of identity in Fig. 4.1.

The error bars were calculated from the propagation of the errors of the quantities entering Eq. 4.1. Fuhrmann points out that the true uncertainties are best reproduced by the scatter in a diagram of the type of Fig. 4.1 (cf. Fuhrmann 2004, fig. 2).

The spectroscopic distances agree with the *Hipparcos* distance within the error bars. Yet the scatter of the data points from the present work is somewhat larger than that of the values taken from Fuhrmann (2004) and König et al. (2006) (see especially the residuals in the upper panel of Fig. 4.1).

The two data points with distances lower than *Hipparcos* reflect the possibly overestimated surface gravities of HD 109647 and HD 110463. As pointed out in Sect. 3.3.2, the analysis of these two objects at the cooler end of the sample was complicated by the lack of *MAFAGS* atmospheres and of Fe II lines.

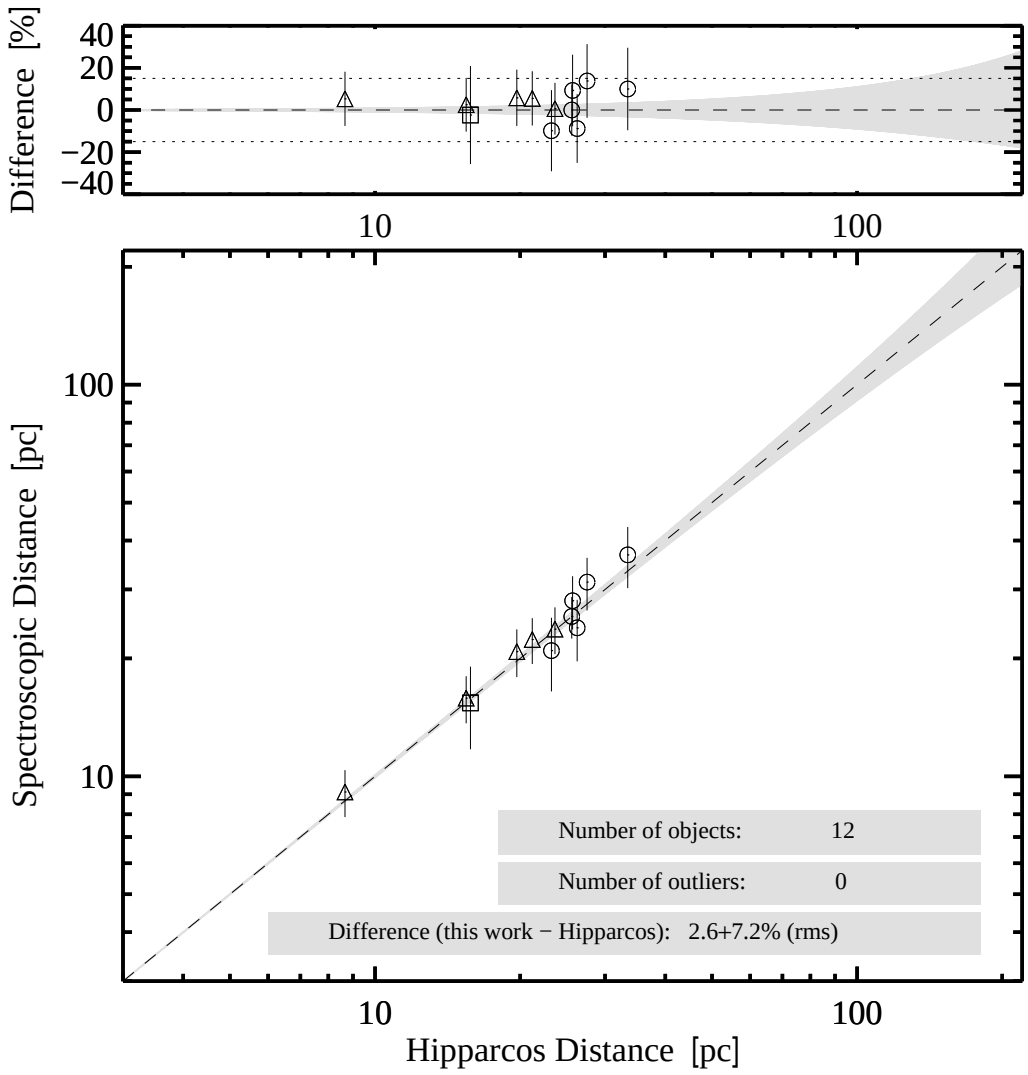

Figure 4.1: Comparison of spectroscopic distances with *Hipparcos* distances – The bottom panel allows a direct comparison of the distances. The dashed line represents perfect agreement with *Hipparcos*. The grey-shaded area displays the *Hipparcos* errors. The top panel shows the residuals and allows to judge the overall quality of the spectroscopic distances. The dashed line represents the typical individual uncertainties of 10 − 15 % experienced by Fuhrmann (2004). This thesis (circles) adds ten to the four analyses of kinematic members from Fuhrmann (2004) (triangles). The square represents the spectroscopic distance of HD 24916 A which was calculated from the parameters given by König et al. (2006).

Table 4.4: Properties determined from the derived parameters – The stellar parameters of the sample stars which were studied following the method of Fuhrmann (1998). The columns give: **(2)** mass, **(3)** radius, **(4)** bolometric correction, **(5)** absolute bolometric magnitude, **(6)** spectroscopic distance, and **(7)** difference from *Hipparcos* distance (Table 1.4) as percentage. The second line gives the corresponding uncertainties. The sources of masses and radii are the same as of the parameters in Table 4.1. The comparison with *Hipparcos* cannot be done for HD 38393, HD 112196, HD 171746 A and B, since their surface gravities were calculated from *Hipparcos* distances.

object	M $[M_\odot]$	R $[R_\odot]$	$B.C._V$	$M_{\rm bol}$	$d_{\rm sp}$ [pc]	$\frac{d_{\rm sp}-d_{\rm HIP}}{d_{\rm HIP}}$ [%]
HD 11131	1.00	1.01	-0.13	4.73	23.8	0.6
	0.05	0.04		0.07	3.3	
HD 24916 A	0.70	0.69	-0.57	6.48	15.4	-2.4
	0.05	0.03		0.09	3.7	
HD 26923	1.07	1.01	-0.11	4.57	22.4	5.5
	0.05	0.04		0.07	3.1	
HD 28495	0.95	0.85	-0.19	5.35	31.3	13.8
	0.10	0.04		0.09	4.8	
HD 38393	1.23	1.33	-0.08	3.74	–	–
	0.05	0.04		0.05	–	
HD 39587	1.04	1.03	-0.12	4.59	9.1	5.3
	0.05	0.04		0.05	1.3	
HD 41593	0.89	0.82	-0.24	5.57	15.8	2.5
	0.05	0.03		0.06	2.2	
HD 59747	0.83	0.76	-0.31	5.90	20.8	5.8
	0.05	0.04		0.08	2.9	
HD 109647	0.83	0.74	-0.36	6.05	24.0	-8.8
	0.05	0.03		0.08	4.3	
HD 110463	0.80	0.75	-0.38	6.05	21.9	-9.8
	0.05	0.03		0.07	4.5	
HD 112196	1.15	1.14	-0.09	4.22	–	–
	0.05	0.08		0.13	–	
HD 115043	1.05	1.03	-0.13	4.64	28.3	10.0
	0.05	0.04		0.06	4.4	
HD 167389	1.05	1.01	-0.12	4.64	36.8	10.0
	0.05	0.04		0.07	6.5	
HD 171746 A	1.15	1.18	-0.10	4.16	–	–
	0.05	0.08		0.14	–	
HD 171746 B	1.10	1.16	-0.10	4.24	–	–
	0.05	0.08		0.14	–	
HD 184960	1.23	1.43	-0.08	3.59	25.6	0.0
	0.05	0.05		0.06	3.1	

The situation of the three data points grouping conspicuously at somewhat too large spectroscopic distance is more complicated. In general, an overestimated spectroscopic distance may indicate binarity. The problem stars are discussed in the following section.

Another point is of importance. Although the spectroscopic distance is hardly sensitive to the explicit dependence on effective temperature in Eq. 4.1, a strong temperature sensitivity enters through the back door by means of the surface gravity. The derived surface gravities strongly vary with effective temperatures as was pointed out in Sect. 3.3.2. This sensitivity indirectly underlies the error bars in Fig. 4.1. These reach the amount of the typical scatter experienced by Fuhrmann (2004).

Nevertheless one has to keep in mind that all the calculated spectroscopic distances still agree with *Hipparcos* within the error bars.

4.1.4 Notes on individual stars

- **HD 28495:** Until recently, the star has not shown any indications of binarity. However binarity is indicated by a discrepancy of 18.3 ± 2.3 mas/yr detected between the proper motion of HD 28495 from the *Hipparcos* catalogue to that of the *Tycho* catalogue (Makarov & Kaplan 2005). Additionally HD 28495 showed a proper motion acceleration of $17.8 \pm 2.8\,\mathrm{mas/yr^2}$. Makarov & Kaplan (2005) gave prescriptions to estimate the lower mass limit of a possible low-mass companion. Assuming a binary system with circular orbit, I estimated a lower mass limit of about $0.20\,M_\odot$ for a possible companion, corresponding to an absolute V-band magnitude $M_\mathrm{V} = 12$ (Baraffe et al. 1998, fig. 3). The brightness difference with respect to the primary is therefore lower than 6.5 mag. A brightness similar to that of the primary would increase the spectroscopic distance by up to 41 %. Such a value is excluded by the small deviation of the spectroscopic distance from the *Hipparcos* distance. Furthermore the procedure of Makarov & Kaplan (2005) only reveals low-mass companions.

  Therefore the analysis might still be affected by a companion but only slightly. More severe problems may arise from the Hα filling-in which is relatively strong for this star (see Table 4.5) and may cause a spurious effective temperature determination.

- **HD 115043:** Lowrance et al. (2005) detected a companion of spectral type M4-M5 at a separation of 1.”58. The spectral type corresponds to an absolute V band magnitude $M_\mathrm{V} \sim 11.8$ (Schmidt-Kaler 1982, table 3). This compares to the much brighter primary with $M_\mathrm{V} = 4.63$. Hence a discrepancy with the *Hipparcos* distance is probably not due to this companion. The distance deviation may still be caused by errors in the derivation of surface gravity. Sect. 3.3.2 already pointed out that the surface gravities of the hotter stars can be underestimated by the iron ionisation equilibrium. This effect is possibly present at the temperature of HD 115043 though at a somewhat smaller scale.

- **HD 167389:** There are no indications of multiplicity at all in the literature. However, the Mg Ib wings may be raised resulting in an underestimation of the surface gravity (cf. Sect. 3.3.2). No such effect can be seen for HD 184960 whose surface gravity was derived from the Mg Ib wings, too.

- **HD 171746 A & B:** This binary has a separation of 1.″718 and a position angle of 158.°8 according to Fabricius & Makarov (2000). They gave *Hipparcos* $H_{\rm P}$ magnitudes for both components which are converted to visual magnitudes of $V_{\rm A} = 6.924 \pm 0.071$ and $V_{\rm B} = 7.009 \pm 0.071$ based on the conversion of Bessell (2000). The binary could be resolved only marginally with *FOCES* so that light from both components may have entered the fibre. Thus the resulting stellar parameters should be regarded with care.

4.1.5 Comparison of single star parameters with previous determinations

The comparison to King & Schuler (2005) is of special interest since they are also interested in the spectroscopic characterisation of the UMa group and have several stars in common with this thesis. Similar to the present work, the analysis of King & Schuler (2005) is differential with respect to the Sun and based on LTE model atmospheres. The most prominent differences arise in the derivation of specific stellar parameters. King & Schuler (2005) determined effective temperatures from a colour-based calibration (Steinhauer 2003) while the values in Table 4.1 are based on the wings of the Balmer lines. They adopted surface gravities from evolutionary models of Yi et al. (2001) in contrast to Table 4.1 where this parameter is derived directly from the spectra (iron ionisation equilibrium and Mg Ib line wings) or from *Hipparcos* distance. The microturbulence parameters are determined iteratively requiring iron abundance to be independent of equivalent width whereas King & Schuler (2005) adopted the microturbulence parameters from the relation given in Allende Prieto et al. (2004). The reader is reminded of the discussion in Sect. 1.4.2.

Effective temperature

Figure 4.2 compares the effective temperatures from Table 4.1 with other previous determinations. The values of almost all authors scatter around the identity line with residuals of less than 200 K. In opposite, the temperatures of King & Schuler (2005) are systematically cooler. The discrepancy is increasing up to almost 400 K towards the coolest stars of the sample. The origin of this discrepancy is probably due to the different methods of temperature determination. In any case, the temperatures of this work and Fuhrmann (2004) are corroborated by the good agreement with other previous determinations.

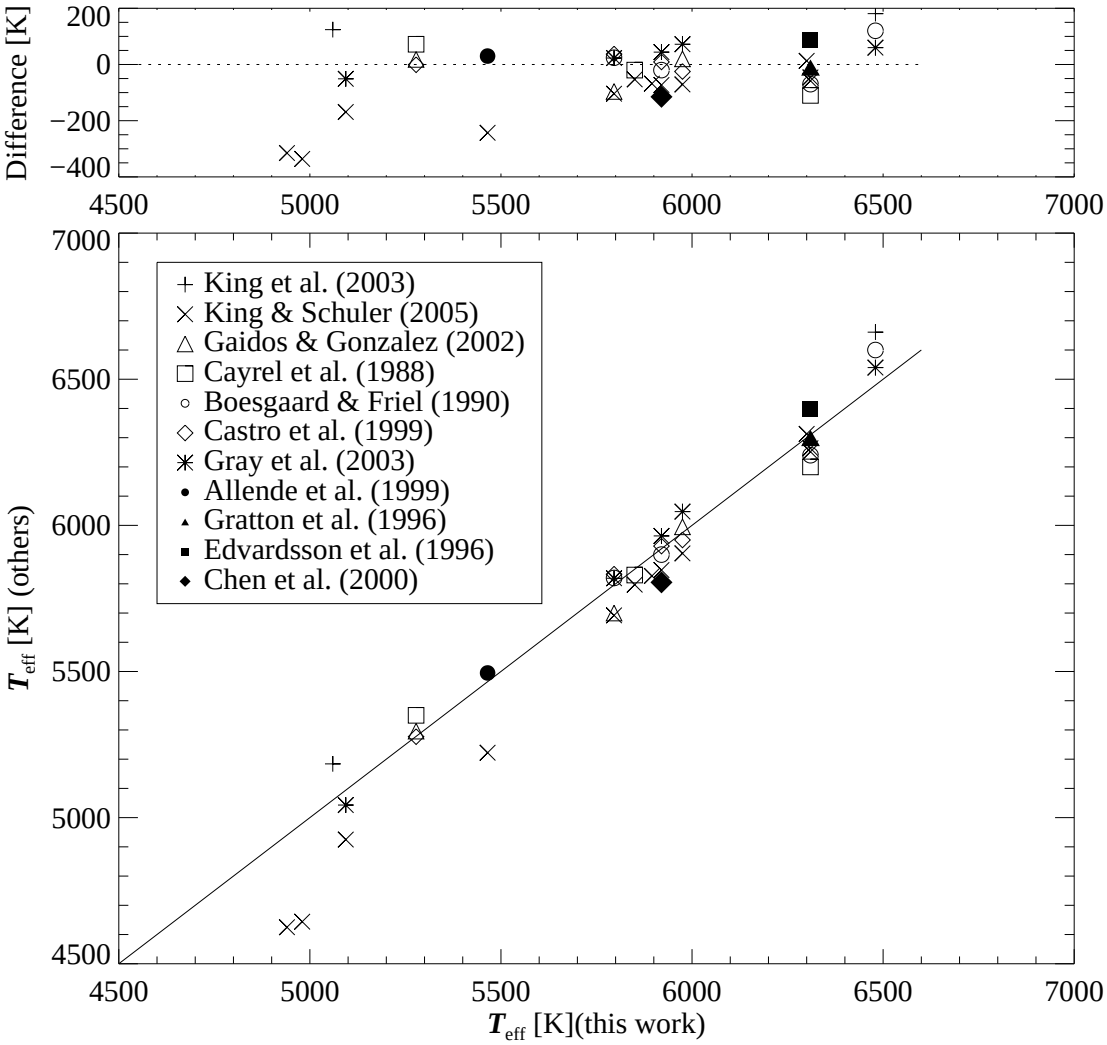

Figure 4.2: Comparison with effective temperatures from previous analyses – The solid line indicates identity with the effective temperatures presented in Table 4.1. Error bars are omitted for clarity.

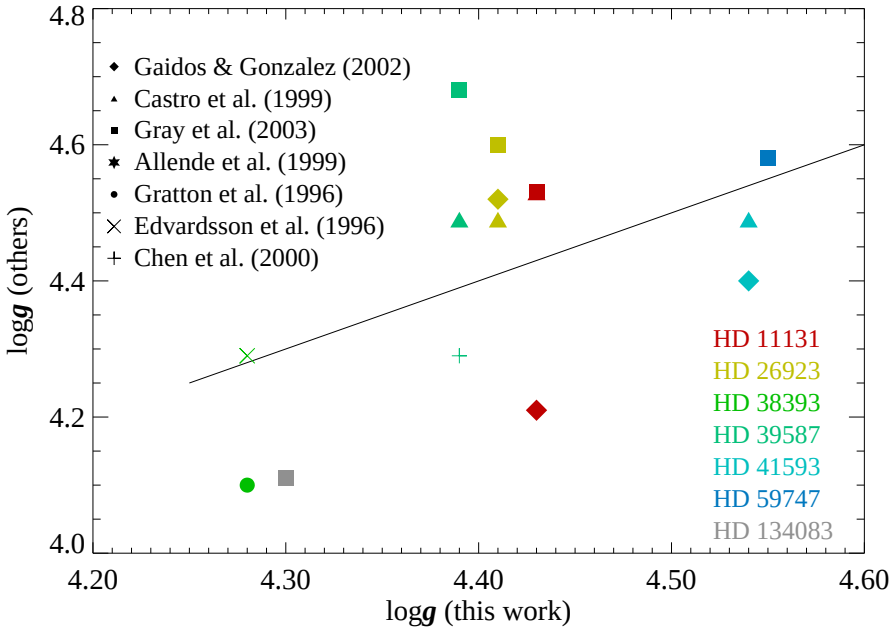

Figure 4.3: Comparison with the surface gravities from other work – Error bars are omitted for clarity.

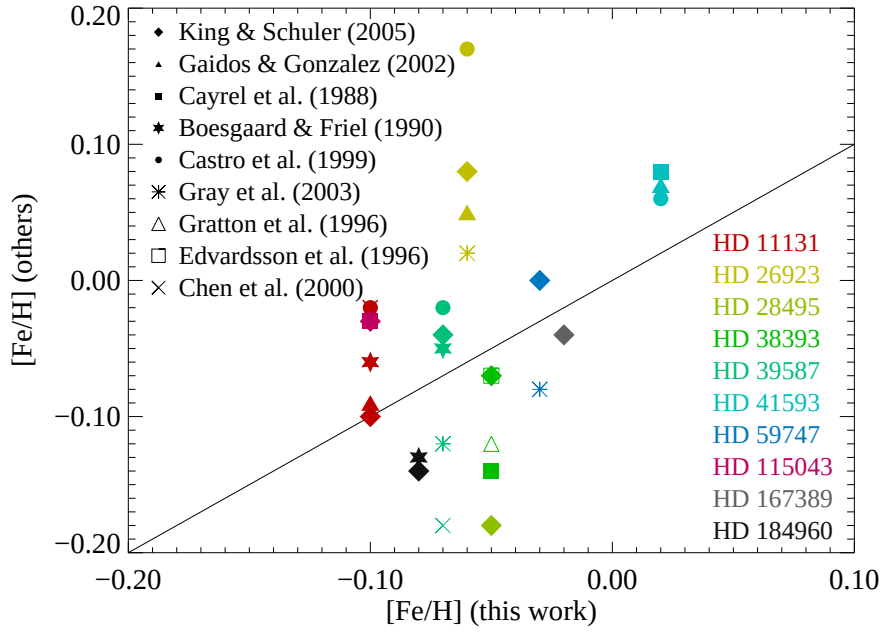

Figure 4.4: Comparison with the iron abundances from other work – Error bars are omitted for clarity.

Surface gravity

See Fig. 4.3 for a comparison of surface gravities from previous work with the values from Table 4.1. The scatter is large though mostly within the typical errors of some 0.10 – 0.15 dex. Two or more values were found for almost all stars. The agreement is good for HD 11131, HD 38393 and HD 39587 while for HD 26923 and HD 41593, the values are quite different from the previous findings.

The reader is reminded of the inhomogeneous values listed in Table 1.3. The present work together with the data from Fuhrmann (2004), Fuhrmann (2000), and König et al. (2006) represents the first homogeneous set of spectroscopic surface gravities of a larger sample of UMa group members. The quality of these surface gravities is approved by Fig. 4.1.

Iron abundance

The iron abundances are of special interest as to the characterisation of the UMa group. See Fig. 4.4 for a comparison with previous spectroscopic determinations. Previous spectroscopic determinations[2] were not found for six stars, namely HD 24916 A, HD 109647, HD 110463, HD 112196, HD 171746 A, and HD 171746 B.

Consider the stars in Fig. 4.4 having more than one value in the literature, i.e. all except of HD 28495, HD 115043, and HD 167389. The values from Table 4.1 are outside the literature range for HD 26923, HD 38393, HD 41593, HD 184960 while they are inside for the remaining three stars HD 11131, HD 39587, HD 59747. In principle, these deviations may be related to the deviations in effective temperature (Fig. 4.2) and surface gravity (Fig. 4.3). However a meaningful comparison is hampered by the inhomogeneity of the literature data. Only the work of King & Schuler (2005) is considered here in more detail since it contributes eight data points to Fig. 4.4. Do the temperature discrepancies in Fig. 4.2 have any consequences on the derived iron abundances? If yes, some correlation is expected when plotting the temperature residuals versus the abundance residuals. Though the large spread in Fig. 4.5 does not allow any firm conclusions. The abundances of King & Schuler (2005) are lower at cooler temperatures if one trusts the rather inconclusive linear fit in Fig. 4.5 and considers Fig. 4.2.

The mean of the iron abundances in Table 4.1 amounts to −0.03 with a standard deviation of 0.04 which is slightly higher than the correspoding value of King & Schuler (2005) for the same stars (-0.06 ± 0.08). Interestingly the scatter of the former value is smaller than that of the latter. Yet any conclusions on the intrinsic scatter of the UMa group abundance would be premature considering the typical errors of abundance determinations (0.07 in the present work).

[2] Only spectroscopic determinations were considered. Values predicted from calibrations or derived from photometry are much less reliable than the spectroscopic determinations (see Sect. 1.3.4).

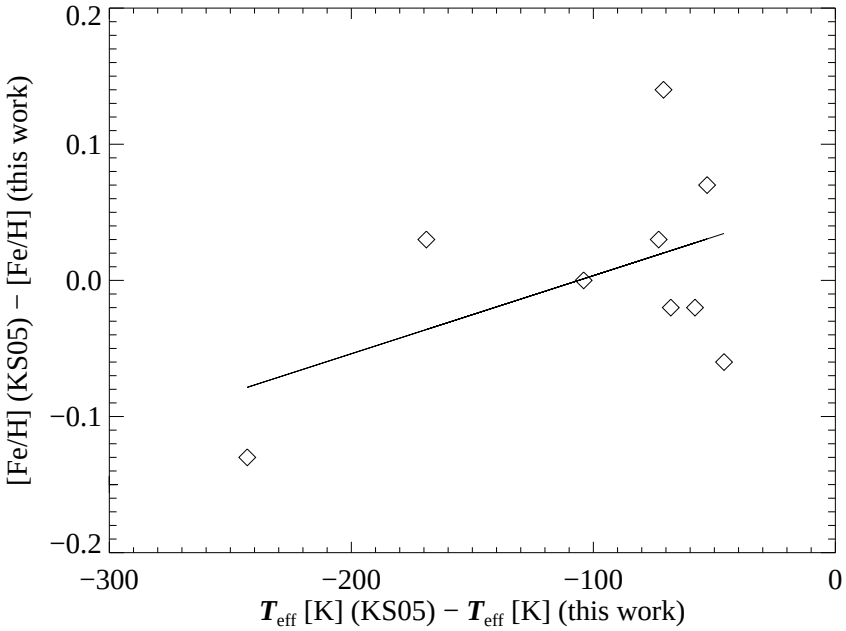

Figure 4.5: Temperature residuals vs. iron abundance residuals of this work with respect to King & Schuler (2005) – The plot shows the temperature residuals (cf. Fig. 4.2) vs. the residuals of the iron abundances (cf. Fig. 4.4). Clearly the fit is only tentative due to the small amount of data points.

Microturbulence

The derived abundances are strongly related to the adopted microturbulences. The iron abundance is underestimated in the case of overestimated microturbulence (cf. Sect. 3.3.3).

The microturbulences from Table 4.1 are displayed versus effective temperatures in Fig. 4.6. The increase of microturbulence with increasing effective temperatures is well-known (see Fuhrmann 2004; Luck & Heiter 2005). The hot star microturbulences added by the present work substantially steepen the UMa group trend indicated by Fuhrmann (2004).

Unlike the comparisons in the preceeding sections, these microturbulences are not compared to further literature values. Such a comparison is difficult since the microturbulence parameters are strongly sensitive to the input data used for the line synthesis. For the Sun, Fuhrmann (1998) gave a value of 0.90 ± 0.15km/s. This value is appropriate when using the same models and methods as Fuhrmann (1998). Of course this choice is not valid for analyses based on other atmospheric models. Then the appropriate value might be quite different. See Allende Prieto et al. (2004), for example, who adopted a solar microturbulence parameter of 1.25 km/s.

Fig. 4.6 also displays the ratio $\frac{\zeta_{\rm RT}}{\xi_{\rm t}}$ versus effective temperature and can be compared to Fuhrmann (2004, fig. 5). As is expected from the microturbulences, these values are

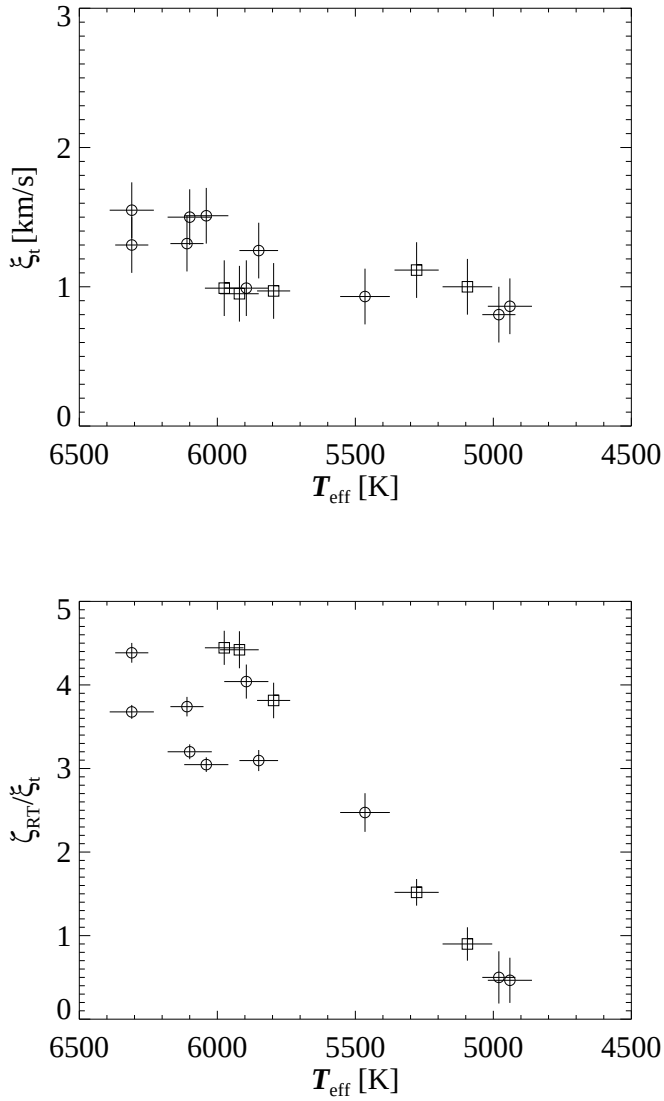

Figure 4.6: Comparison of the microturbulence parameter ξ_t with Fuhrmann (2004) – top: The microturbulence parameters from the present work (circles) steepen the trend indicated by the data points from Fuhrmann (2004) (squares). **bottom:** Consequently the trend of ζ_{RT}/ξ_t is changed.

substantially lower for the hotter stars than the values expected from the usual trend for young stars.

4.2 The properties of the UMa group

The Kiel diagram indicates the evolutionary state of the UMa group (Sect. 4.2.1). Considering the abundances, the most interesting question is whether these are distinct from other groups of stars (Sect. 4.2.2). The projected rotational velocities are related to the age when underlying a Skumanich law (Sect. 4.2.3). Stronger age constraints are given by lithium equivalent widths (Sect. 4.2.4). The filling-in of Hα is compared to the homogenous level encountered by Fuhrmann (2004) (Sect. 4.2.5).

4.2.1 Kiel diagram

Besides the Hertzsprung-Russell diagram and the colour-magnitude diagram, stellar evolution is traced in the $T_{\rm eff}$–log$g$ diagram, the so-called *Kiel diagram* (see Fig. 4.7). It is particularly appropriate for this thesis since both effective temperature and surface gravity are derived consistently from the spectra. See Holweger, Hempel, & Kamp (1999) for a discussion of the general advantage of the Kiel diagram.

King & Schuler (2005) derived similar age for the UMa group (400 − 800 Myrs), the Hyades (500 − 900 Myrs), and the Coma Berenices cluster (400 − 800 Myrs) when comparing $B-V$ and $M_{\rm V}$ with the isochrones of Yi et al. (2001). The age estimates depend critically on the turn-off which is however sparsely populated in all of these systems. The Kiel diagram in the top panel of Fig. 4.7 does not give any further age constraints with exception of the hotter stars which give an upper age limit, namely ≈3 Gyrs. Early-type stars close to the turn-off are more conclusive (King et al. 2003).

Strikingly the stars are placed systematically above the zero-age main sequence. These positions in the diagram ambiguously conincide with the pre-main sequence. Therefore the diagram is repeated in the bottom panel of Fig. 4.7 but now with pre-main sequence models of Baraffe et al. (1998) matched to fit the Sun. Again the age constraint is rather poor giving a lower limit of $\approx 10^7$ Myrs.

4.2.2 Abundances of iron and magnesium

The iron abundances in Table 4.1 range from [Fe/H]= −0.10 up to [Fe/H]= +0.05 with an average of $\langle$[Fe/H]$\rangle$ − 0.03 and a standard deviation of 0.04 dex. Previous means of -0.08 ± 0.09 and -0.09 ± 0.02 were given by Soderblom & Mayor (1993) and Boesgaard & Friel (1990), respectively. The new average is higher by 0.05 dex and 0.06 dex, respectively. The UMa group abundances can be compared to other groups of stars, e.g. the Pleiades and the Hyades. Boesgaard & Friel (1990) gave [Fe/H]= −0.03 ± 0.02 for the Pleiades and [Fe/H]= 0.13 ± 0.05 for the Hyades. Grupp (2004) presented a somewhat higher value for the Pleiades of [Fe/H]= 0.04 ± 0.02 higher by 0.07 dex than the value from Boesgaard & Friel (1990). This fact is remarkable, since the work of Grupp (2004)

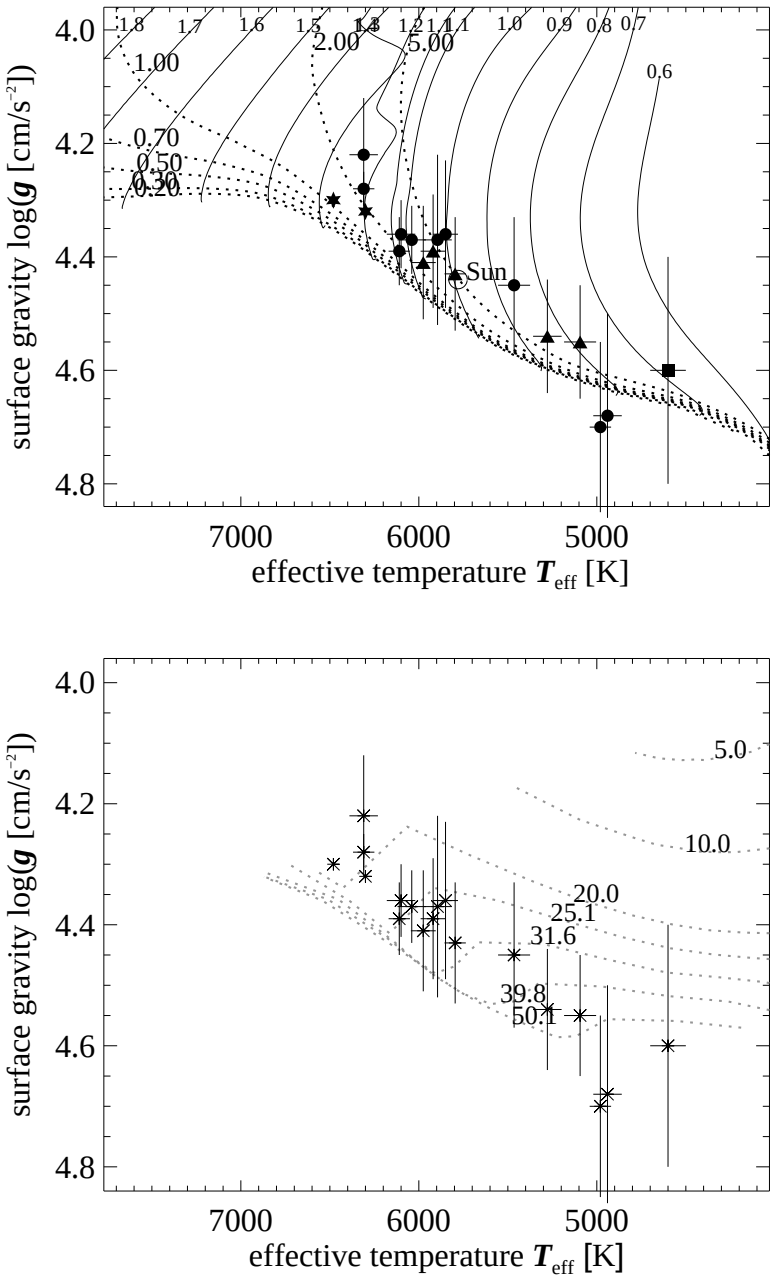

Figure 4.7: Kiel diagram of the UMa group – Top: Post-main sequence models. Surface gravities log$g$ and effective temperatures $T_{\rm eff}$ for the sample are taken from the present work (circles), Fuhrmann (2004) (triangles), Fuhrmann (2000) (stars), and König et al. (2006) (square). Evolutionary post-main sequence tracks (solid lines, labelled with mass [$M_{\odot}$]) and isochrones (dotted lines, labelled with age [Gyrs]) from VandenBerg et al. (2006) (scaled-solar, [Fe/H]=-0.04, [α/Fe]=0.0) are overplotted. **Bottom: Pre-main sequence models.** Isochrones (dotted, labelled with age [Myrs]) of Baraffe et al. (1998) are plotted. The models with mixing length parameter α = 1.9 are chosen since these were constructed in order to match the Sun. The data points are the same as in the top panel.

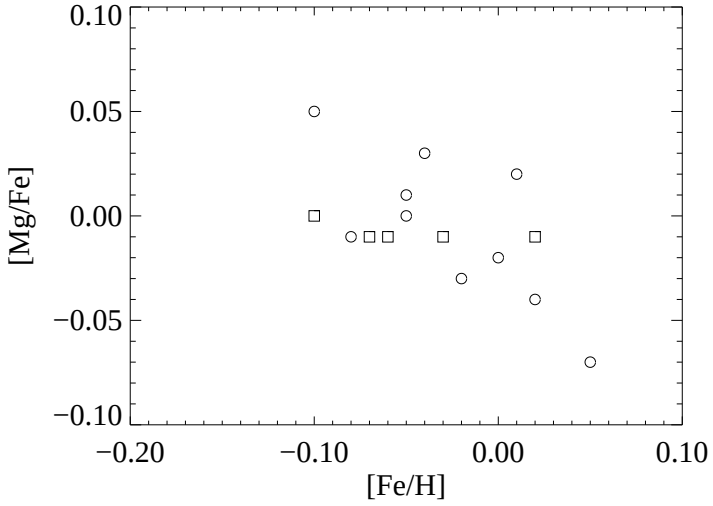

Figure 4.8: Magnesium vs. iron abundance – Own results (circles) compared to Fuhrmann (2004) (squares). Error bars are omitted for clarity.

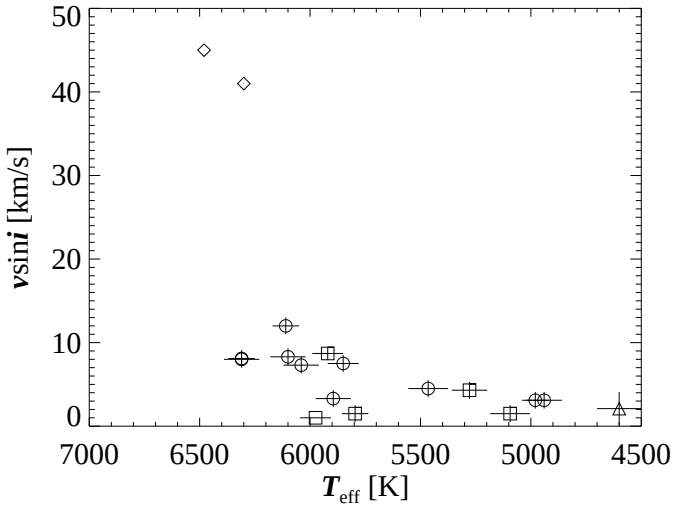

Figure 4.9: Projected rotational velocity of UMa group members – Effective temperature vs. projected rotational velocity (circles) compared to results of Fuhrmann (2000) (diamonds), Fuhrmann (2004) (squares) and König et al. (2006) (triangle). Uncertainties for the fast-rotating HD 134083 and HD 111456 were not given.

was based on an improved version of *MAFAGS*. In the present work on the UMa group, a similar offset with respect to the values of Boesgaard & Friel (1990) is encountered, namely 0.06 dex.

All in all, the UMa group iron abundance is quite different from the Hyades while it is at best marginally different from the Pleiades.

Fig. 4.8 shows magnesium overabundance [Mg/Fe] versus iron abundance [Fe/H]. A slight trend of decreasing [Mg/Fe] with increasing [Fe/H] is indicated. In general, the distribution coincides well with the thin disk population of Fuhrmann (2004, fig. 34).

4.2.3 Rotation

The hypothesis of *magnetic braking* explains the slow-down of the rotation rate of late-type main-sequence stars. Stellar magnetic fields transfer angular momentum to ionised stellar winds braking the stellar rotation. See Mestel (1999) for further details. Hotter stars on the main sequence do not have convective envelopes and keep their initial high rotation rates of up to several hundred km/s during their main sequence lifetime.

The measurement of the stellar rotation by means of line broadening is hampered by the unknown *inclination* of the rotation axis relative to the line of sight. The true rotation rate is only obtained if the inclination i equals 90°, i.e. the rotation axis forms a right angle with the line of sight. Therefore rotational line broadening only indicates the *projected rotational velocity* $v\sin i$.

Figure 4.9 displays projected rotational velocity $v\sin i$ versus effective temperatures $T_{\rm eff}$ from Table 4.1. This diagram is an effect of both true rotational velocity and inclination angle, formed by stars with different inclination angles. The envelope of the distribution in Fig. 4.9 nicely traces a relation which monotonously decreases with decreasing effective temperature. The distribution further coincides with the onset of magnetic braking on the main sequence at ≈6200 K. The projected rotational velocities of HD 111456, HD 134083 are substantially higher than these of the rest of the sample.

The rotational velocities allow conclusions on the age since they decrease with time (Skumanich 1972). Only the projected rotational velocity is measured so that age estimates are valid in a statistical sense only. Gray (2005) gives a *Skumanich relation* for solar-mass stars

$$v\sin i\,[\mathrm{km/s}] \approx \frac{5}{\sqrt{t\,[\mathrm{Gyrs}]}} \tag{4.2}$$

where t is the age of the star. Adopting an UMa group value of $v\sin i = 5 - 10$ km/s at the position of the Sun in Fig. 4.9, Eq. 4.2 gives an age estimate of 250 – 1000 Myrs which perfectly agrees with previous age estimates. Due to the inclination of the rotation axis, the projected rotational velocity can hardly be used to decide on membership.

Rotation rates are not compared to other groups of stars in the present work. King et al. (2003) state that rotation cannot be distinguished from the Hyades but is decreased with respect to the Pleiades and M 34 clusters.

4.2.4 Equivalent width of the Li I λ6707.8 Å absorption line

Table 4.5 tabulates lithium abundances derived from the equivalent widths of the Li I λ6708 Å feature. The measurements follow two different approaches. First, the lithium equivalent widths were found by integrating the observed profiles so that the abundances could be derived by interpolation in the LTE curves of growth in Soderblom et al. (1993b, table 2). In the second approach, the lithium abundances were determined by fitting the observed lithium feature with a synthetic profile. Then the equivalent width followed by integration of the synthetic profile.

In most cases, the neighbouring Fe I λ6707.441 Å line is resolved (see Fig. E.1) and excluded from the integration. Uncertainties of the equivalent widths from direct integration are found by varying the integration limits and the position of the continuum under guidance of noise and blends with neighbouring lines. Uncertainties of the interpolated abundances are found by varying the input parameters, i.e. the equivalent widths, effective temperatures and surface gravities within their error bars. The resulting total formal error amounts to typically 0.04 – 0.09 dex.

Similarly the synthetic line fits were done repeatedly at the limits of the stellar parameters. The variation of effective temperature and iron abundance dominated the changes in lithium abundance so that only these two parameters were changed. The resulting errors amount to 0.06 – 0.11 dex.

The equivalent widths emerging from these methods agree remarkably good – except of HD 115043 – although most values from direct integrations are somewhat higher. Considering the problem of line blends, Hünsch et al. (2004) derived Li abundances by both methods, too: synthetic line fits and curves of growth. Following their fig. 3, the values from synthetic fits exceeded those from curves of growth (Soderblom et al. 1993b) by 0.1 – 0.3 dex. This effect can be reproduced from Table 4.5 though being lower in magnitude, i.e. up to 0.08 dex for HD 115043.

The age-dependent lithium absorption can be used as membership criterion in the case that it is distinct from the lithium absorption in other groups. The amount of absorption is correlated with effective temperature as is shown in Fig. 4.10.

In order to compare to the level of absorption in other stellar groups, I follow the presentation in Montes et al. (2001b, fig. 2). I added the upper and lower boundaries of lithium absorption in the Pleiades. The upper boundary follows Neuhäuser et al. (1997, fig. 3) based on results of Soderblom et al. (1993a) and García Lopéz, Rebolo, & Martín (1994). The lower boundary is taken from Soderblom et al. (1993a, fig. 2d). Furthermore the fit to Hyades lithium data from Soderblom et al. (1990, fig. 3a) is shown[3]. Moreover members of the open cluster M 35 (Barrado y Navascués et al. 2001) are displayed.

The absorption of the hotter stars of the sample overlaps with the distributions of the Pleiades and the Hyades while the absorption of the cooler stars is quite distinct from

[3] Soderblom et al. (1993a) and Soderblom et al. (1990) gave the lower Pleiades boundary and the Hyades fit, respectively, not as function of effective temperature but as function of intrinsic colour $(B-V)_0$. Similar to Neuhäuser et al. (1997), the colours are converted to effective temperatures using Bessell (1979, 1991). In detail, table 2 from Bessell (1979) is used for stars hotter than 4000 K and table 2 from Bessell (1991) for stars cooler than 4000 K.

Table 4.5: Lithium equivalent widths, lithium abundances, and filling-in of the Hα line – In a first approach, the equivalent width of the Li I λ6707.8 Å is calculated by integrating the observed profile ($W_{\rm Li}^{\rm int}$). Then the Li abundance is estimated by interpolation in the curves of growth of Soderblom et al. (1993b) ($\log N_{\rm Li}^{\rm cog}$). In a second approach, the abundance is derived by fitting the observed feature with a synthetic Li doublet ($\log N_{\rm Li}^{\rm fit}$). Integration of the matching synthetic profile gives the equivalent width ($W_{\rm Li}^{\rm fit}$). The last column tabulates the minimum intensity at the core of the Hα line. The relative continuum corresponds to 100 %.

object	$T_{\rm eff}$ [K]	$W_{\rm Li}^{\rm int}$ [mÅ]	$W_{\rm Li}^{\rm fit}$ [mÅ]	$\log N_{\rm Li}^{\rm cog}$	$\log N_{\rm Li}^{\rm fit}$	Hα [%]
HD 11131	5796[4]					29
HD 24916 A	4600[3]	<8.0± 3.0				33
HD 26923	5975[4]	88.0± 5.0	87.0			25
HD 28495	5465[2]	69.0± 4.0	72.4	2.14±0.06	2.22±0.06	42
HD 38393	6310[2]	65.0± 3.0	63.5	2.87±0.04	2.95±0.06	17
HD 39587	5920[4]					28
HD 41593	5278[4]					30
HD 59747	5094[4]					32
HD 71974 A	5480[6]	68.0± 4.0	66.7			32
HD 95650	3634[5]	<45.0± 5.0				73
HD 238087	4350[8]	<20.0± 5.0				39
HD 109647	4980[2]	46.0± 5.0	44.2	1.37±0.09	1.36±0.11	34
HD 110463	4940[2]	22.0± 5.0	22.5	0.97±0.09	1.05±0.11	34
HD 112196	6110[2]	110.0± 5.0	109.5	3.03±0.04	3.09±0.06	28
HD 115043	5850[2]	94.0± 6.0	84.0	2.70±0.09	2.78±0.11	27
HD 238224	4350[8]	<11.0± 4.0				61
HD 152863 A[1]	4980[7]	< 7.0± 5.0				17
HD 155674 A	<4800[2]	< 9.0± 6.0				37
HD 155674 B	3900[8]	<10.0± 2.0				39
HD 167389	5895[2]	60.0± 4.0	58.2	2.47±0.05	2.47±0.07	21
HD 171746 A	6100[2]	85.0± 5.0	83.2	2.84±0.05	2.90±0.07	17
HD 171746 B	6040[2]	50.0± 5.0	45.3	2.51±0.05	2.51±0.11	28
HD 184960	6310[2]	62.1± 6.0	60.4	2.83±0.04	2.88±0.06	17
HD 205435[1]	5060[9]	<15.0± 5.0				20

[1]giant [2]$T_{\rm eff}$ from this work [3]from König et al. (2006) [4]from Fuhrmann (2004) [5]from Alonso, Arribas, & Martínez-Roger (1996) [6]from Strassmeier et al. (2000) [7]from de Laverny et al. (2003) [8]converted from spectral type with the calibration from Kenyon & Hartmann (1995) [9]from McWilliam (1990)

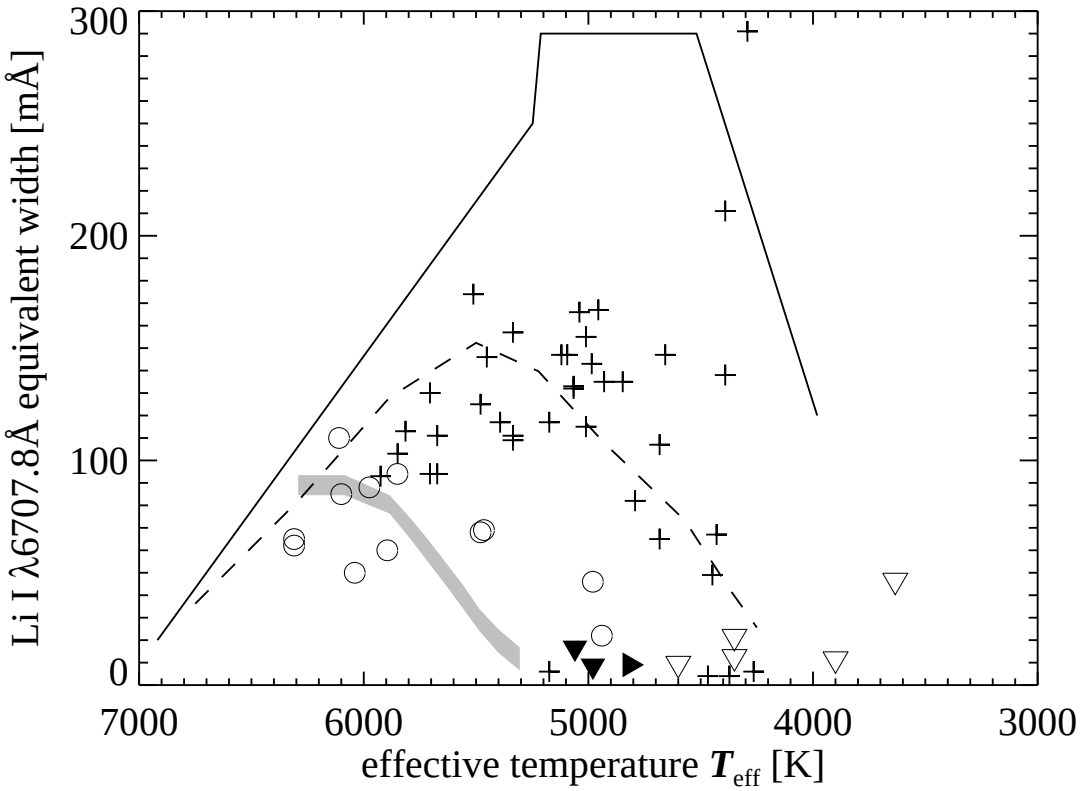

Figure 4.10: Effective temperature vs. lithium equivalent width – Almost all own measurements for the certain kinematic UMa group members are indicated by circles. For some stars, only upper limits could be determined (triangles pointing downwards). Filled triangles represent the upper limits for the giants HD 152863 A and HD 205435. The filled triangle pointing to the right is the location of HD 155674 A. Only upper limits are available for both lithium equivalent width and effective temperature. The upper (solid) and the lower boundary (dashed) of lithium absorption in the Pleiades as well as the distribution of the Hyades (grey-shaded) are overplotted. The crosses represent members of M 35. See the text for references. Error bars were omitted for clarity.

these distributions. Lithium absorption may be used as membership criterion at least for UMa group candidates cooler than the Sun and hotter than $T_{\rm eff} \approx 5000$ K. In this temperature regime, lithium absorption of young stars strongly depends on the age. The Pleiades have an age of roughly 110 Myrs (Terndrup et al. 2000) while the Hyades are much older with an age of ≈ 625 Myrs (Perryman et al. 1998). M 35 is somewhat older than the Pleiades (175 Myrs, Barrado y Navascués et al. 2001). Below solar temperature, the UMa group sample is distinguished well from the other stellar groups down to 5000 K although this region is sparsely populated. Two stars, HD 152863 A and HD 205435, have upper limits only possibly related to their giant status. The UMa group values are distinguished well from the Pleiades, the Hyades, and the bulge of M 35. I do not follow the reasoning of King & Schuler (2005). Instead the youth of the UMa group is confirmed with an age of $\approx 200 - 600$ Myrs. The reader is reminded of the discussion in Sect. 1.3.6.

Two important points have to be kept in mind when considering Fig. 4.10:

- Uncertainties in the effective temperature may shift the Li sequence considerably. Except of the coolest stars, the effective temperatures of the whole UMa group sample of this work were derived with the method of Fuhrmann (1998), by fitting the Balmer lines.

- The quality of the measured equivalent widths strongly depends on the resolution and the signal-to-noise ratio of the underlying spectra. In the present work, a signal-to-noise ratio of ≈ 200 with a resolving power of ≈ 60000 could be achieved for almost all stars. The blend with the Fe I line mostly has been resolved.

4.2.5 Filling-in of the Hα line core

This thesis presents a preliminary estimation of the Hα filling-in. Only the relative core intensities are measured in order to compare to Fuhrmann (2004). More information can be obtained from the measurement of equivalent width of the central emission not done in the present work. Such equivalent widths can be measured following the *spectral subtraction technique* described in Montes et al. (2001b), for example. Line profiles from standard stars of same spectral type have to be obtained first. These are subtracted from the observed spectrum. The residual is related to chromospheric emission.

In principle, a subtraction of synthetic lines is possible. However, the LTE line synthesis used in the present work fails in predicting the line cores (see Figs. E.2 through E.4). Figure F.1 shows the residuals when subtracting theoretical LTE profiles from the observed profiles. Only the outer wings are modelled reliably.

The subtraction of synthetic lines can be done only for the stars with solved stellar parameters whereas the intensity in the Hα core can be measured for all observed stars of the sample. Fig. 4.11 displays the Hα core intensity levels versus effective temperatures. All values are taken from Table 4.5. Additionally the theoretical LTE prediction is shown. The LTE profiles do not reproduce the core of the Hα lines and thus are shifted by a constant amount in order to match the solar data point. Considering the values from

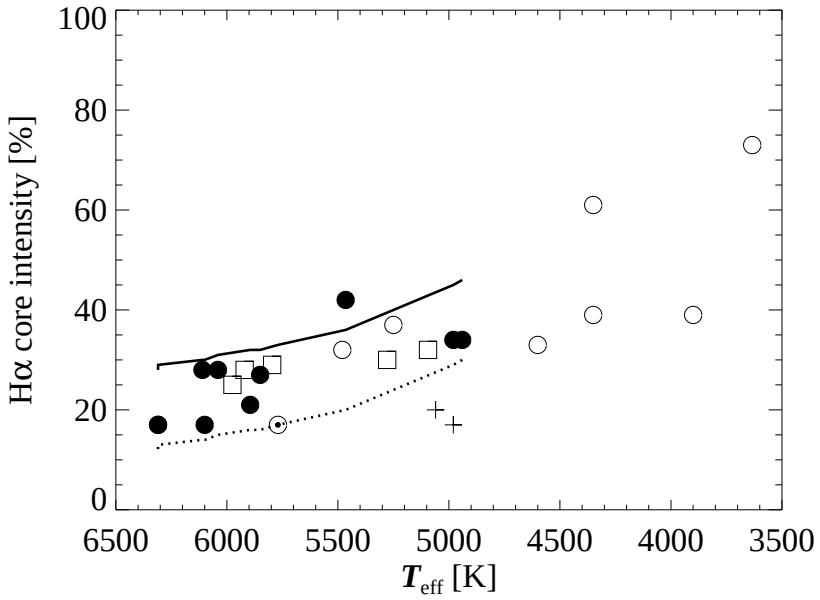

Figure 4.11: Effective temperature vs. Hα core intensity – The core intensity with respect to the relative continuum is plotted. Circles denote values from this work with the filled circles being the stars with solved stellar parameters (Table 4.1). Squares indicate values for the certain UMa group members taken from Fuhrmann (2004). The plus signs display the values of the two giants HD 152863 A and HD 205435. $\odot$ denotes the solar value. The solid line represents the theoretical values from LTE synthesis and the dotted line is the same but shifted to match the solar value. The homogeneity of the values from Fuhrmann (2004) is not supported.

Fuhrmann (2004) alone, we clearly perceive the homogeneous filling-in encountered by Fuhrmann (2004). However the new data strongly blur this nice relation. What remains regardless of the two giants, is a systematically higher Hα core level with respect to the Sun, yet with a substantial spread of at least 15 % in the relative units.

4.3 Conclusions on the age

In order to summarise, following age constraints are inferred:

property	age
rotation	$\approx 250 - 1000$ Myrs
lithium	180-630 Myrs
Kiel diagram	$\approx 10^7 - 10^9$ years
[Fe/H], [Mg/Fe]	$\lesssim 4$ Gyrs (thin disk, Fuhrmann 2004)

The new determinations do not change the limits on the age given by the literature. However some progress may be seen in the dependence of lithium equivalent width on effective temperature. Having in mind that there are not enough data points in the decisive temperature range, the lithium equivalent widths indicate a common age rather than an age spread. If the age spread of 200 – 600 Myrs in the literature was intrinsic to the UMa group, the homogeneously measured lithium equivalent widths were expected to scatter strongly between the distributions of the Pleiades and the Hyades.

4.4 Concluding remarks on membership criteria

Certainly a large age spread would inhibit a common level of activity from the outset and thus the existence of appropriate activity-based spectroscopic membership criteria.

Some more words have to be said on the meaning of “common” in this context. First of all, it is important to distinguish carefully the steps in the construction of membership criteria. The prerequisite is the agreement on a sample of assured members, the “canonical” members defining the properties of the stellar group. The distribution of these properties can be characterised by some limits which may be used to define the membership criterion, i.e. the limits used to select new members. This reasoning does not need any further deepening at this point. Instead an example is given by the work of King et al. (2003). The canonical members are the UMa nucleus or UMa cluster stars, respectively. The photometric criterion is given by the isochrones of 400 and 600 Myrs in the colour-magnitude diagram. These isochrones limit the distribution of the UMa nucleus. Similarly in their *UV* diagram, the $3\,\sigma$ ellipse encloses the kinematic distribution of the nucleus stars and represents a selection limit for the kinematic membership criterion. Now let us turn back to the term “common”. It does not mean that the considered stellar property is described by a sharp distribution. Rather it is of importance whether this distribution can be distinguished well from the distributions of other stellar groups,

i.e. the degree of distinctness is decisive. That means that “common” is always used in a relative sense and not in an absolute sense.

In this respect, the distribution of UMa group lithium abundances appears distinct in the present study while the iron abundance can only be distinguished from the Hyades and not from the Pleiades. It is important to keep in mind that this thesis does not present systematic comparisons with all nearby group of stars. Instead only some examples were chosen.

A further improvement can be made by abandoning any list of canonical members. Such a list always biases the resulting membership criteria as already has been pointed out in Sect. 1.3.2. The kinematical clustering discussed in Sect. 1.3.3 allows to fix group properties without any canonical member list. Herewith an underlying unbiased sample is essential. Fuhrmann (2004) extends this principle to a sort of “spectroscopic clustering” based on an underlying volume-complete and magnitude-limited sample (see Sect. 1.3.6).

5 Summary and outlook

The Ursa Major (UMa) group consists of the UMa open cluster and many more stars moving into the same direction. The stars are close and thus suited for many kinds of studies. The UMa group would be an ideal sample for evolutional analyses if the age constraints could be improved. The adopted age depends on the exact member list as do the overall properties of the group. Yet recent member lists disagree.

Therefore I selected a sample of stars comprised of the certain kinematic members in order to readdress the spectroscopic properties of the UMa group. The lack of homogeneous analyses of stellar parameters, i.e. effective temperature, surface gravity, and abundances, of a larger sample of mid- and late-type UMa group members motivated new analyses based on spectroscopic observations with high resolving power ($\approx$60000) and signal-to-noise ratio ($\gtrsim$200).

Spectra for twenty late-type kinematic members were obtained within a larger project on the UMa group during eleven observing campaigns in 2002-2004 with *FOCES* on Calar Alto and the Coudé-Échelle spectrograph in Tautenburg.

I followed the quantitative spectral analyses of Fuhrmann (2004, and preceeding work) who already had analysed five of the certain kinematic UMa group members. Stellar parameters for ten more members with spectral types late-F to early-K were derived extending Fuhrmann's work on the UMa group beyond 25 pc. The spectral analysis is strictly differential with respect to the Sun. Effective temperatures were derived from the wings of Balmer lines based on *MAFAGS* model atmospheres in local thermal equilibrium. Surface gravities were determined from the iron ionisation equilibrium and the wings of the Mg Ib triplet. For four stars, neither of these methods could be used so that surface gravities had to be calculated from *Hipparcos* distance. Otherwise all stellar parameters were obtained consistently from the spectra only. The lines of ionised iron yielded iron abundance and projected rotational velocity. The magnesium abundance could be estimated from a few lines of neutral magnesium.

The analyses were exposed to several tests. The overall validity of the analysis was confirmed by reproducing the solar parameters from moon exposures obtained twice in each observing run. The application on young stars was approved by reproducing the values obtained by Fuhrmann (2004) for HD 217813. The spectroscopic distances were calculated from the derived stellar parameters of the UMa group members and agree well with the *Hipparcos* distances. Finally the measurements were compared to values of individual stars taken from the literature. The effective temperatures are consistent with previous findings whereas the agreement of surface gravities and iron abundances is worse. Primarily this finding does not question the accuracy of the parameters derived in this thesis. Rather the inconsistencies reflect the inhomogeneity of the literature data.

The interpretation of the results took advantage of the fact that five stars already had been analysed by Fuhrmann (2004) and one further star by König et al. (2006) by means of the same methods. Therefore homogeneous stellar parameters are available for in total sixteen mid- and late-type kinematic UMa group members including seven beyond 25 pc.

The surface gravities and effective temperatures are consistent with the main sequence but do not allow further conclusions on the age. The new mean abundance of the UMa group is [Fe/H]= -0.03 ± 0.04, higher by 0.06 dex relative to previous estimations. It is still different from the Hyades' value but cannot be distinguished from the iron abundance of the Pleiades. The iron and magnesium abundances of the UMa group members agree with the abundances of the thin disk population. Homogeneous projected rotational velocities are available for in total eighteen stars of the sample, including ten stars from the present work and two stars from Fuhrmann (2000). They show the onset of main sequence magnetic braking at effective temperatures of ≈6200 K. The rotation rates are consistent with an age of 250 – 1000 Myrs. More information can be obtained when considering photometric periods (cf. Fuhrmann 2004).

The equivalent width of the Li I λ6707.8 Å resonance doublet of all twenty observed kinematic mid- and late-type members was measured in this work. The amount of lithium absorption is different from the Pleiades, M 35, and the Hyades at effective temperatures between ≈5000 K and that of the Sun, indicating an age between 180 Myrs and 630 Myrs. However this conlusion is based on a rather small number of data points. It's noteworthy at this point that a substantial part of the kinematic UMa group sample is located on the southern sky and spectra for this work could not have been obtained yet. New insights may be given by comparing the abundances instead of the equivalent widths to other groups of stars. A homogeneous comparison to Sestito & Randich (2005) will be possible by applying non-LTE corrections (following Carlsson et al. 1994) to the LTE abundances based on Soderblom et al. (1993b).

The chromospheric filling-in of the Hα line was estimated for the same twenty stars the same way as in Fuhrmann (2004) so that measurements of additional four kinematic UMa group members could be included from the latter work. While Fuhrmann (2004) realised a quite homogeneous filling-in considering his UMa group sample, the scatter in the present kinematic sample is substantial. Nevertheless the data confirm that the $H\alpha$ core intensity is systematically higher than that of the Sun. This corroborates previous findings that the UMa group members are more active and younger than the Sun.

In spite of the presented age estimates, the overall limits on the age of the UMa group did not improve. The strongest constraint is the lithium age of 180 – 630 Myrs found by comparing the lithium absorption with nearby stellar groups. Certainly this constraint will be sharpened by a systematic comparison to more clusters. More important than the overall age limit is the fact that the correlation of Li equivalent width with effective temperature shows little scatter similar to the Hyades arguing against the rather larger age spread of 200 – 600 Myrs found in the literature.

The interesting question now is whether all these properties can be used to affirm the membership of further UMa group candidates. Strong membership criteria have to be based on properties which can be distinguished from other groups of stars. In this

respect, the iron abundance and the lithium absorption appear to be suited to decide on membership of late-type UMa group candidates while the surface gravities, the projected rotational velocity, and the filling-in of the Hα line are rather inconclusive. In praxis, lithium equivalent widths and iron abundance have to be compared systematically with other stellar groups first. Of course, their use as membership criteria will gain strength when combined with kinematics.

An important work not done here is the systematic comparison of two completely different approaches. I discussed that this work is based on a selection of kinematic members, a list of "canonical" members. In contrast, Fuhrmann (2004) isolated the UMa group by clustering in the "spectroscopic space", i.e. filling-in of the Hα line core and lithium absorption. Similar to Soderblom & Mayor (1993), he realised that the kinematics of the spectroscopically constrained UMa group are close to the previously known space velocity of the UMa cluster. The approach of Fuhrmann (2004) is only possible because of the underlying volume-complete and magnitude-limited sample. Interesting questions arise: What would the kinematics of the UMa group look like when based on an extended sample which is selected by Fuhrmann's spectroscopic criteria? Are the spectroscopic criteria more distinct than the kinematic criteria?

Bibliography

Adelman, S. J., Coursey, B. C., & Harris, E. A. 2000, Informational Bulletin on Variable Stars, 5003, 1

Ali, A. W. & Griem, H. R. 1965, Physical Review, 140, 1044

Ali, A. W. & Griem, H. R. 1966, Physical Review, 144, 366

Allende Prieto, C., Barklem, P. S., Lambert, D. L., & Cunha, K. 2004, A&A, 420, 183

Allende Prieto, C. & Lambert, D. L. 1999, A&A, 352, 555

Alonso, A., Arribas, S., & Martínez-Roger, C. 1995, A&A, 297, 197

Alonso, A., Arribas, S., & Martínez-Roger, C. 1996, A&AS, 117, 227

Ammler, M., Guenther, E. W., König, B., & Neuhäuser, R. 2005, in Proceedings of 'The 13th Cambridge Workshop on Cool Stars, Stellar Systems and the Sun', ed. F. Favata, G. Hussain, & B. Battrick, Vol. 1, ESA, 391

Asiain, R., Figueras, F., Torra, J., & Chen, B. 1999, A&A, 341, 427

Asplund, M. 2005, ARA&A, 43, 481

Asplund, M., Grevesse, N., & Sauval, A. J. 2005, in ASP Conf. Ser. 336: Cosmic Abundances as Records of Stellar Evolution and Nucleosynthesis, ed. T. G. Barnes & F. N. Bash, 25–+

Axer, M., Fuhrmann, K., & Gehren, T. 1994, A&A, 291, 895

Baraffe, I., Chabrier, G., Allard, F., & Hauschildt, P. 1998, A&A, 337, 403

Barklem, P. S., Stempels, H. C., Allende Prieto, C., et al. 2002, A&A, 385, 951

Barrado y Navascués, D., Deliyannis, C. P., & Stauffer, J. R. 2001, ApJ, 549, 452

Bessell, M. S. 1979, PASP, 91, 589

Bessell, M. S. 1991, AJ, 101, 662

Bessell, M. S. 2000, PASP, 112, 961

Biazzo, K., Frasca, A., Catalano, S., & Marilli, E. 2006, A&A, 446, 1129

Biemont, E., Baudoux, M., Kurucz, R. L., Ansbacher, W., & Pinnington, E. H. 1991, A&A, 249, 539

Biemont, E., Hibbert, A., Godefroid, M., & Vaeck, N. 1993, ApJ, 412, 431

Blackwell, D. E. & Shallis, M. J. 1977, MNRAS, 180, 177

Boesgaard, A. M. 1989, ApJ, 336, 798

Boesgaard, A. M., Budge, K. G., & Burck, E. E. 1988, ApJ, 325, 749

Boesgaard, A. M. & Friel, E. D. 1990, ApJ, 351, 467

Bohlin, K. 1905, Astronomische Nachrichten, 167, 209

Böhm-Vitense, E. 1958, Zeitschrift für Astrophysik, 46, 108

Burrows, A., Marley, M., Hubbard, W. B., et al. 1997, ApJ, 491, 856

Campbell, B., Walker, G. A. H., & Yang, S. 1988, ApJ, 331, 902

Carlsson, M., Rutten, R. J., Bruls, J. H. M. J., & Shchukina, N. G. 1994, A&A, 288, 860

Castellani, V., Chieffi, A., & Straniero, O. 1992, ApJS, 78, 517

Castro, S., Porto de Mello, G. F., & da Silva, L. 1999, MNRAS, 305, 693

Cayrel, R., Cayrel de Strobel, G., & Campbell, B. 1988, in IAU Symp. 132: The Impact of Very High S/N Spectroscopy on Stellar Physics, 449–+

Cayrel de Strobel, G., Soubiran, C., & Ralite, N. 2001, A&A, 373, 159

Chang, T. N. 1990, Phys. Rev. A, 41, 4922

Chen, Y. Q., Nissen, P. E., Zhao, G., Zhang, H. W., & Benoni, T. 2000, A&AS, 141, 491

Chereul, E., Crézé, M., & Bienaymé, O. 1999, A&AS, 135, 5

Chupina, N. V., Reva, V. G., & Vereshchagin, S. V. 2001, A&A, 371, 115

Croswell, K. 2005, Descendants of the Dipper, Astronomy, p. 40

de Laverny, P., do Nascimento, J. D., Lèbre, A., & De Medeiros, J. R. 2003, A&A, 410, 937

Delhaye, J. 1948, B.A.N., 10, 409

Duncan, D. K. 1981, ApJ, 248, 651

Dziewulski, W. 1916, Bull. Internat. Acad. Sci. Cracovie, A, 251

Edmonds, F. N., Schlüter, H., & Wells, D. C. 1967, Mem. R. Astron. Soc., 71, 271

Edvardsson, B., Andersen, J., Gustafsson, B., et al. 1993, A&A, 275, 101

Eggen, O. J. 1958, MNRAS, 118, 65

Eggen, O. J. 1989, PASP, 101, 366

Eggen, O. J. 1992, AJ, 104, 1493

Eggen, O. J. 1994, in Galactic and Solar System Optical Astrometry, 191–+

Eggen, O. J. 1995, AJ, 110, 2862

Eggen, O. J. 1998, AJ, 116, 782

ESA. 1997, VizieR Online Data Catalog, 1239, 0

Fabricius, C. & Makarov, V. V. 2000, A&A, 356, 141

Feautrier, P. 1964, C. R. Acad. Sci. Paris, 258, 3189

Forrest, W. J., Shure, M., & Skrutskie, M. F. 1988, ApJL, 330, L119

Friel, E. D. & Boesgaard, A. M. 1992, ApJ, 387, 170

Fuhrmann, K. 1993, PhD thesis, LMU München

Fuhrmann, K. 1998, A&A, 338, 161

Fuhrmann, K. 2000, http://www.usm.uni-muenchen.de/people/gehren/topics/pap_100.pdf

Fuhrmann, K. 2004, Astronomische Nachrichten, 325, 3

Fuhrmann, K., Axer, M., & Gehren, T. 1993, A&A, 271, 451

Fuhrmann, K., Axer, M., & Gehren, T. 1994, A&A, 285, 585

Fuhrmann, K., Pfeiffer, M., Frank, C., Reetz, J., & Gehren, T. 1997a, A&A, 323, 909

Fuhrmann, K., Pfeiffer, M. J., & Bernkopf, J. 1997b, A&A, 326, 1081

Gaidos, E. J. & Gonzalez, G. 2002, New Astronomy, 7, 211

García Lopéz, R. J., Rebolo, R., & Martín, E. L. 1994, A&A, 282, 518

Giannuzzi, M. A. 1979, A&A, 77, 214

Gliese, W. 1941, Astronomische Nachrichten, 272, 97

Gliese, W. & Jahreiß, H. 1991, Preliminary Version of the Third Catalogue of Nearby Stars, Tech. rep.

Gould, B. A. 1879, Resultados del Observatorio Nacional Argentino en Cordoba, 1, 354

Gratton, R. G., Carretta, E., & Castelli, F. 1996, A&A, 314, 191

Gray, D. 1992, The observation and analysis of stellar atmospheres, 2nd edn. (Cambridge: Cambridge University Press)

Gray, D. 2005, The observation and analysis of stellar photospheres, 3rd edn. (Cambridge: Cambridge University Press)

Gray, D. F. 1984, ApJ, 281, 719

Gray, R. O., Corbally, C. J., Garrison, R. F., McFadden, M. T., & Robinson, P. E. 2003, AJ, 126, 2048

Grupp, F. 2003, A&A, 412, 897

Grupp, F. 2004, PhD thesis, LMU München

Gustafsson, B. 1971, A&A, 10, 187

Haas, J. 1931, Astronomische Nachrichten, 241, 233

Halley, E. 1718, Phil. Trans., 30, 736

Hanbury Brown, R., Davis, J., & Allen, L. R. 1974, MNRAS, 167, 121

Hatzes, A. P., Guenther, E. W., Endl, M., et al. 2005, A&A, 437, 743

Heis, E. 1872, Neuer Himmels-Atlas (Coeln: M. duMont-Schauberg)

Herbig, G. H. 1985, ApJ, 289, 269

Hertzsprung, E. 1909, ApJ, 30, 135

Høg, E., Fabricius, C., Makarov, V. V., et al. 2000, A&A, 355, L27

Holweger, H. 1972, Solar Phys., 25, 14

Holweger, H. 1979, in Les Elements et leurs Isotopes dans l'Univers, 22nd Liège Symp., Liège

Holweger, H., Hempel, M., & Kamp, I. 1999, A&A, 350, 603

Horne, K. 1986, PASP, 98, 609

Huggins, W. 1871, Royal Society of London Proceedings Series I, 20, 379

Hünsch, M., Randich, S., Hempel, M., Weidner, C., & Schmitt, J. H. M. M. 2004, A&A, 418, 539

Joy, A. H. 1945, ApJ, 102, 168

Kenworthy, M., Hofmann, K.-H., Close, L., et al. 2001, ApJL, 554, L67

Kenyon, S. & Hartmann, L. 1995, ApJS, 101, 117

King, J., Villarreal, A., Soderblom, D., Gulliver, A., & Adelman, S. 2003, AJ, 125, 1980

King, J. R. & Schuler, S. C. 2005, PASP, 117, 911, kS05

Kirkpatrick, J. D. 2001, in ASP Conf. Ser. 231: Tetons 4: Galactic Structure, Stars and the Interstellar Medium, ed. C. E. Woodward, M. D. Bicay, & J. M. Shull, 17–+

Kitchin, C. 1998, Astrophysical Techniques, 3rd edn. (Bristol and Philadelphia: Institute of Physics Publishing)

Klinkerfues, W. 1873, Göttingen Nachr.

König, B. 2003, PhD thesis, LMU Munich

König, B., Fuhrmann, K., Neuhäuser, R., Charbonneau, D., & Jayawardhana, R. 2002, A&A, 394, L43

König, B., Guenther, E. W., Esposito, M., & Hatzes, A. 2006, MNRAS, 365, 1050

König, B., Guenther, E. W., Woitas, J., & Hatzes, A. P. 2005, A&A, 435, 215

Korn, A. J. 2002, in Scientific Drivers for ESO Future VLT/VLTI Instrumentation Proceedings of the ESO Workshop held in Garching, Germany, 11-15 June, 2001. p. 199., 199–+

Kroupa, P. 2002, Science, 295, 82

Kupka, F., Piskunov, N., Ryabchikova, T. A., Stempels, H. C., & Weiss, W. W. 1999, A&AS, 138, 119

Kupka, F. G., Ryabchikova, T. A., Piskunov, N. E., Stempels, H. C., & Weiss, W. W. 2000, Baltic Astronomy, 9, 590

Kurucz, R. 1995, in Highlights of Astronomy, ed. I. Appenzeller, Vol. 10, 407–410

Kurucz, R. L. 1979, ApJS, 40, 1

Kurucz, R. L. 1992, Revista Mexicana de Astronomia y Astrofisica, vol. 23, 23, 181

Kurucz, R. L., Furenlid, I., & Brault, J. T. L. 1984, Solar flux atlas from 296 to 1300 nm (National Solar Observatory Atlas, Sunspot, New Mexico: National Solar Observatory, 1984)

Lambert, D. L. 1978, MNRAS, 182, 249

Lowrance, P. J., Becklin, E. E., Schneider, G., et al. 2005, AJ, 130, 1845

Luck, R. E. & Heiter, U. 2005, AJ, 129, 1063

Ludendorff, H. 1910, Astronomische Nachrichten, 183, 113

Ludwig, H.-G. & Kučinskas, A. 2005, in 13th Cambridge Workshop on Cool Stars, Stellar Systems and the Sun, ed. F. Favata, G. Hussain, & B. Battrick, Vol. 1, 319–325, held 5-9 July 2004, Hamburg, Germany

Makarov, V. V. & Kaplan, G. H. 2005, AJ, 129, 2420

Mallik, S. V. 1998, A&A, 338, 623

McLean, I. 1997, Electronic imaging in astronomy – Detectors and Instrumentation, Wiley-Praxis Series in Astronomy and Astrophysics (John Wiley & Sons Ltd in association with Praxis Publishing Ltd)

McWilliam, A. 1990, ApJS, 74, 1075

Mestel, L. 1999, Stellar Magnetism (New York: Oxford University Press, INc.)

Mihalas, D. 1978, Stellar Atmospheres, 2nd edn. (San Francisco: W.H. Freeman and Company)

Montes, D. 2001, in ASP Conf. Ser. 223: 11th Cambridge Workshop on Cool Stars, Stellar Systems and the Sun, ed. R. J. Garcia Lopez, R. Rebolo, & M. R. Zapaterio Osorio, 1471–+

Montes, D., López-Santiago, J., Gálvez, M. C., et al. 2001a, MNRAS, 328, 45

Montes, D., López-Santiago, J., Fernández-Figueroa, M. J., & Gálvez, M. C. 2001b, A&A, 379, 976

Neckel, T. 1994, Compendium of Practical Astronomy, ed. G. D. Roth (Springer-Verlag), 129

Neuhäuser, R., Torres, G., Sterzik, M. F., & Randich, S. 1997, A&A, 325, 647

Nordström, B., Mayor, M., Andersen, J., et al. 2004, A&A, 418, 989

O'Mara, B. J. 1976, MNRAS, 177, 551

Pasquini, L. & Pallavicini, R. 1991, A&A, 251, 199

Pavlenko, Y. V. 1995, Memorie della Societa Astronomica Italiana, 66, 441

Perrin, G., Coudé du Foresto, V., Ridgway, S., et al. 1998, A&A, 331, 619

Perryman, M. A. C., Brown, A. G. A., Lebreton, Y., et al. 1998, A&A, 331, 81

Perryman, M. A. C., Lindegren, L., Kovalevsky, J., et al. 1997, A&A, 323, L49

Pfeiffer, M. J., Frank, C., Baumueller, D., Fuhrmann, K., & Gehren, T. 1998, A&AS, 130, 381

Pinsonneault, M. 1997, ARA&A, 35, 557

Piskunov, N. E., Kupka, F., Ryabchikova, T. A., Weiss, W. W., & Jeffery, C. S. 1995, A&AS, 112, 525

Pöppel, W. 1997, Fundamentals of Cosmic Physics, 18, 1

Potter, D., Martín, E. L., Cushing, M. C., et al. 2002, ApJL, 567, L133

Proctor, R. A. 1869, Royal Society of London Proceedings Series I, 18, 169

Reile, C. 1987, Master's thesis, LMU München

Richichi, A., Ragland, S., Stecklum, B., & Leinert, C. 1998, A&A, 338, 527

Roman, N. G. 1949, ApJ, 110, 205

Ryabchikova, T. A., Piskunov, N. E., Kupka, F., & Weiss, W. W. 1997, Baltic Astronomy, 6, 244

Sandage, A. 1956, PASP, 68, 498

Scheffler, H. & Elsässer, H. 1992, Bau und Physik der Galaxis (Leipzig; Wien; Zürich: BI-Wiss.-Verl.)

Schmidt-Kaler, T. 1982, in Landolt-Börnstein, ed. K. Schaifers & H. Voigt, Vol. 2 (Berlin: Springer), 449

Sesti, G. M. 1991, The glorious constellations – History and mythology (New York: Abrams Inc.)

Sestito, P. & Randich, S. 2005, in 13th Cambridge Workshop on Cool Stars, Stellar Systems and the Sun, ed. F. Favata, G. Hussain, & B. Battrick, Vol. 2, 959–962, held 5-9 July 2004, Hamburg, Germany

Sestito, P. & Randich, S. 2005, A&A, 442, 615

Skumanich, A. 1972, ApJ, 171, 565

Smart, W. M. 1939a, MNRAS, 99, 441

Smart, W. M. 1939b, MNRAS, 99, 710

Soderblom, D. R., Jones, B. F., Balachandran, S., et al. 1993a, AJ, 106, 1059

Soderblom, D. R. & Mayor, M. 1993, AJ, 105, 226

Soderblom, D. R., Oey, M. S., Johnson, D. R. H., & Stone, R. P. S. 1990, AJ, 99, 595

Soderblom, D. R., Stauffer, J. R., MacGregor, K. B., & Jones, B. F. 1993b, ApJ, 409, 624

Stahler, S. W. & Palla, F. 2004, The Formation of Stars (Weinheim, Germany: Wiley-VCH)

Steffen, M. & Holweger, H. 2002, A&A, 387, 258

Steinhauer, A. 2003, PhD thesis

Stix, M. 1989, The Sun – An Introduction (Berlin, Heidelberg, New York: Springer-Verlag)

Strassmeier, K., Washuettl, A., Granzer, T., Scheck, M., & Weber, M. 2000, A&AS, 142, 275

Stürenburg, S. & Holweger, H. 1990, A&A, 237, 125

Terndrup, D. M., Stauffer, J. R., Pinsonneault, M. H., et al. 2000, AJ, 119, 1303

Thorburn, J., Hobbs, L., Deliyannis, C., & Pinsonneault, M. 1993, ApJ, 415, 150

Unsöld, A. 1955, Physik der Sternatmosphären, 2nd edn. (Berlin-Göttingen-Heidelberg: Springer)

Unsöld, A. & Baschek, B. 1999, Der neue Kosmos – Einführung in die Astronomie und Astrophysik, 6th edn. (Berlin, Heidelberg: Springer)

van Bueren, H. G. 1952, BAN, 11, 385

VandenBerg, D. A., Bergbusch, P. A., & Dowler, P. D. 2006, ApJS, 162, 375

VandenBerg, D. A., Swenson, F. J., Rogers, F. J., Iglesias, C. A., & Alexander, D. R. 2000, ApJ, 532, 430

Vernazza, J. E., Avrett, E. H., & Loeser, R. 1981, ApJS, 45, 635

Vidal, C. R., Cooper, J., & Smith, E. W. 1970, JQSRT, 10, 1011

Vidal, C. R., Cooper, J., & Smith, E. W. 1973, ApJS, 25, 37

von Hoerner, S. 1957, Zeitschrift fur Astrophysik, 42, 273

Walter, F. M., Linsky, J. L., Simon, T., Golub, L., & Vaiana, G. S. 1984, ApJ, 281, 815

Wielen, R. 1971, A&A, 13, 309

Wielen, R. 1977, A&A, 60, 263

Wielen, R. 1978, BAAS, 10, 408

Wielen, R. 1991, in ASP Conf. Ser. 13: The Formation and Evolution of Star Clusters, ed. K. Janes, 343–349

Yi, S., Demarque, P., Kim, Y.-C., et al. 2001, ApJS, 136, 417

A The kinematic membership criteria of Eggen (1958, 1995)

A.1 Preliminaries

The kinematic properties of a cluster are fully described by the galactic space velocity components. However the observed quantity is not the space velocity but proper motion given in the ecliptical coordinate system centred at the observer. Consequently the projection of the space velocity onto the celestial sphere depends on the position of the star considered. Therefore for the full description of the problem, the following stellar kinematic parameters are needed:

α	right ascension
δ	declination
μ	total proper motion
π [mas]	parallax
$\rho \left[\frac{\text{km}}{\text{s}}\right]$	radial velocity
$\nu \left[\frac{\text{mas}}{\text{yr}}\right]$	proper motion component in direction of the convergent point
$\tau \left[\frac{\text{mas}}{\text{yr}}\right]$	proper motion component perpendicular to the direction of the convergent point
λ	angular separation between the star and the cluster's convergent point
U, V, W	galactic velocity components in the direction of the galactic centre, of the galactic rotation, and perpendicular to the galactic plance, respectively
$V_{\text{tot,c}} = U_{\text{c}}^2 + V_{\text{c}}^2 + W_{\text{c}}^2$	the cluster's total space velocity
$V_{\text{tan,c}} = V_{\text{tot,c}} \cdot \sin\lambda$	tangent velocity of a cluster member at an angular separation λ from the convergent point
$\rho_c = V_{\text{tot,c}} \cdot \cos\lambda$	expected radial velocity of a cluster member at an angular separation λ from the convergent point

A.2 Moving cluster method

The tangent velocity of a star is given by Eq. 1.1:

$$V_{\text{tan}} = r\,[\text{km}] \cdot \mu \left[\frac{\text{rad}}{\text{s}}\right] = 4.738 \frac{\mu[''/yr]}{\pi['']} \tag{A.1}$$

where the first equation follows from elementary geometry and the second equation results from conversion of units (Unsöld & Baschek 1999, p. 174).

In case that the star belongs to a moving cluster, we have $V_{\rm tot} = V_{\rm tot,c}$, $\rho = \rho_{\rm c}$ and $V_{\rm tan} = V_{\rm tan,c}$. With Eq. A.1 follows:

$$\pi = \frac{4.74{\cdot}\mu}{V_{\rm tan}} = \frac{4.74{\cdot}\mu}{V_{\rm tot} \cdot \sin\lambda} = \frac{4.74{\cdot}\mu}{\rho \cdot \tan\lambda} \tag{A.2}$$

The resulting parallaxes are very accurate once the cluster's convergent point is well-known and the star's membership established.

A.3 Peculiar velocity criterion

The first membership criterion is to compare the proper motion of the candidate to the proper motion expected if the star was a member of the cluster. The amount of deviation is given by the *peculiar velocity* of the candidate:

$$PV \equiv \frac{4.74}{\pi}\tau \tag{A.3}$$

A candidate then is accepted as a member of the cluster if the peculiar velocity is sufficiently small. "Sufficiently small" means that the peculiar velocity is much smaller than the cluster's total space velocity.

Until the end of the last century, the parallax has been the most uncertain parameter so that it has been expressed by Eq. A.2 but using the proper motion component ν in direction of the convergent point instead of the total proper motion μ (Eggen 1958, 1995)[1]. Eggen (1995) considered a candidate to be a member if its peculiar velocity was less than 10 % of the cluster's total space velocity:

$$|PV| \leq 0.1{\cdot}V_{\rm tot,c} \Longleftrightarrow \frac{|\tau|}{\nu} \leq \frac{0.1}{\sin\lambda} \tag{A.4}$$

A.4 Radial velocity criterion

Likewise the parallaxes did not enter the second criterion, too, which compared the expected radial velocity ρ_c with the actual radial velocity ρ of the candidate. Eggen (1958) accepted a deviation of $\leq\ 3 - 5$ km/s for members.

A.5 Adaption by Montes et al. (2001a)

The criteria are slightly modified by Montes et al. (2001a) inasmuch precise parallaxes entered from the *Hipparcos* and *Tycho* catalogues (ESA 1997; Høg et al. 2000). This

[1] Of course, with the advent of precise *Hipparcos* parallaxes for most of the bright nearby stars, space velocities can be calculated accurately and compared directly to the cluster's space velocity.

allowed to reinterpret A.2 in order to derive an expected total space velocity V_{tot} of the candidate from its total proper motion μ, and the actually co-moving component V_{T} from its proper motion component ν:

$$V_{\mathrm{tot}} = \frac{4.74}{\pi \sin \lambda} \cdot \mu$$
$$V_{\mathrm{T}} = \frac{4.74}{\pi \sin \lambda} \cdot \nu$$

Then the peculiar velocity is related to V_{T} instead the cluster's total velocity $V_{\mathrm{tot,c}}$ leaving the right hand side expression of Eq. A.4 unchanged. However the radial velocity criterion is modified as the expected radial velocity is now expressed by:

$$\rho_{\mathrm{T}} = V_{\mathrm{T}} \cos \lambda$$

Referring to early works of Eggen, Montes et al. (2001a) adopted a tolerance of $4 - 8 \frac{\mathrm{km}}{\mathrm{s}}$ for members.

The application of both criteria to the individual stars accounts for the errors in V_{T}, in the peculiar velocity PV, and in the radial velocity ρ.

B Details on the used spectra

Table B.1: List of the spectra which were included in this work – Spectra with sufficient signal-to-noise ratio ($S/N < 200$) could not be obtained for several stars. Improvements were achieved by adding two spectra if available, i.e. in the cases of HD 95650, HD 115043, HD 155674 A, HD 238087, and HD 238224. The signal-to-noise ratio was measured in the order with the Hα line.

exposure	object	run identifier	S/N
uma_Oct03_0179.FITS	HD 24916A	Oct03	240
uma_Feb04_0176.FITS	HD 26923	Feb04	293
uma_Oct03_0106.FITS	HD 28495	Oct03	242
uma_Oct03_0107.FITS	HD 28495	Oct03	249
uma_Oct03_0112.FITS	HD 38393	Oct03	382
uma_Oct03_0113.FITS	HD 38393	Oct03	332
planetXVI_0196.FITS	HD 71974A	Mar03	194
HD95650_coad.FITS	HD 95650	Feb04	212
uma_May04_0377.FITS	HD 109647	May04	173
uma_Feb04_0317.FITS	HD 110463	Feb04	148
uma_Feb04_0318.FITS	HD 110463	Feb04	224
uma_May04_0155.FITS	HD 112196	May04	302
uma_May04_0156.FITS	HD 112196	May04	286
HD115043_COAD.FITS	HD 115043	Mar03	216
planetX_0641.FITS	HD 152863A	Jul02	194
HD155674A_coad.FITS	HD 155674A	May04	200
uma_May04_380.FITS	HD 155674B	May04	107
planetXVIII_0149.FITS	HD 167389	Jul03	201
planetXVIII_0150.FITS	HD 167389	Jul03	204
uma_May04_0381.FITS	HD 171746A	May04	240
uma_May04_0323.FITS	HD 171746A	May04	209
uma_May04_0322.FITS	HD 171746B	May04	142
planetXVIII_0193.FITS	HD 184960	Jul03	250
uma_Oct03_0088.FITS	HD 184960	Oct03	342
uma_Oct03_0093.FITS	HD 205435	Oct03	423
planetXVIII_0296.FITS	HD 217813	Jul03	267
HD238087_coad.FITS	HD 238087	Feb04	165
HD238224_coad.FITS	HD 238224	Feb04	178
planetXVI_0248.FITS	MOON KSO	Mar03	620
planetXVI_0249.FITS	MOON KSO	Mar03	424
planetXVIII_0205.FITS	MOON KSO	Jul03	498
planetXVIII_0206.FITS	MOON KSO	Jul03	471
uma_Oct03_0094.FITS	MOON CA	Oct03	432
uma_Oct03_0095.FITS	MOON CA	Oct03	469
uma_Feb04_0112.FITS	MOON CA	Feb04	323
uma_Feb04_0113.FITS	MOON CA	Feb04	345
uma_May04_0082.FITS	MOON CA	May04	411
uma_May04_0083.FITS	MOON CA	May04	357

C Line data

Table C.1: Line data – Following values are listed: **(1)** central wavelength, **(2)** element number, **(3)** ionisation stage, **(4)** lower excitation potential, **(5)** oscillator strength, **(6)** van der Waals damping constant, **(7)** radiative damping constant, **(8)** quadratic Stark effect damping constant. See Sect. 3.2.6 for the exact definitions. The effect of quadratic Stark broadening ($\log C_4$) on weak iron lines is negligible so that in this work, it is usually not taken into account for these lines. The radiation damping constant ($\gamma_{\rm rad}$) is calculated with the classical formula within *LINFOR* in case it is missing in the table.

λ [Å]	Z	ion. stage	$\chi_{\rm low}$ [eV]	$\log gf$	$\log C_6$	$\gamma_{\rm rad}$ 10^8 [1/s]	$\log C_4$
4481.330	12	2	8.83	0.70	-30.20	6.9600	-15.00
4571.100	12	1	0.00	-5.59	-31.50	–	-15.00
4607.330	38	1	0.00	0.04	-31.61	–	-15.00
4613.910	40	2	0.97	-0.62	-32.27	–	-15.00
4703.000	12	1	4.33	-0.52	-29.55	4.9520	-15.00
4730.030	12	1	4.33	-2.34	-28.80	4.7680	-15.00
4883.690	39	2	1.08	0.15	-32.18	–	-15.00
4923.930	26	2	2.89	-1.48	-31.90	3.0800	-15.00
4993.350	26	2	2.80	-3.73	-31.60	3.0500	-15.00
4994.140	26	1	0.91	-3.01	-31.97	15.000	-15.00
5018.450	26	2	2.89	-1.33	-31.90	3.0600	-15.00
5087.420	39	2	1.08	-0.19	-32.21	–	-15.00
5127.370	26	1	0.91	-3.20	-31.97	16.600	-15.00
5167.340	12	1	2.70	-0.87	-30.88	1.0020	-14.50
5172.700	12	1	2.70	-0.39	-30.88	1.0020	-14.50
5183.620	12	1	2.70	-0.17	-30.88	1.0020	-14.50
5197.580	26	2	3.23	-2.31	-31.80	3.0300	-15.00
5198.720	26	1	2.22	-2.12	-31.50	1.6100	-15.00
5217.400	26	1	3.21	-1.08	-30.60	76.000	-15.00
5223.190	26	1	3.64	-2.25	-31.91	78.600	-15.00
5232.950	26	1	2.94	-0.11	-30.90	10.203	-15.00
5234.630	26	2	3.22	-2.23	-31.80	3.0700	-15.00
5242.500	26	1	3.63	-0.87	-31.70	57.500	-15.00
5264.810	26	2	3.23	-3.11	-32.19	4.1100	-15.00

Table C.1 continued next page

Table C.1 continued

λ [Å]	Z	ion. stage	$\chi_{\rm low}$ [eV]	loggf	logC_6	$\gamma_{\rm rad}$ 10^8 [1/s]	logC_4
5281.800	26	1	3.04	-0.91	-30.90	1.0200	-15.00
5284.110	26	2	2.89	-3.12	-32.11	3.4300	-15.00
5295.320	26	1	4.42	-1.52	-31.15	1.8380	-15.00
5302.310	26	1	3.28	-0.75	-30.60	74.900	-15.00
5324.190	26	1	3.21	-0.13	-30.60	75.600	-15.00
5325.560	26	2	3.22	-3.22	-31.80	3.1000	-15.00
5339.940	26	1	3.27	-0.65	-30.60	74.900	-15.00
5364.880	26	1	4.45	0.39	-31.15	1.8550	-15.00
5367.480	26	1	4.42	0.49	-31.15	1.8500	-15.00
5379.580	26	1	3.69	-1.44	-31.70	57.500	-15.00
5383.380	26	1	4.31	0.68	-31.15	1.7580	-15.00
5393.170	26	1	3.24	-0.74	-30.60	74.800	-15.00
5414.070	26	2	3.22	-3.61	-32.19	4.1200	-15.00
5425.250	26	2	3.20	-3.28	-31.80	2.9900	-15.00
5434.530	26	1	1.01	-2.13	-31.99	14.000	-15.00
5497.520	26	1	1.01	-2.82	-31.99	14.200	-15.00
5522.450	26	1	4.21	-1.40	-30.80	89.800	-15.00
5528.420	12	1	4.33	-0.50	-30.43	4.9080	-13.10
5534.850	26	2	3.24	-2.83	-32.18	2.9900	-15.00
5546.510	26	1	4.37	-1.05	-31.20	1.7860	-15.00
5560.220	26	1	4.43	-0.96	-31.50	1.6410	-15.00
5576.100	26	1	3.43	-0.79	-30.85	75.300	-15.00
5611.360	26	1	3.64	-2.93	-31.91	1.2500	-15.00
5618.640	26	1	4.21	-1.22	-31.46	1.0450	-15.00
5636.700	26	1	3.64	-2.52	-31.94	39.000	-15.00
5638.270	26	1	4.22	-0.65	-31.00	1.9430	-15.00
5651.470	26	1	4.47	-1.77	-31.30	1.6310	-15.00
5679.030	26	1	4.65	-0.64	-30.80	1.3990	-15.00
5711.090	12	1	4.33	-1.70	-30.00	4.8170	-15.00
5741.850	26	1	4.26	-1.63	-31.10	2.1080	-15.00
5785.280	12	1	5.11	-1.76	-30.20	–	-15.00
5853.680	56	2	0.60	-0.81	-32.04	–	-15.00
5855.080	26	1	4.61	-1.54	-31.75	1.9110	-15.00
5856.090	26	1	4.29	-1.55	-31.91	86.200	-15.00
5862.360	26	1	4.55	-0.16	-31.30	1.8970	-15.00
5991.380	26	2	3.15	-3.59	-31.60	3.4600	-15.00
6027.060	26	1	4.08	-1.02	-31.91	88.503	-15.00
6056.010	26	1	4.73	-0.31	-30.80	1.8480	-15.00
6065.490	26	1	2.61	-1.38	-31.92	1.0200	-15.00

Table C.1 continued next page

Table C.1 continued

λ [Å]	Z	ion. stage	$\chi_{\rm low}$ [eV]	loggf	logC_6	$\gamma_{\rm rad}$ 10^8 [1/s]	logC_4
6084.110	26	2	3.20	-3.84	-31.60	3.4300	-15.00
6093.650	26	1	4.61	-1.32	-31.75	1.9350	-15.00
6096.670	26	1	3.98	-1.79	-31.10	45.250	-15.00
6113.320	26	2	3.22	-4.16	-31.60	3.4100	-15.00
6125.020	14	1	5.59	-1.52	-30.00	–	-15.00
6142.490	14	1	5.59	-1.45	-30.01	–	-15.00
6149.250	26	2	3.89	-2.75	-31.90	3.3900	-15.00
6151.620	26	1	2.18	-3.29	-31.86	1.5500	-15.00
6157.730	26	1	4.08	-1.10	-31.70	50.203	-15.00
6173.340	26	1	2.22	-2.84	-31.86	1.6700	-15.00
6200.320	26	1	2.61	-2.31	-31.92	1.0300	-15.00
6213.440	26	1	2.22	-2.51	-31.86	1.6500	-15.00
6226.740	26	1	3.88	-2.11	-31.10	54.140	-15.00
6232.650	26	1	3.65	-1.20	-30.70	80.600	-15.00
6239.940	26	2	3.89	-3.50	-31.90	3.3800	-15.00
6240.650	26	1	2.22	-3.27	-31.95	15.700	-15.00
6246.330	26	1	3.60	-0.73	-30.70	79.600	-15.00
6247.560	26	2	3.89	-2.34	-31.90	3.3800	-15.00
6252.570	26	1	2.40	-1.56	-31.92	87.000	-15.00
6330.850	26	1	4.73	-1.15	-31.69	2.3840	-15.00
6335.340	26	1	2.20	-2.22	-31.86	1.6600	-15.00
6336.830	26	1	3.69	-0.80	-30.70	81.100	-15.00
6369.460	26	2	2.89	-4.19	-31.50	2.9000	-15.00
6380.750	26	1	4.19	-1.24	-31.70	73.503	-15.00
6393.610	26	1	2.43	-1.39	-31.92	93.200	-15.00
6411.660	26	1	3.65	-0.56	-30.70	80.300	-15.00
6416.930	26	2	3.89	-2.67	-31.90	3.3700	-15.00
6430.850	26	1	2.18	-2.02	-31.86	1.6500	-15.00
6432.680	26	2	2.89	-3.63	-31.50	2.9000	-15.00
6436.410	26	1	4.19	-2.39	-31.96	30.403	-15.00
6446.400	26	2	6.22	-1.97	-32.18	5.2200	-15.00
6456.390	26	2	3.90	-2.09	-31.90	3.3700	-15.00
6496.910	56	2	0.60	-0.05	-32.10	–	-15.00
6516.090	26	2	2.89	-3.34	-31.50	2.9100	-15.00
6608.030	26	1	2.28	-3.99	-31.91	1.6600	-15.00
6627.550	26	1	4.55	-1.48	-31.44	1.7530	-15.00
6704.480	26	1	4.22	-2.62	-31.16	–	-15.00
6707.760	3	1	0.00	0.00	-31.86	–	-15.00
6707.910	3	1	0.00	-0.31	-31.86	–	-15.00

Table C.1 continued next page

Table C.1 continued

λ [Å]	Z	ion. stage	$\chi_{\rm low}$ [eV]	loggf	logC_6	$\gamma_{\rm rad}$ 10^8 [1/s]	logC_4
6713.750	26	1	4.80	-1.42	-31.30	2.3550	-15.00
6725.360	26	1	4.10	-2.21	-31.37	2.0910	-15.00
6733.150	26	1	4.64	-1.43	-31.37	2.2680	-15.00
6750.160	26	1	2.42	-2.53	-31.95	770.00	-15.00
6786.870	26	1	4.19	-1.90	-31.36	1.9860	-15.00
6806.850	26	1	2.73	-3.11	-31.83	1.0200	-15.00
6810.270	26	1	4.61	-0.94	-30.90	2.3010	-15.00
6820.370	26	1	4.64	-1.11	-30.90	2.2200	-15.00
6837.010	26	1	4.59	-1.74	-31.81	52.405	-15.00
6843.660	26	1	4.55	-0.73	-31.10	1.9230	-15.00
7222.400	26	2	3.89	-3.26	-31.60	4.1400	-15.00
7224.480	26	2	3.89	-3.24	-31.60	4.1400	-15.00
7301.570	26	2	3.89	-3.69	-32.18	3.0700	-15.00
7479.700	26	2	3.89	-3.70	-32.18	3.1000	-15.00
7495.080	26	1	4.22	0.04	-30.80	1.6810	-15.00
7511.030	26	1	4.18	0.18	-30.80	1.6750	-15.00
7515.840	26	2	3.90	-3.45	-31.60	4.0900	-15.00
7711.730	26	2	3.90	-2.56	-31.60	4.1200	-15.00
8923.560	13	1	4.07	-2.12	-30.00	–	-15.00
8923.570	12	1	5.39	-1.57	-29.70	41.250	-15.00

End of Table C.1

D Solution of the model atmosphere problem with *MAFAGS*

D.1 Flux conservation

The energy is produced in the stellar core and lost at the stellar surface. Therefore, the divergence of the energy flux vanishes in the stellar photosphere so that the total energy flux is the same at every depth. The energy flux is composed of the radiative energy flux F_λ and the convective energy flux $\phi(z) =< \rho v_z h >$ with the projected velocity v_z and the specific enthalpy h.
In plane-parallel geometry, we have:

$$F_0 = \phi(z) + \int_0^\infty F_\lambda \mathrm{d}\lambda = \phi(z) + 4\pi \int_0^\infty H_\lambda \mathrm{d}\lambda \tag{D.1}$$

or in differential form:

$$0 = 4\pi \int_0^\infty H_\lambda \mathrm{d}\lambda + \partial_z \phi(z) \tag{D.2}$$

where the so-called *Eddington flux* is defined by:

$$H_\lambda = \frac{1}{2} \int_{-1}^{1} \mu I_\lambda(\mu) \mathrm{d}\mu = \frac{F_\lambda}{4\pi} \tag{D.3}$$

with $\mu = \cos\theta$ (Reile 1987).

D.2 Solution of the model atmosphere

The Feautrier-Rybicki method for temperature correction is used (cf. Gustafsson 1971). The model is iterated until flux constancy is maintained throughout the atmosphere.

The *radiation pressure* is expressed in terms of the K integral $K_\lambda(\tau_\lambda)$:

$$K_\lambda = \oint I_\lambda \cos^2\theta \mathrm{d}\omega \tag{D.4}$$

For the mean intensity and the radiation pressure, spherical coordinates and independence on the azimuthal angle give with $\mu = \cos\theta$:

$$J_\lambda = \frac{1}{2}\int_0^\pi I_\lambda \sin\theta \mathrm{d}\theta = \frac{1}{2}\int_{-1}^{1} I_\lambda \mathrm{d}\mu \tag{D.5}$$

$$K_\lambda = 2\pi\int_0^\pi I_\lambda \cos^2\theta \sin\theta \mathrm{d}\theta = 2\pi\int_{-1}^{1} \mu^2 I_\lambda \mathrm{d}\mu \tag{D.6}$$

In Sect. 3.2.5 we saw that the equation of radiative transfer cannot be solved easily. In *MAFAGS*, J_λ is determined with H_λ and K_λ using the approximate boundary condition (Reile 1987):

$$f_\lambda^{\mathrm{K}} J_\lambda \equiv K_\lambda \tag{D.7}$$

The *Eddington factor* f_λ^{K} is determined iteratively. The solution of the problem is coupled to the determination of the temperature stratification and the calculation of other thermodynamic quantities, all accounting for flux conservation and hydrostatic equilibrium. *MAFAGS* adopts the following procedure (Reile 1987, p. 56 et seq.) for each iteration step:

- *Grey atmosphere*[1] as initial approximation for temperature and pressure stratification.
- Determination of occupation numbers from these stratifications using the ionisation equilibria amongst others.
- Calculation of opacities.
- Solution of radiative transfer, Eddington factors and energy flux (including convection).
- New temperature stratification using the method of temperature corrections following Feautrier (1964) and Gustafsson (1971).
- New gas pressure stratification using the hydrostatic equation.

Convergence is achieved using *Newton-Raphson iteration* warranting fast convergence. However convergence is only achieved as long as the initial grey atmosphere is not too far from the true solution. This is no longer the case in cool ($T_{\mathrm{eff}} \lesssim 5000\,\mathrm{K}$) metal-rich ([Fe/H] $\gtrsim 0.20$) atmospheres. This limit is encountered in the analysis of the two cool stars HD 109647 and HD 110463 (cf. Sect. 3.3.2).

[1] The opacity then is independent of wavelength and equals the *Rosseland mean of opacity*

$$\frac{1}{\kappa_{\mathrm{R}}} \equiv \frac{\int_0^\infty \frac{1}{\kappa_\lambda}\partial_T B_\lambda \mathrm{d}\lambda}{\int_0^\infty \partial_T B_\lambda \mathrm{d}\lambda}$$

(for details, see e.g. Mihalas 1978, p. 57 et seq.)

E Individual spectra near Hα and Li I 6707.8 Å

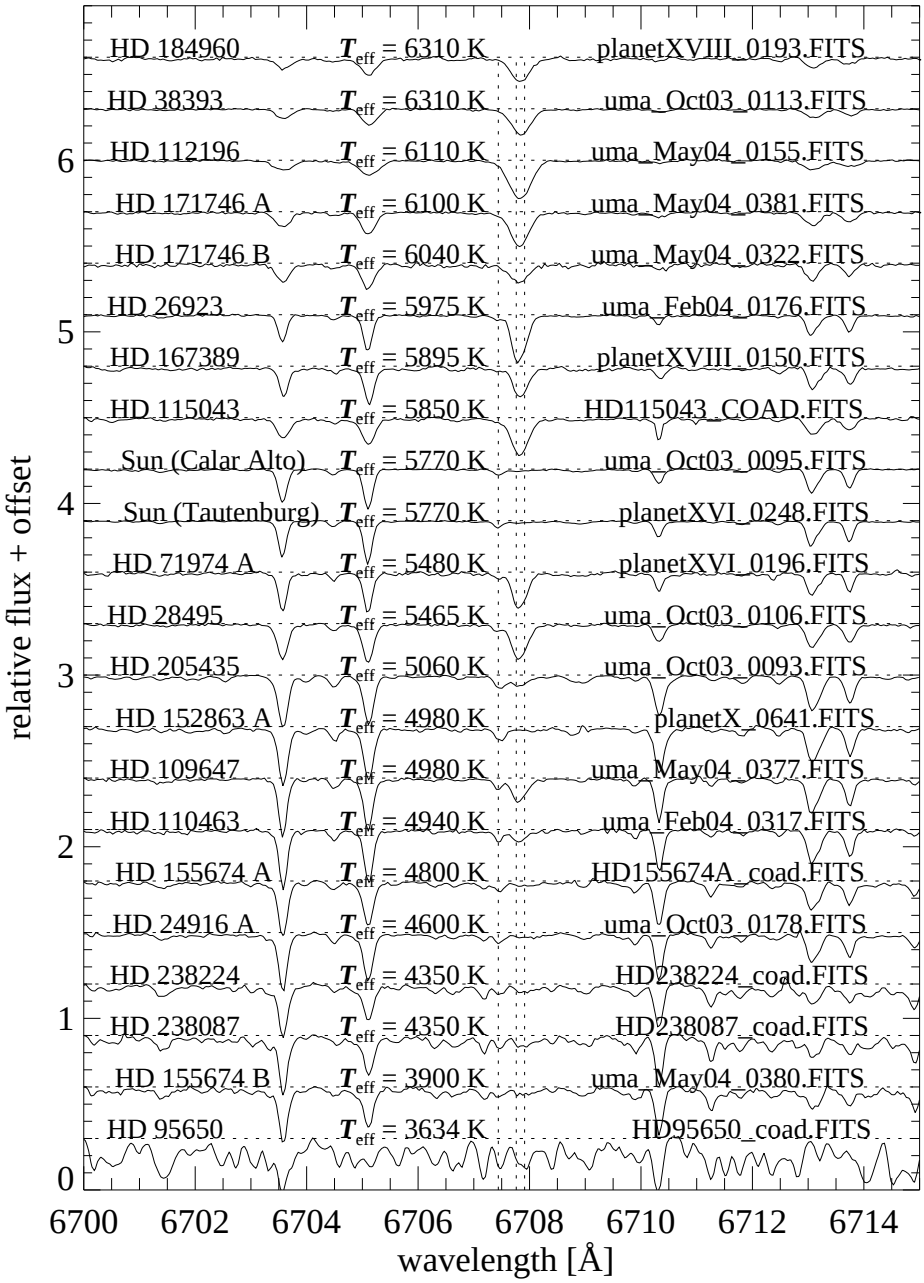

Figure E.1: The Li I resonance doublet at 6707.8 Å of UMa group candidates – The spectra are shifted along the ordinate by arbitrary values for clarity. The dotted lines indicate the position of following lines: Fe I λ 6707.44 Å (Sestito & Randich 2005), ^{7}Li I λ 6707.76 Å and ^{7}Li I λ 6707.91 Å (Pavlenko 1995). The given effective temperatures are the values derived from the individual exposures indicated at the right (see Table B.1).

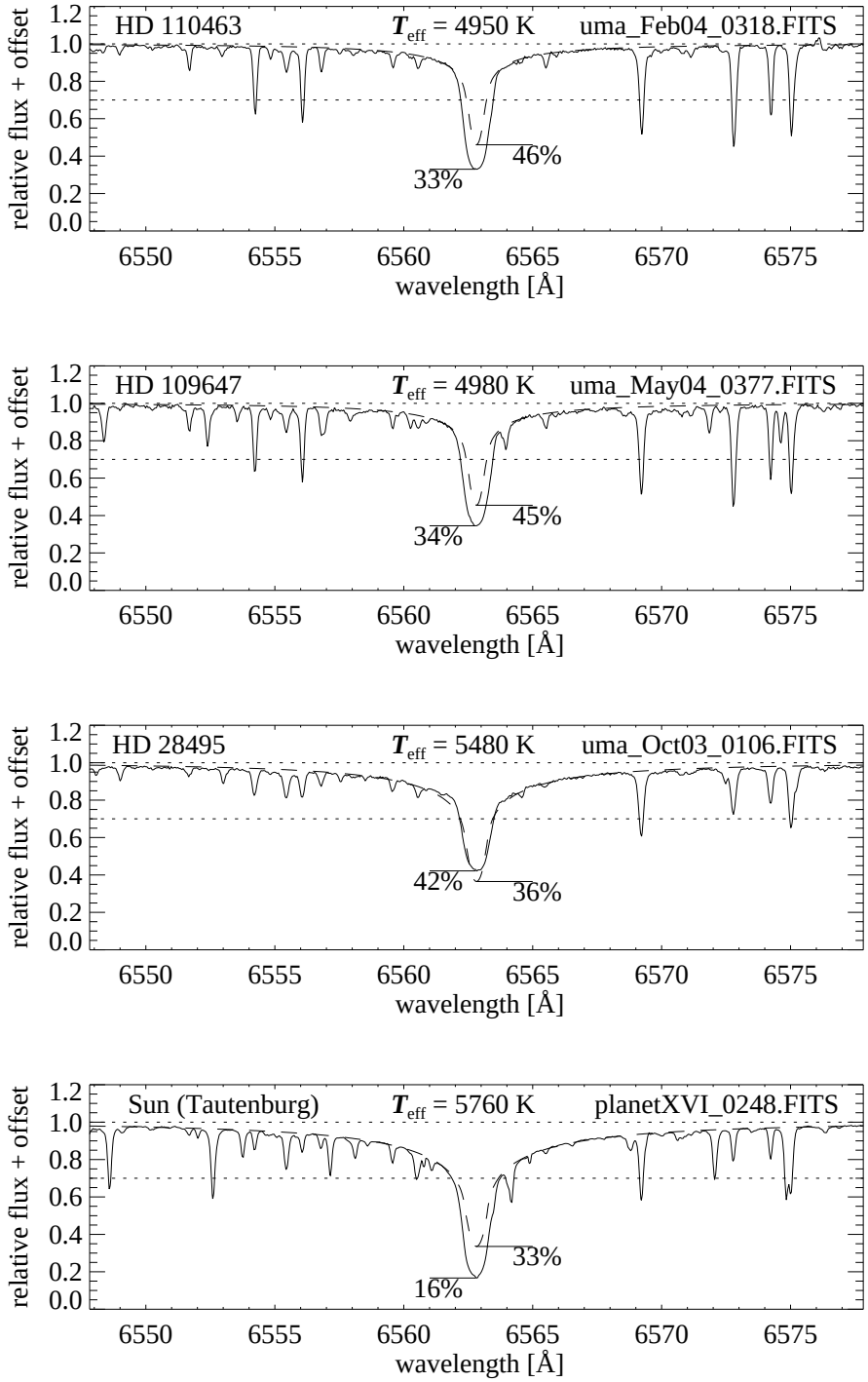

Figure E.2: The Hα line of UMa group candidates – For each object including the Moon, one exposure was chosen (solid). Theoretical spectra were calculated with the stellar parameters derived from these exposures (dashed, name of frame given at the right, see Table B.1). Core intensities are indicated by relative percentage. Furthermore the dotted lines represent the relative continuum and the relative level of 0.7, the lower boundary for the temperature determination.

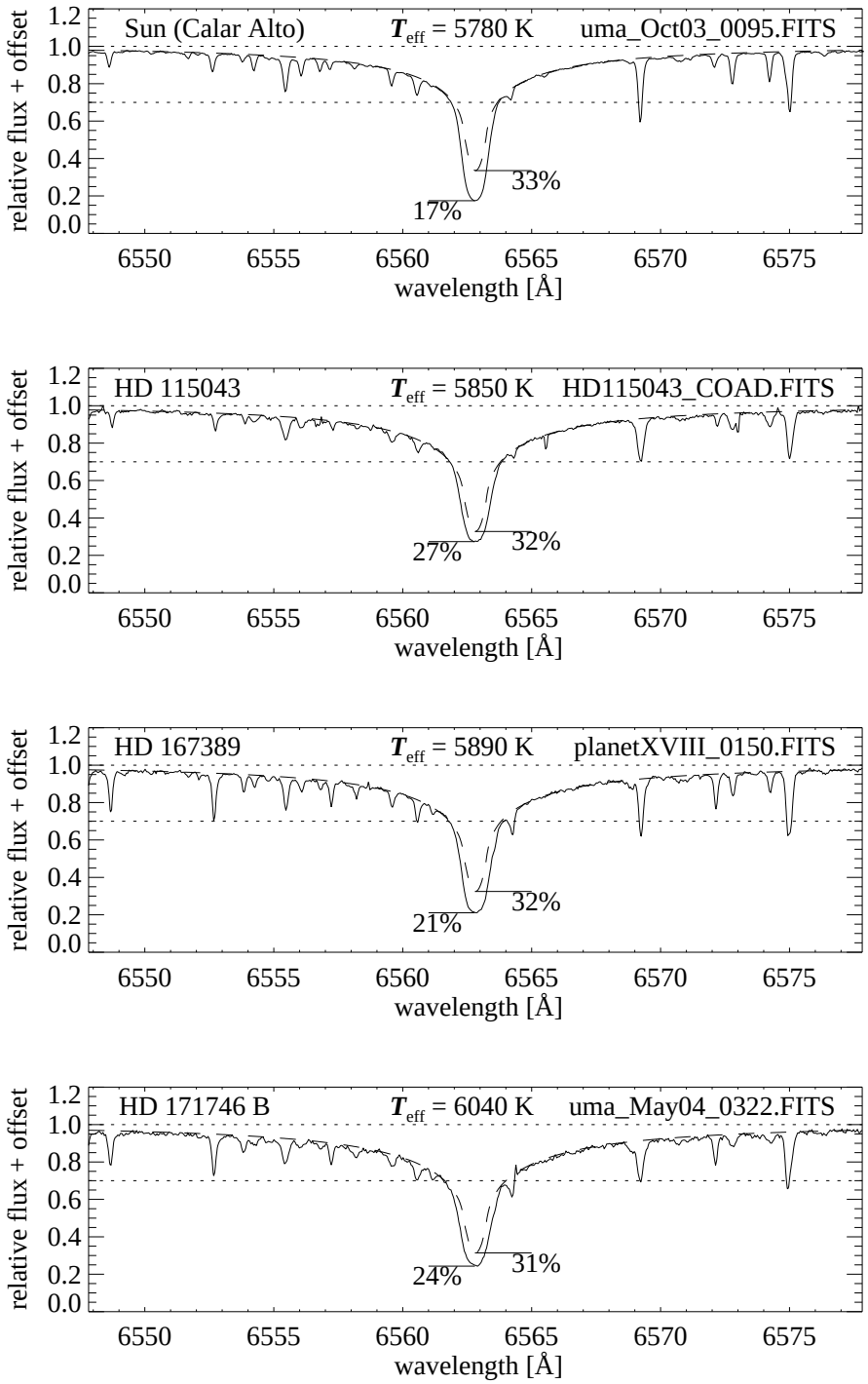

Figure E.3: The Hα line of UMa group candidates – Same as Fig. E.2 for the remaining spectra.

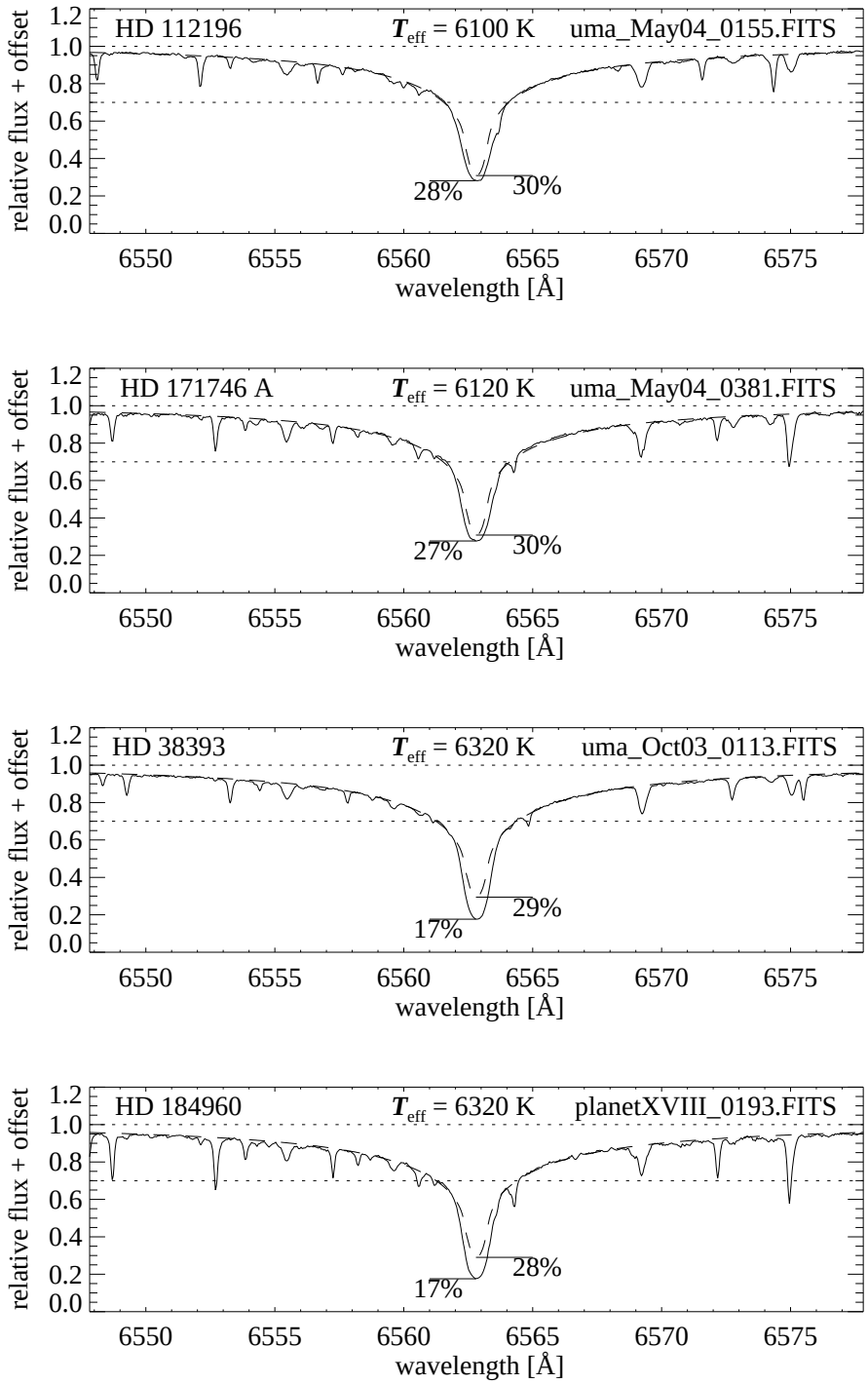

Figure E.4: The Hα line of UMa group candidates – Same as Fig. E.2 for the remaining spectra.

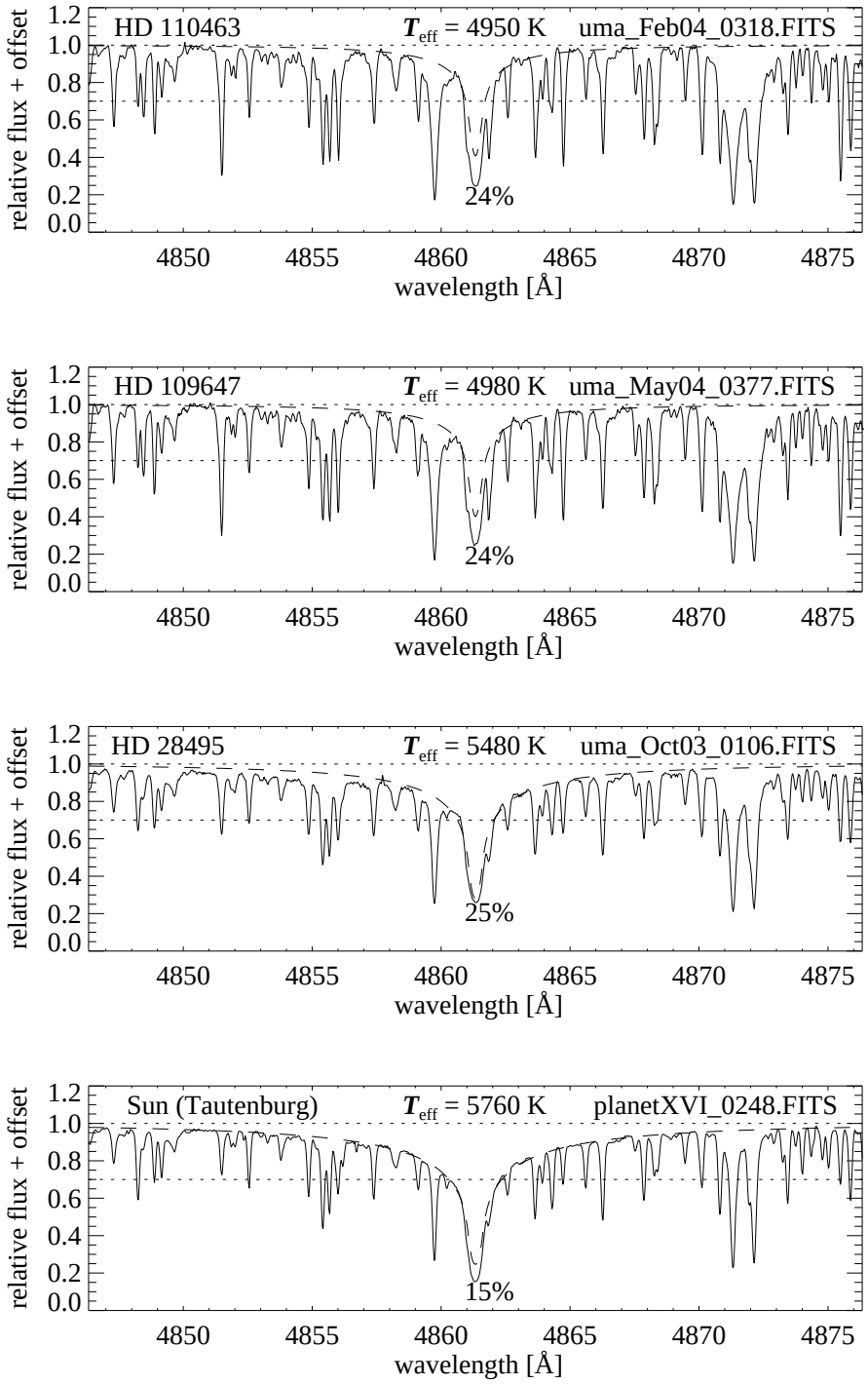

Figure E.5: The Hβ line of UMa group candidates – Same as Fig. E.2 but for Hβ. The synthetic lines were calculated with the effective temperatures derived from the Hα line and allow to judge the overall consistency with the Hβ profile. The intensity at the core of only the observed line is indicated.

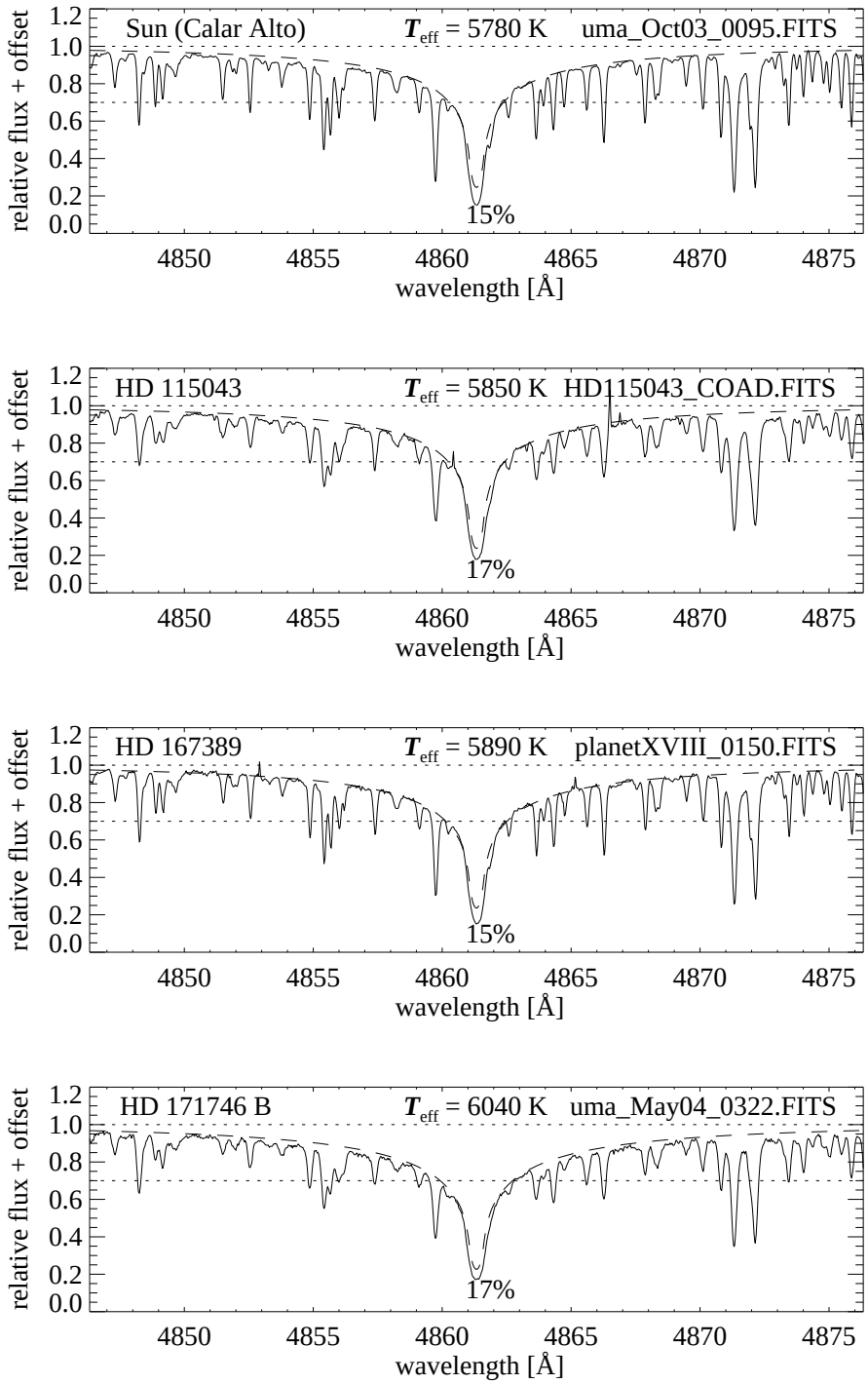

Figure E.6: The Hβ line of UMa group candidates – Same as Fig. E.5 for the remaining spectra.

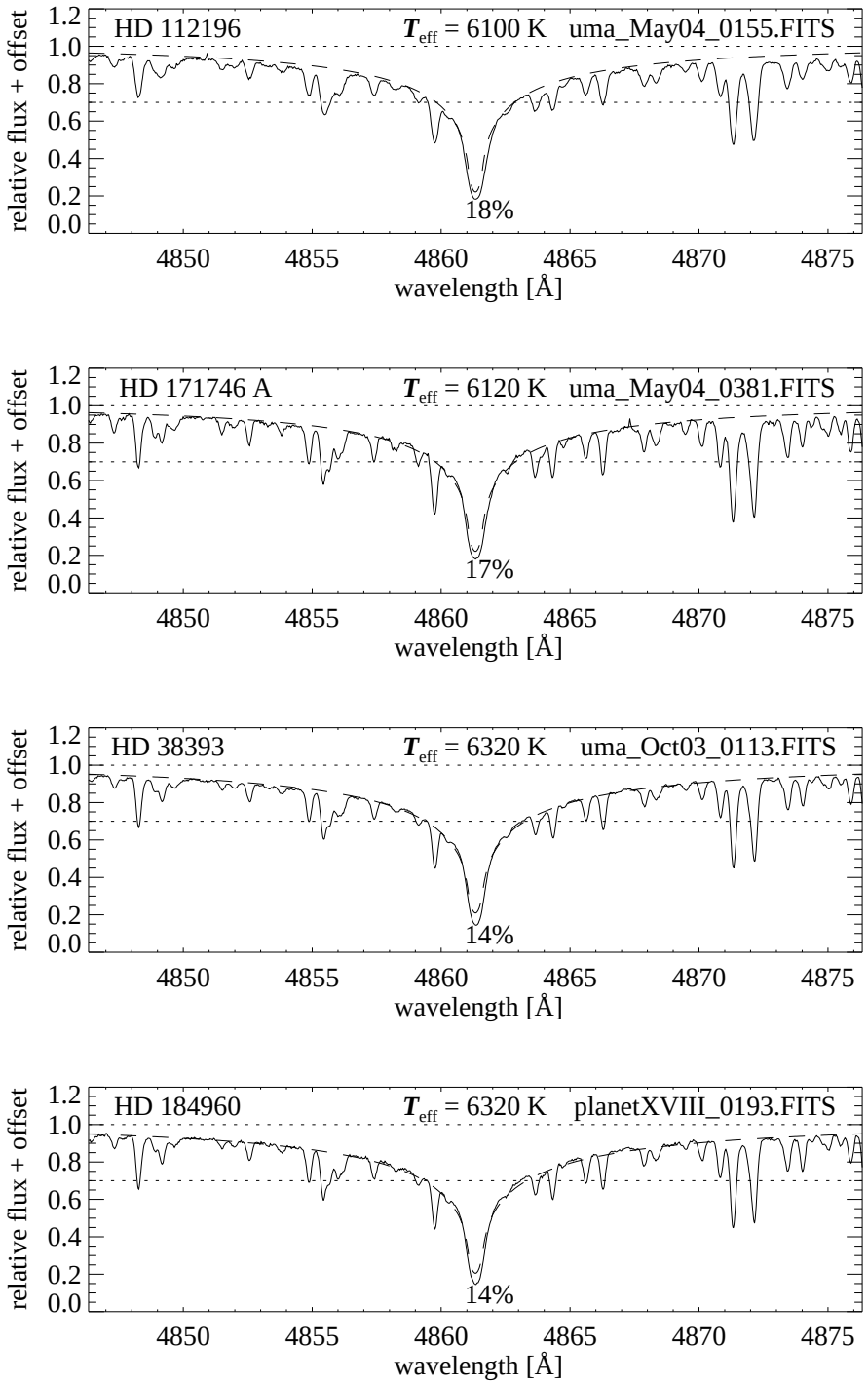

Figure E.7: The Hβ line of UMa group candidates – Same as Fig. E.5 for the remaining spectra.

F Residuals of LTE fits to the observed Hα profile.

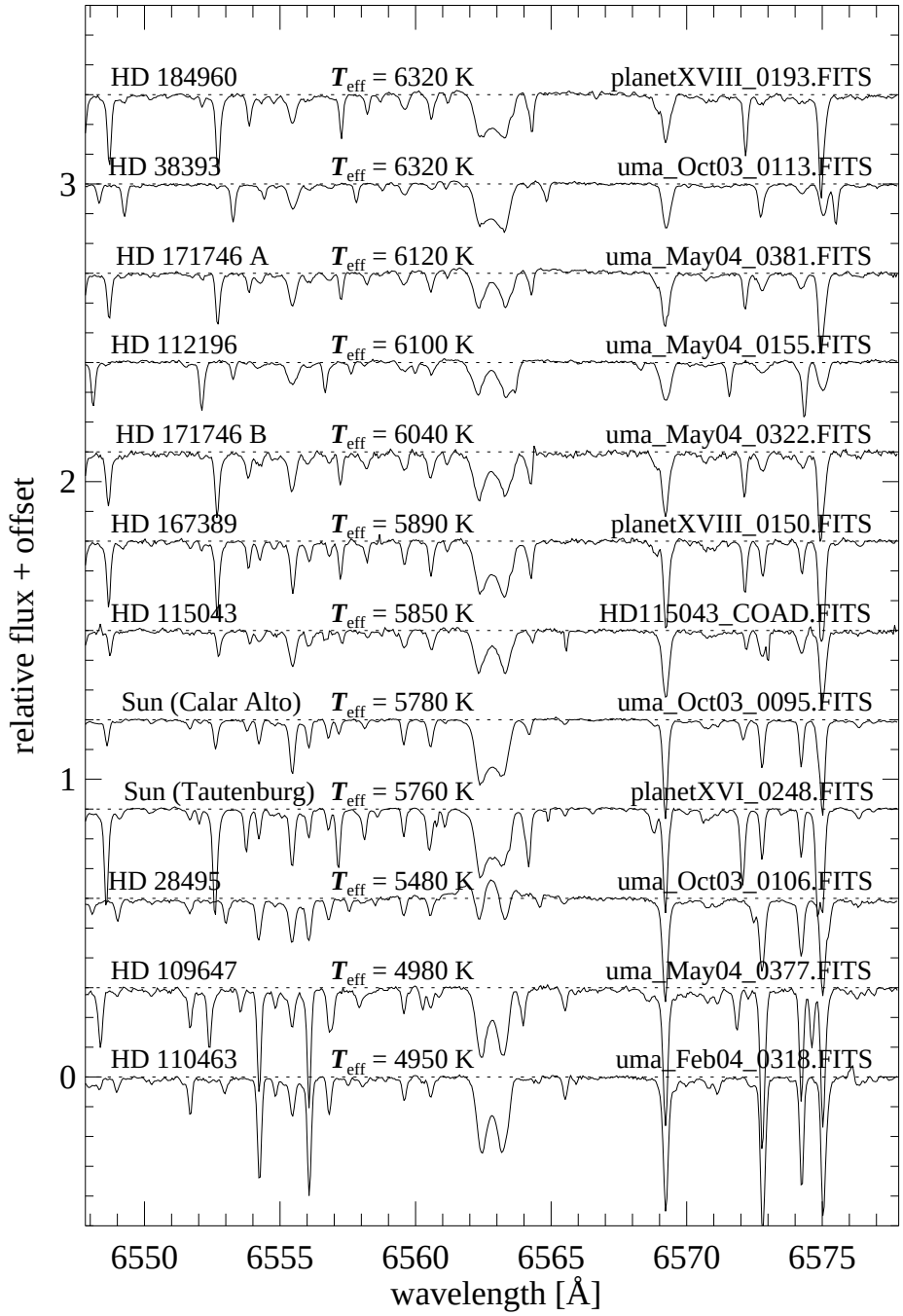

Figure F.1: LTE Hα residual fluxes – For each object including the Moon, one exposure was chosen. Synthetic LTE spectra were calculated with the stellar parameters derived from these individual exposures (see Table B.1). The residual Hα fluxes are shown with an arbitrary ordinate offset.

Index

Persönliche Danksagung

Am Schluss dieser Arbeit ist es Zeit, sich bewusst zu werden, dass ohne die begleitende Unterstützung vieler anderer Menschen mein Projekt “Ursa Major” nicht zu Stande gekommen wäre.

Als erstes möchte ich mich bei Prof. Ralph Neuhäuser bedanken, der mich bereits seit meiner Diplomarbeit am MPE Garching stets unterstützt hat. Er motivierte mich zu der Arbeit an den jungen, nahen Sternen, an denen ich bald viel Freude fand. Nach dem Umzug an die Unisternwarte in Jena konnte ich mich neben fachlichem Rat immer auf seine Hilfe bei allerlei Anträgen und organisatorischen Dingen verlassen. Ihm habe ich die Freude zu verdanken, in einem der schönstgelegenen Institute dieses Landes gearbeitet zu haben.

Die Doktorarbeit wurde nicht komplett in Jena durchgeführt. Daher danke ich Prof. Morfill, in dessen Theoriegruppe am MPE ich das erste Jahr als Doktorand verbringen durfte. Ich danke ihm für die Ermöglichung mehrerer Beobachtungsaufenthalte und Konferenzbesuche. Der Datenverarbeitungsgruppe am MPE, vor allem Harald Baumgartner, danke ich für die professionelle Unterstützung.

Nun ist es an der Zeit, Dr. Klaus Fuhrmann zu danken, der mir bereits in der Zeit am MPE in vielen Diskussionen die Begeisterung an der präzisen Analyse der Sternatmosphähren vermittelte. Er überliess mir seine *IDL*-Programme und wies mich in die Arbeit mit *LINFOR* und *MAFAGS* ein. Weiterhin danke ich ihm für die Anpassung der Reduktionsprogramme an den Coudé-Échelle- Spektrographen in Tautenburg. Obwohl er nach 2003 nicht mehr der Gruppe angehörte, war von Jena immer noch ein Draht zu ihm ans MPE und dann später nach Teneriffa gespannt, über den er mich nach wie vor bis zum Ende dieser Arbeit mit wichtigen Informationen und Ratschlägen versorgte.

Auch Dr. Brigitte König stand mir mit Rat und Tat zu Seite, wenn es mit der Linienanpassung mal nicht so ging, wie ich es mir vorstellte, oder die Programme Sachen machten, die ich nicht zu träumen gewagt hätte. Viele unserer Beobachtungsanträge profitierten von ihrer unmittelbaren und effizienten Kritik. Dies gilt ebenso für Teile des Manuskripts, die sie Korrektur gelesen hat; vor allem das Manuskript dieser Arbeit, als sie bereits in Pittsburgh war. Ich danke ihr weiterhin für das Überlassen ihres Programms zur Anpassung von Lithium-Linien sowie einer hervorragenden Korrelationsvorlage zur Radialgeschwindigkeitsmessung.

Als ich 2002 als Fremder die ersten Male nach Thüringen kam – zunächst nur zu Beobachtungen in Tautenburg – war es Dr. Eike Guenther, der mir half, hier Fuß zu fassen. Ich danke ihm für die hervorragende Zusammenarbeit in Tautenburg und die Einblicke in die Radialgeschwindigkeitssuche nach Planeten, die mir in vielen nächtlichen Diskussionen zu Teil wurden. Auch ihm danke ich für das Lesen des Manuskripts dieser Arbeit und das kritische Hinterfragen vieler Dinge, die ich als selbstverständlich nahm, vor allem in Hinblick auf die theoretischen Grundlagen der Analysen.

Was wäre diese Arbeit, wenn das Wissen um die theoretischen Grundlagen fehlte? Gerade in dieser Hinsicht danke ich Dr. Günther Wuchterl für die vielen Diskussionen über Sternentwicklung und Sternatmosphären. Er war eine echte Bereicherung für die in erster Linie auf Beobachtung ausgerichtete Gruppe.

An dieser Stelle danke ich meinem Zimmerkollegen Chris Broeg, der ebenfalls viele hilfreiche Kritik zu theoretischen Aspekten der Arbeit beisteuerte. Darüber hinaus schätze ich sein Talent, viele nützliche LINUX-Programme und LaTeX-Helferlein auszugraben, die er mir sogleich weitergab. Auch über die Arbeit hinausgehend konnte ich immer mit ihm rechnen, vor allem Anfang 2003, als wir noch recht fremd in Jena waren.

Eine große Bereicherung für mich als Spektroskopiker war die Aufnahme von Dr. Marc Hempel in das Institut. Ihm verdanke ich viele Einsichten in die spektroskopische Analyse von Sternen, vor allem bezüglich des statistischen Gleichgewichtes. Ich danke ihm für das Lesen des Manuskripts und die vielen nützlichen Vorschläge.

Ich danke allen Angehörigen des Jenaer Instituts für die angenehme Atmosphäre. Monika Müller und Jürgen Weiprecht habe mich im weitesten Sinne bei technischen Dingen aller Art unterstützt. Ohne Jürgens schnelle Hilfe bei Rechnerproblemen und seinen effizienten Lösungen, mit denen meine Programme zum Laufen gebracht werden konnten, wäre meine Arbeit von vornherein zum Scheitern verurteilt gewesen.

Besonders möchte ich jenen danken, die mit kleinerem und größerem Engagement das Leben im Institut aufgewertet haben. Das DVD-Seminar, das von Andreas Seifahrt begründet und von Ansgar Gaedke sowie Dr. Marc Hempel und Sebastian Krause weitergeführt wurde und wird, ist bereits zu einem regelmäßigen Bestandteil des Institutslebens geworden. Furthermore, I'd like to thank Ana Bedalov, Akemi Tamanai, Bettina Posselt, Helge Rehwald, Tobias Schmidt and Jürgen Weiprecht for the precious big and little things of everyday's life. Moreover, I thank Akemi for her critical reading of a part of the manuscript.

Außerhalb des Instituts danke ich Dr. Andreas Korn für die Bereitstellung seines Programms zur Addition von Spektren, Dr. Matthias Hünsch und Prof. Thomas Gehren für ihre Hilfe bei der Suche nach verloren geglaubter Literatur. Darüberhinaus danke ich allen, deren Anwesenheit und Unterstützung das Beobachterdasein leichter machte: Dr. Miriam Rengel, Dr. Eike Guenther, Christian Högner, Uwe Laux, Steffen Richter und Johannes Winkler. Finally I'm grateful to Noel Carboni who left his photograph of the Big Dipper to me.

Sehr wichtig war für mich die Förderung durch das Cuasanuswerk, welches die drei Jahre in Jena finanzierte. Ich danke all den Cusanern und Cusanerinnen und den Referenten des Cusanuswerks, die mir in vielen Veranstaltungen ermöglichten, Bekanntschaft mit anderen Fachgebieten und anderen Denkweisen zu machen.

Mein besonderer Dank gilt meinen Eltern, für ihre jahrelange und geduldige Unterstützung, obwohl sie nie wussten, woran genau ich arbeitete.

Schließlich möchte Dir, liebe Caroline, danken. Du gabst mir mit Deiner Liebe und Unterstützung die Kraft, durchzuhalten und die Arbeit zu einem Abschluss zu bringen.

Ehrenwörtliche Erklärung

Ich erkläre hiermit ehrenwörtlich, dass ich die vorliegende Arbeit selbständig, ohne unzulässige Hilfe Dritter und ohne Benutzung anderer als der angegebenen Hilfsmittel und Literatur angefertigt habe. Die aus anderen Quellen direkt oder indirekt übernommenen Daten und Konzepte sind unter Angabe der Quelle gekennzeichnet.

Weitere Personen waren an der inhaltlich-materiellen Erstellung der Arbeit nicht beteiligt. Insbesondere habe ich hierfür nicht die entgeltliche Hilfe von Vermittlungs- bzw. Beratungsdiensten in Anspruch genommen. Niemand hat von mir unmittelbar oder mittelbar geldwerte Leistungen für Arbeiten erhalten, die im Zusammenhang mit dem Inhalt der vorgelegten Dissertation stehen.

Die Arbeit wurde bisher weder im In- noch im Ausland in gleicher oder ähnlicher Form einer anderen Prüfungsbehörde vorgelegt.

Die geltende Promotionsordnung der Physikalisch-Astronomischen Fakultät ist mir bekannt.

Ich versichere ehrenwörtlich, dass ich nach bestem Wissen die reine Wahrheit gesagt und nichts verschwiegen habe.

Jena, den 19. April 2006

Lebenslauf

Matthias Ammler

Geboren: 10.01.1977, Neuburg a. d. Donau
Staatsangehörigkeit: deutsch

09.1983 - 07.1987	Grundschule Bergheim
09.1987- 06.1996	Descartes-Gymnasium Neuburg a. d. Donau
28.06.1996	Allg. Hochschulreife
11.1996 - 12.2001	Studium der Physik an der Ludwig-Maximilians-Universität München
08. - 09.1998	Werkstudent in der techn. Entwicklung der Audi AG
03. - 04.1999	Werkstudent bei Daimler-Chrysler Aerospace AG zur Arbeit an Navigationsprogrammen
08. - 09.1999	Sommerstudent bei DESY Zeuthen
10.1999	Praktikum in der Plasmaphysikgruppe der Universitätssternwarte (USM) München
03. - 04.2000	wissenschaftl. Hilfskraft am Wendelsteinobservatorium der USM
12.2000 - 12.2001	Diplomarbeit am MPI für Extraterrestrische Physik (MPE) bei Dr. R. Neuhäuser und Prof. G. Morfill: *Photometrische Untersuchung von T Tauri-Sternen – Test von Vorhauptreihenentwicklungsmodellen*
17.12.2001	Physikdiplom
01.2002 - 04.2003	Doktorand am MPE Garching bei Dr. R. Neuhäuser und Prof. G. Morfill: *"Characterisierung der jungen nahen Sterne"*
05.2002 - 04.2003	Graduiertenstudium an der *International Max-Planck Research School for Astrophysics*
SoSe 2003 - SoSe 2006	Graduiertenstudium an der Friedrich-Schiller-Universität Jena, Doktorand bei Prof. R. Neuhäuser

05.2003 - 04.2006	Graduiertenstipendium der Bischöflichen Studienförderung Cusanuswerk: *Charakterisierung der jungen, nahen Sterne*

Jena, den 19. April 2006